High Resolution X-Ray Scattering

E. Ercan Alp

Advanced Photon Source

Argonne National Laboratory, Argonne, Illinois 60439

JASS'02, October 19-28, 2002
Amman, Jordan


SOURCE
EXPLORING MOLECULES AT WORK WITH BRILLIANT X-RAYS
IE ADVANCED PHOTON SOURCE
dvanced Photon Source Explore Molecules
Scientists At The Advanced Photon Source Will Use Four Different Experimental Techniques With X-Rays
Imaging With X-Rays

W. Sturhahn, T. Toellner,
J. Zhao, H. Sinn,
C. L'abbé, A. Alatas,
A. Said, S. Hwang, H. Yavas

Advanced Photon Source
Argonne National Laboratory

Y. Shvydko, H.C. Wille
M. Lucht, M. Lerche
E. Gerdau, K. Geske,
H.-D. Rüter

Hamburg University,

R. Röhlsberger
G. Wortmann
W. Keune

Rostock
Paderborn
Duisburg

F. Parak, K. Achterhold
U. Van Bürck, W. Potzel
H. Franz

Münich
HASYLAB

What is high resolution in the hard x-ray regime ?

Resolution power, $R = E/\Delta E$

This talk is focused for the following energy and resolution range:

$7 < E < 30$ keV

$10^{-9} < \Delta E < 10^{-3}$ eV

$10^{7} < R < 10^{13}$

The beamline 3-ID at the APS is built for this energy range to study collective excitations in condensed matter and hyperfine interactions for nuclear resonance scattering

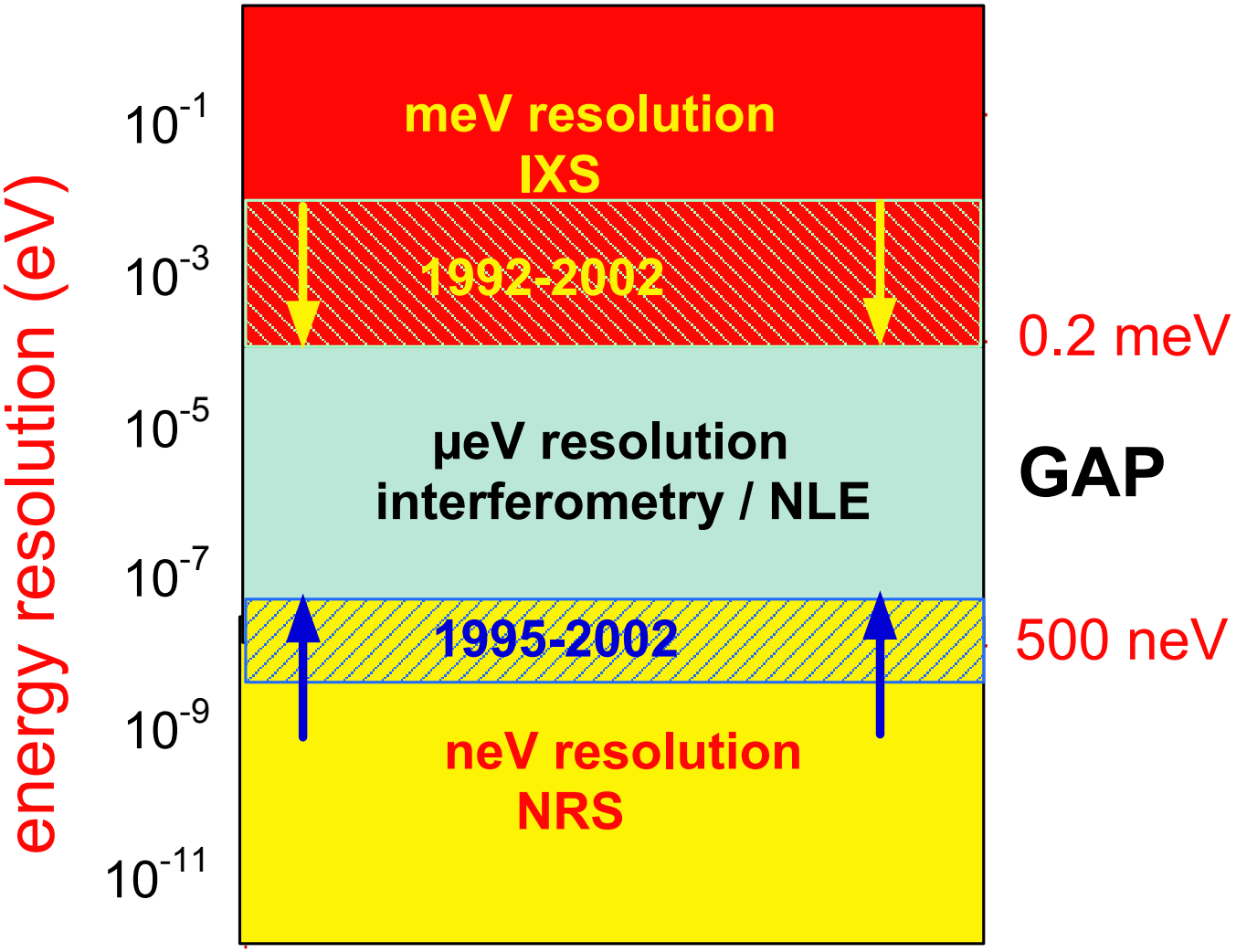
energy resolution (eV)
10-1
10-3
10-5
10-7
10-9
10-11
meV resolution
IXS
1992-2002
0.2 meV
μeV resolution
interferometry / NLE
GAP
1995-2002
500 neV
neV resolution
NRS

Inelastic X-Ray Scattering in the Synchrotron Era

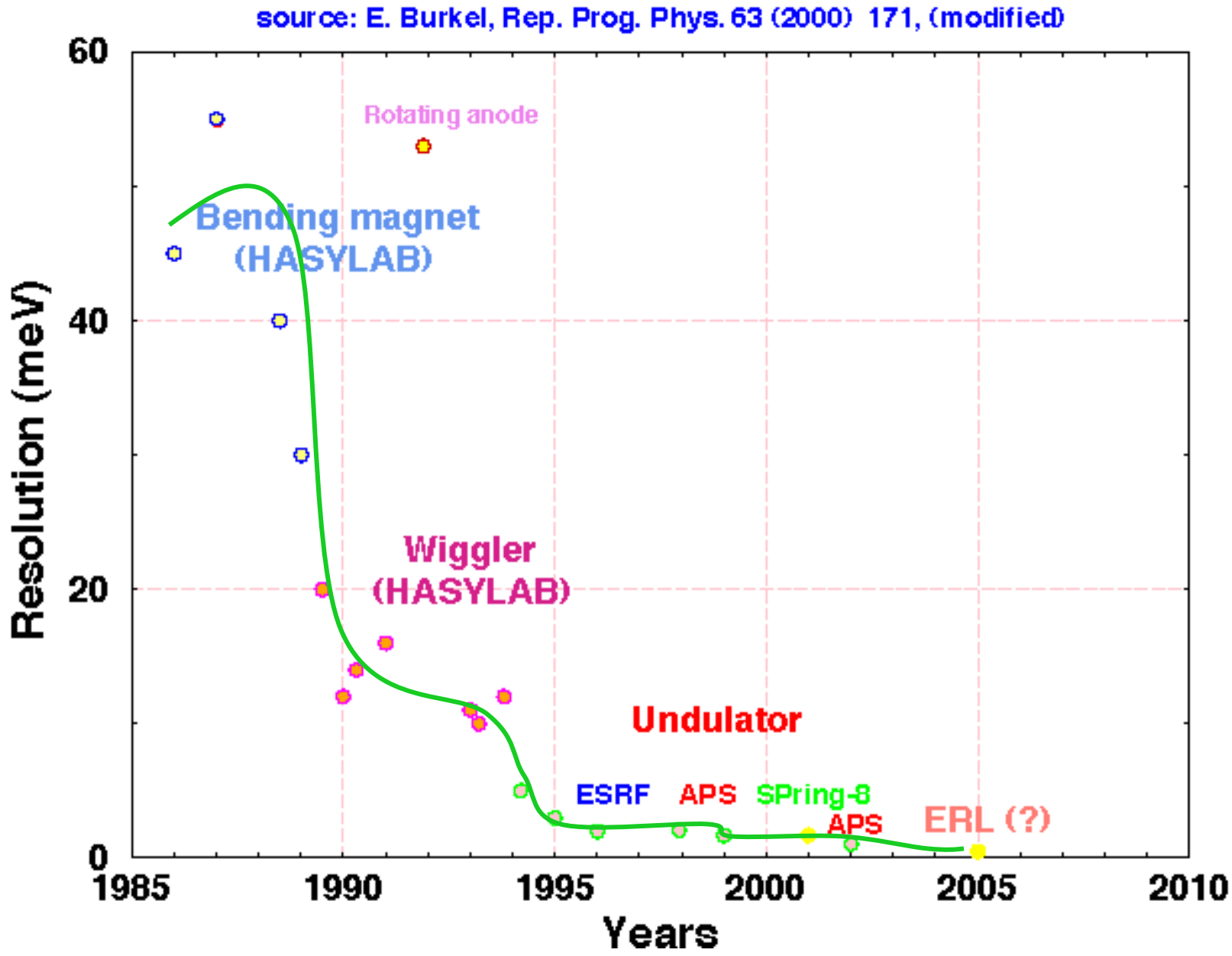

Key concepts in crystal Monochromatization

Angular acceptance
Reflectivity
Energy bandpass
Asymmetric diffraction
Debye-Waller factor
Low-order vs high order reflections
Extinction length
DuMond diagram
Dispersive vs non-dispersive arrangements: (++) or (+-)

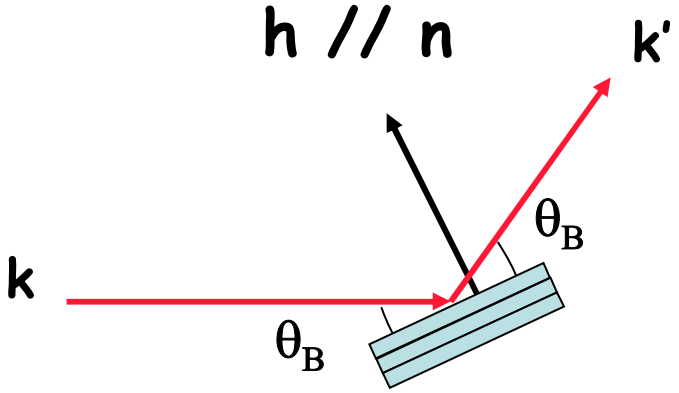

Symmetric: Bragg planes are parallel to the surface of the crystal

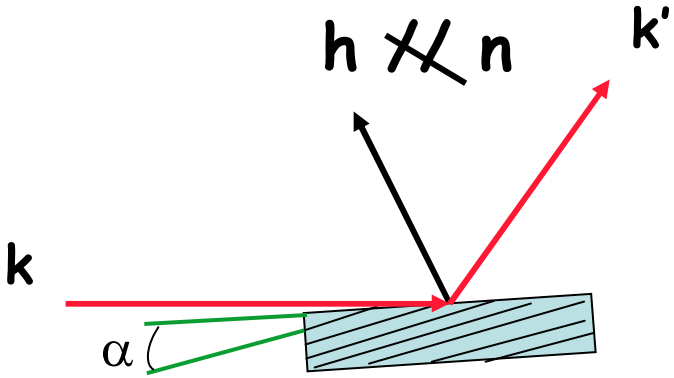

Asymmetric, Bragg planes are not parallel to the surface of the crystal

$$b = -\frac{\sin(\theta_B - \alpha)}{\sin(\theta_B + \alpha)}$$

b < 1	asymmetric,	beam enlarges
b = 1	symmetric,	$\alpha = 0$
b > 1	asymmetric	beam shrinks

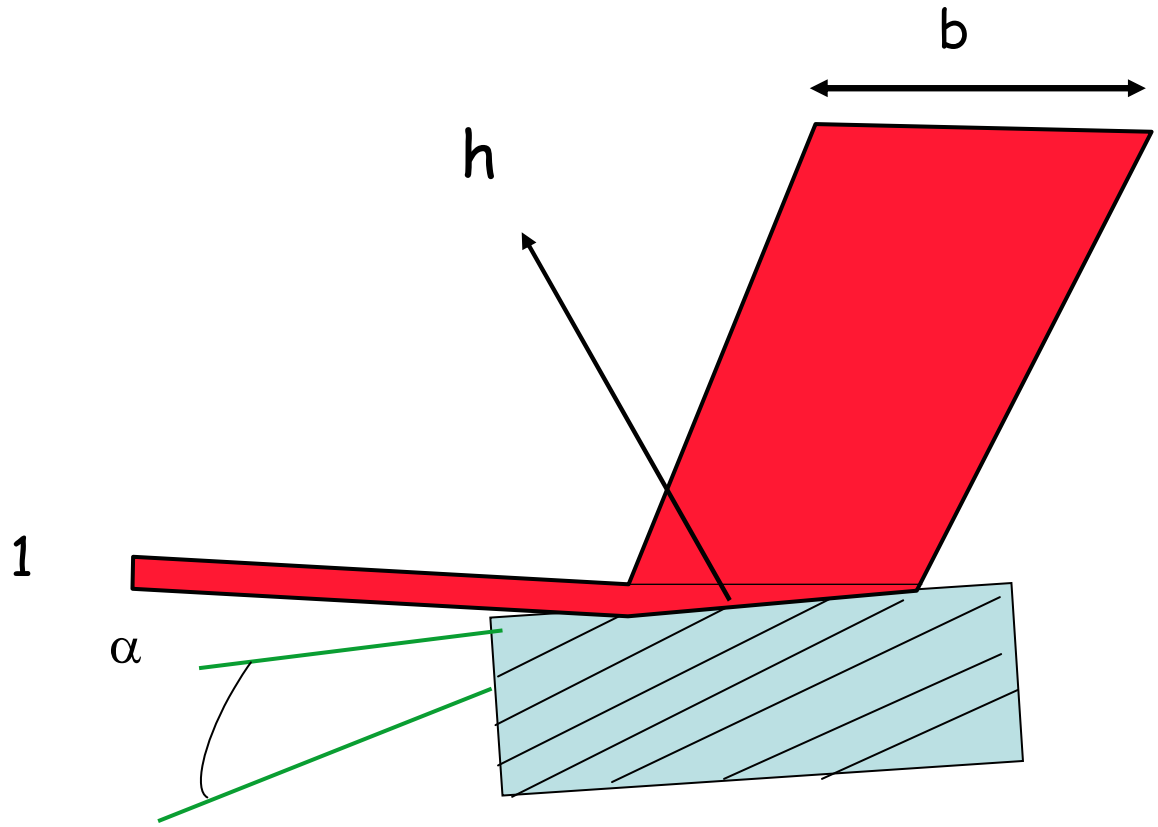

$$b = -\frac{\sin(\theta_B - \alpha)}{\sin(\theta_B + \alpha)}$$

$0.05 < b < 50$

Collimation by asymmetric Bragg diffraction

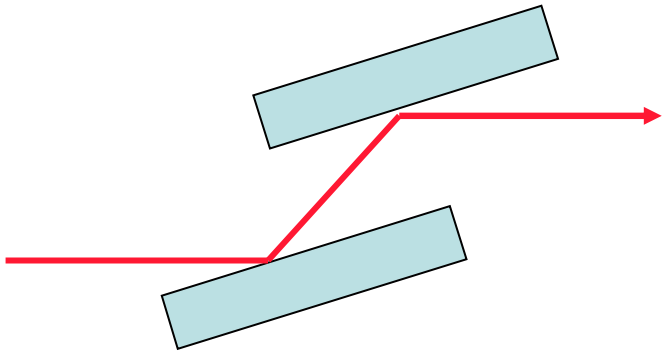

non-dispersive: (+ -)

Does not select energy per se
Beam leaves in the same direction

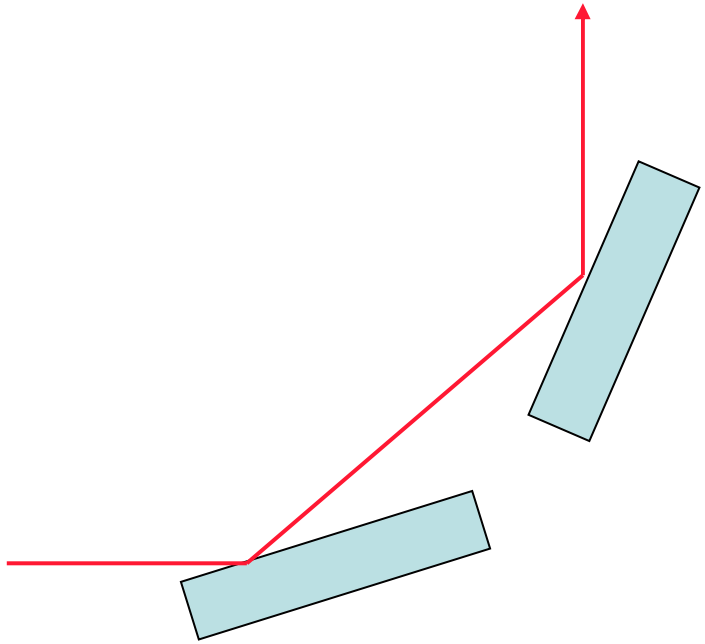

dispersive: (+ +)

energy selective, beam
Leaves in a different direction

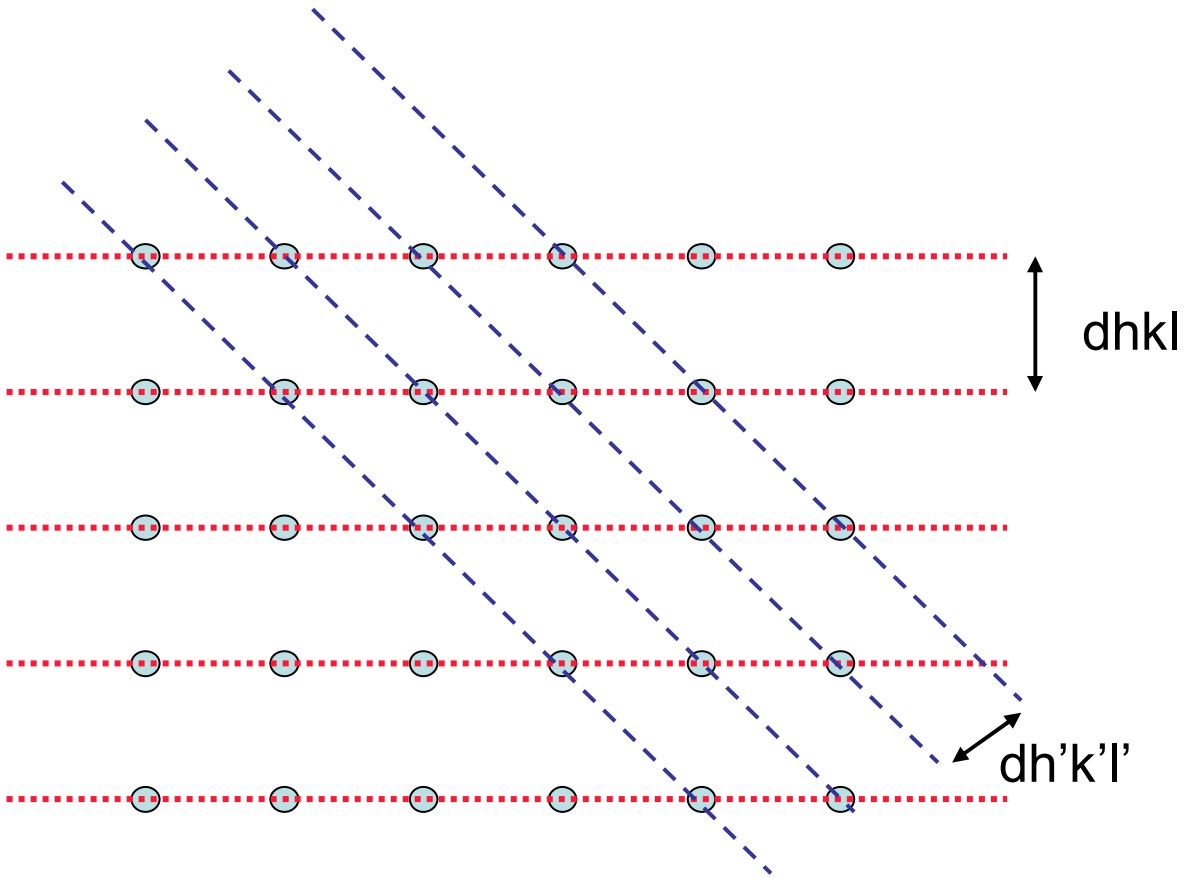

$d_{hkl} > d_{h'l'k'}$ higher order reflections have smaller d

$n\lambda = 2d\sin\theta$, smaller d for a given λ means higher Bragg angle

Si (800), 4 crystal set for 9.4 keV

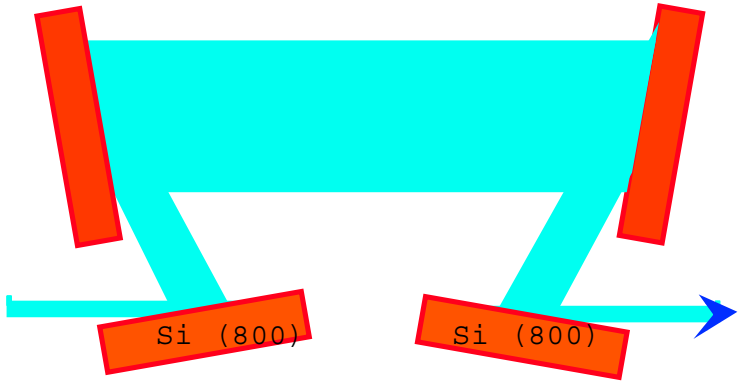

ΔE = 0.97 meV,
$\Delta\Theta$=32 μrad

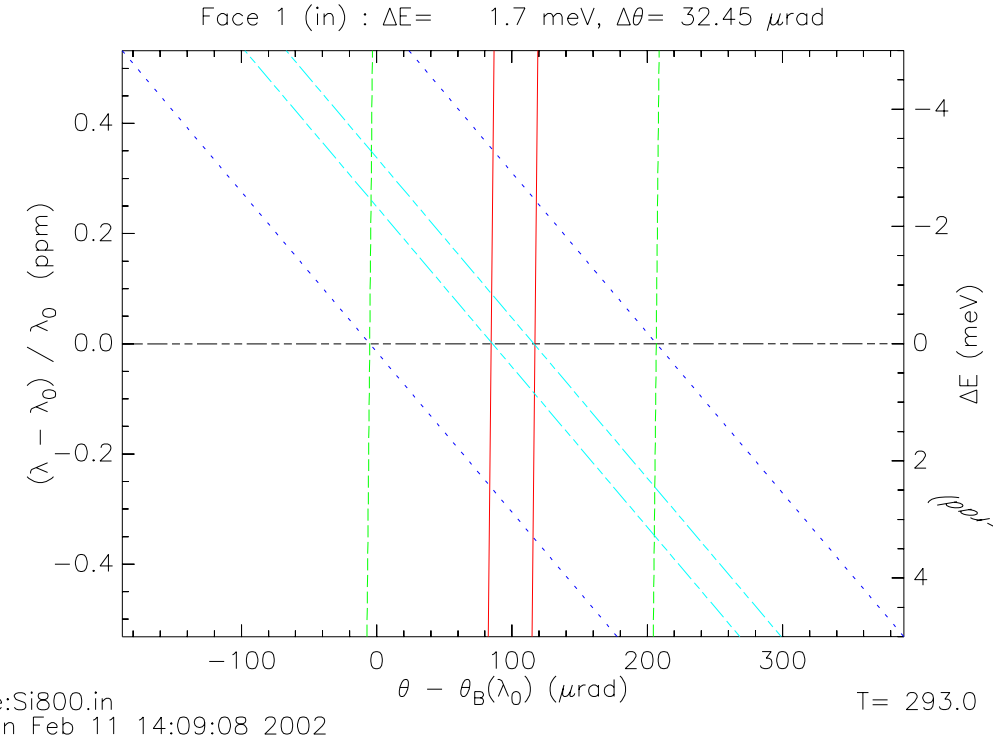

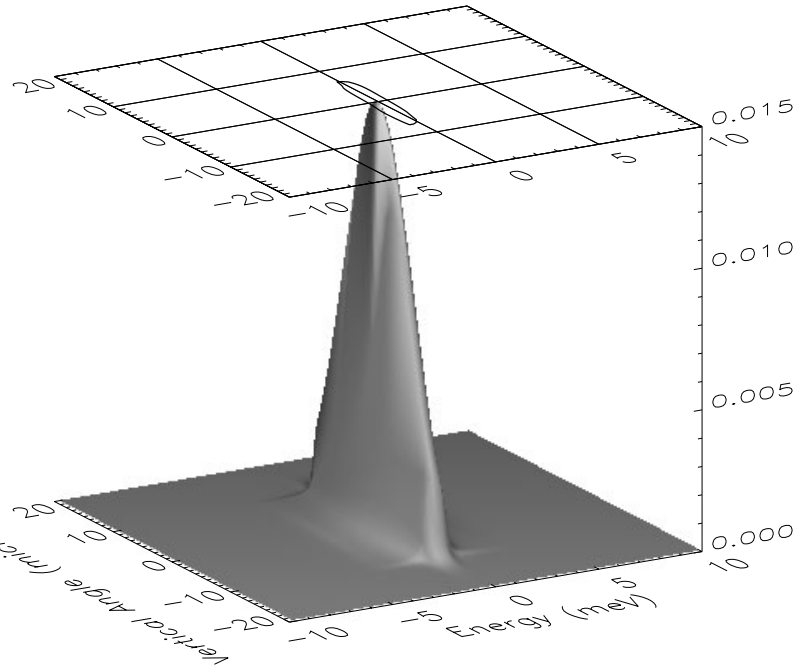

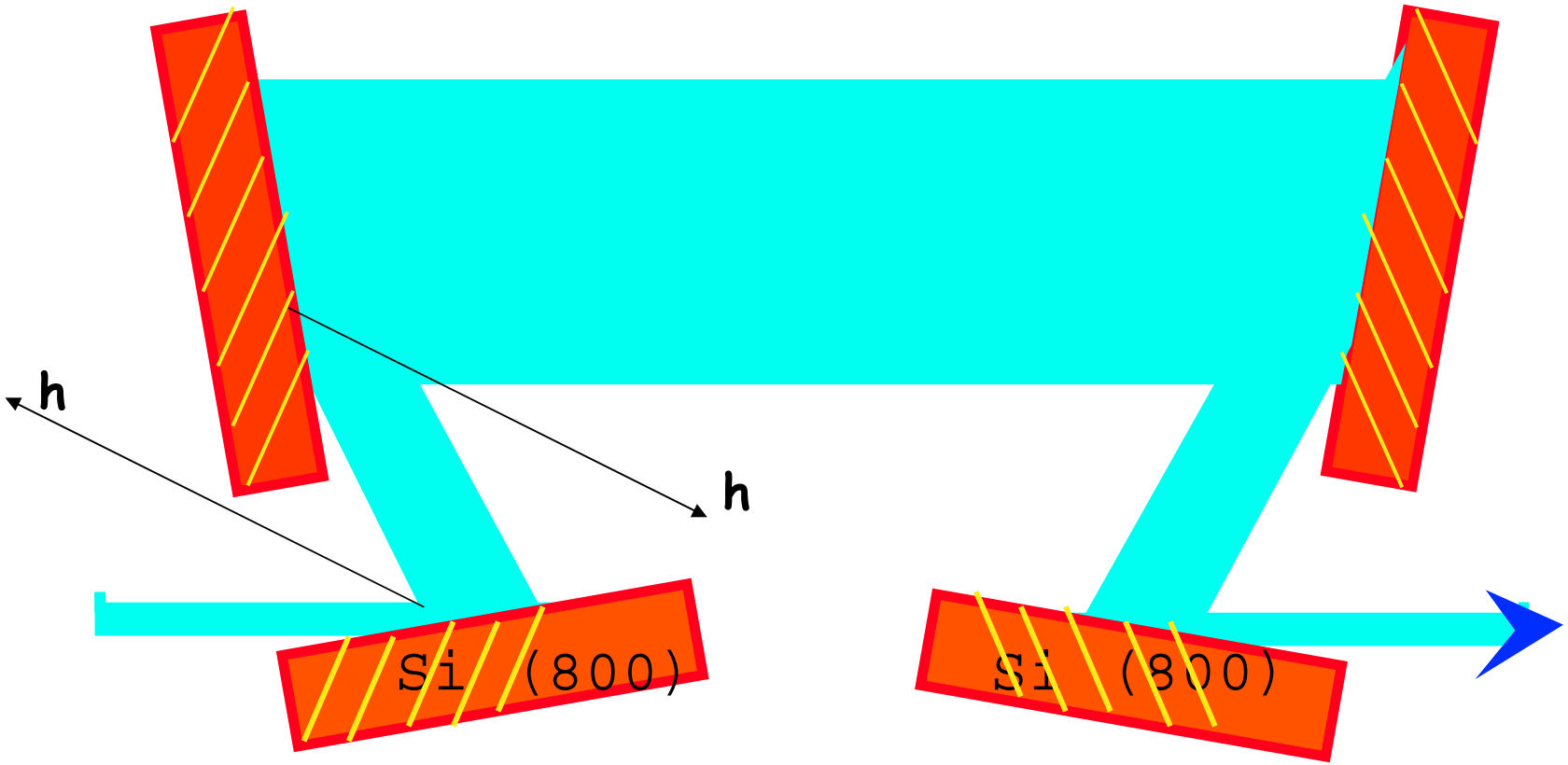

energy dispersive, artificially linked "channel-cut" in (+ - - +) geometry
(T. Toellner, et al, 2002, Yabashi, et al (2001, PRL)

DuMond diagram (J. DuMond, 1932)

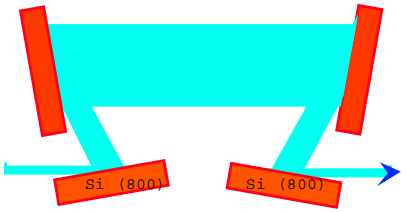

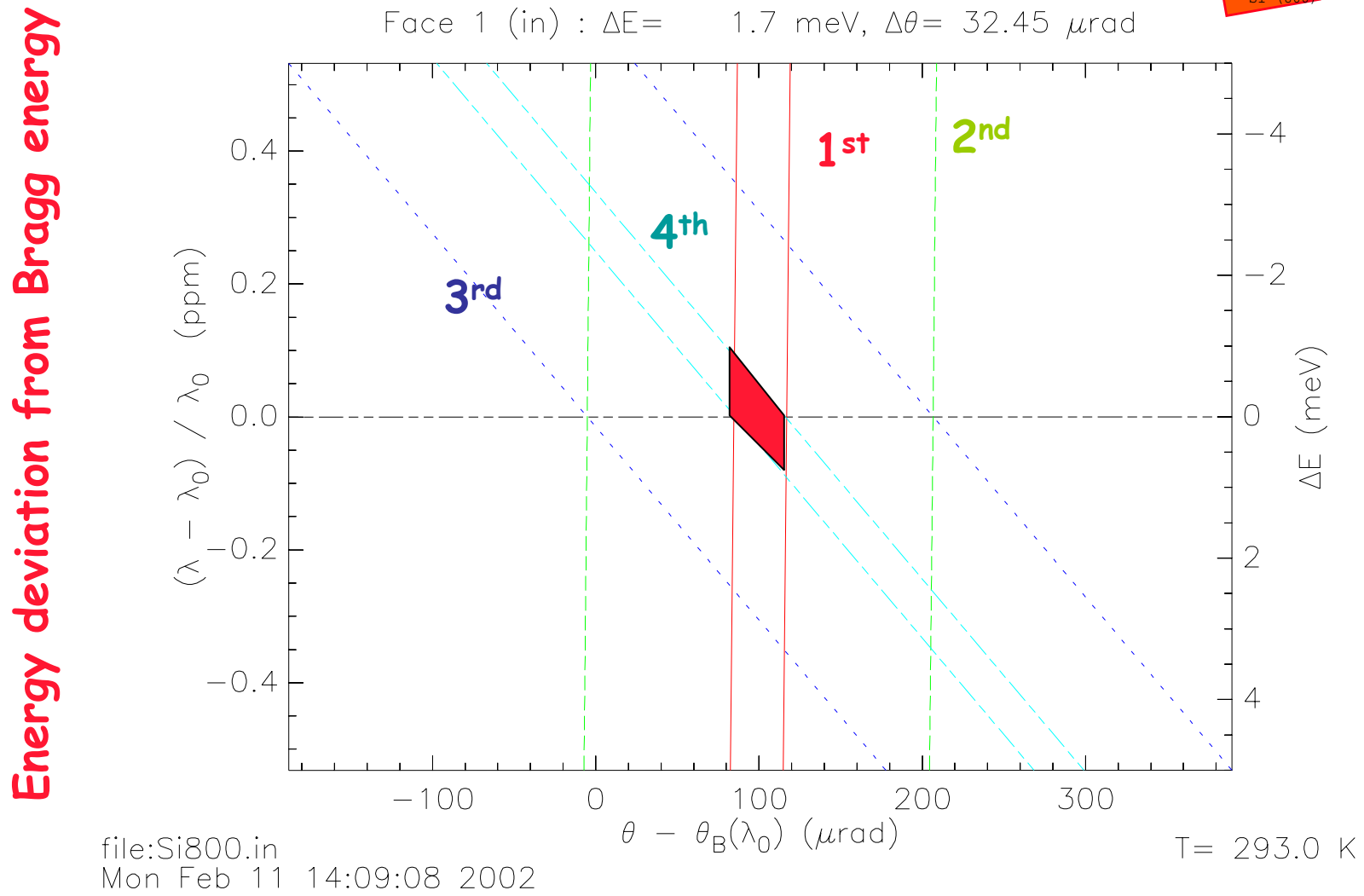

Energy deviation from Bragg energy

Angular deviation from Bragg angle

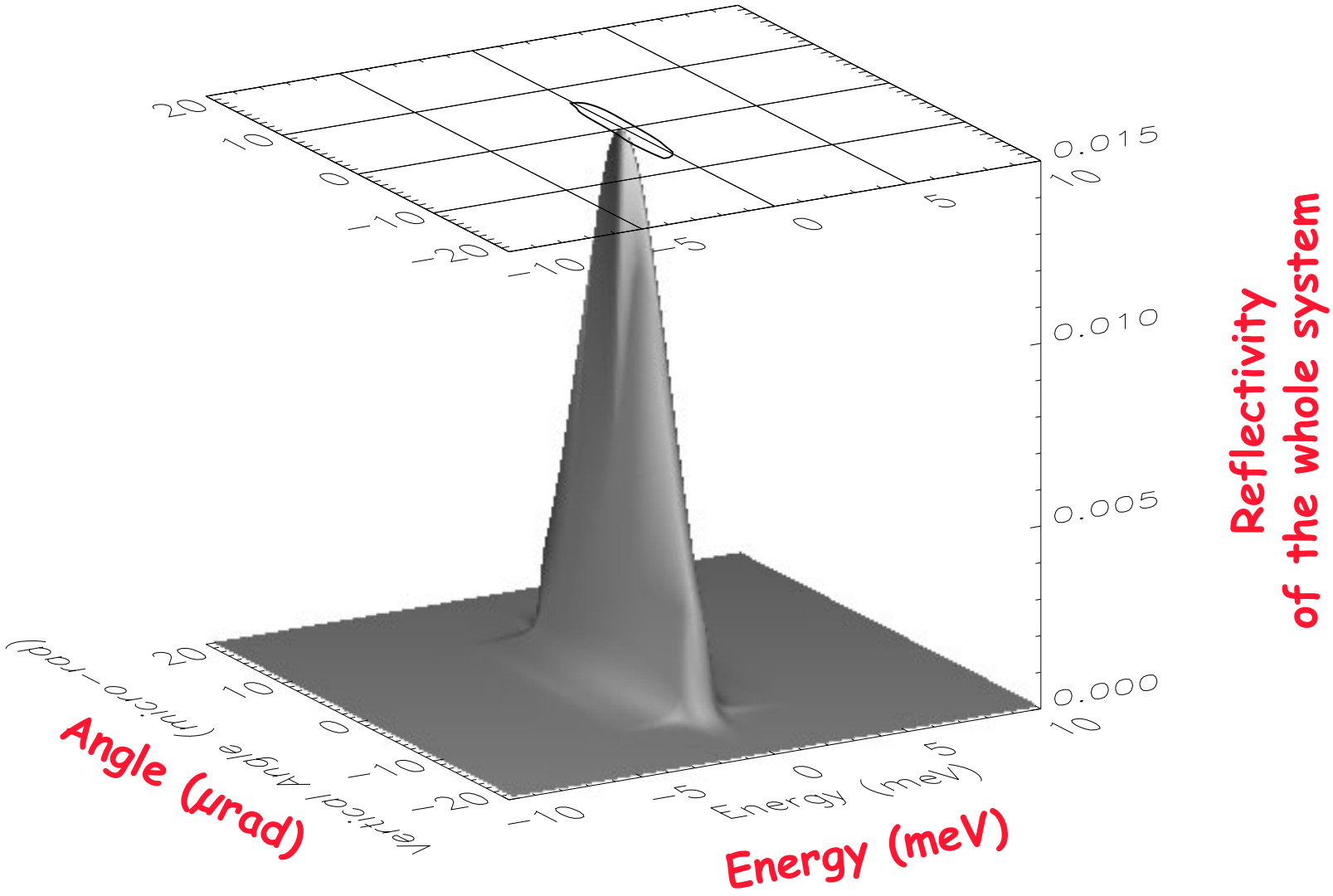
20
10
0
−10
−20
−10
−5
0
5
Vertical Angle (micro−rad)
Angle (μrad)
Energy (meV)
0.015
0.010
0.005
0.000
Reflectivity
of the whole system

Si (800), 4 crystal set for 9.4 keV

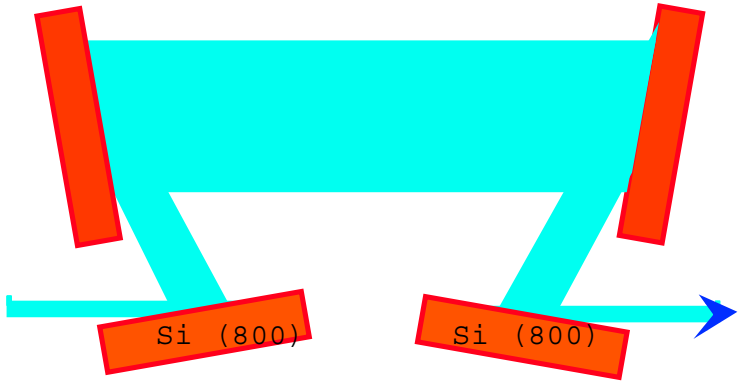

ΔE = 0.97 meV,
$\Delta\Theta$=32 μrad

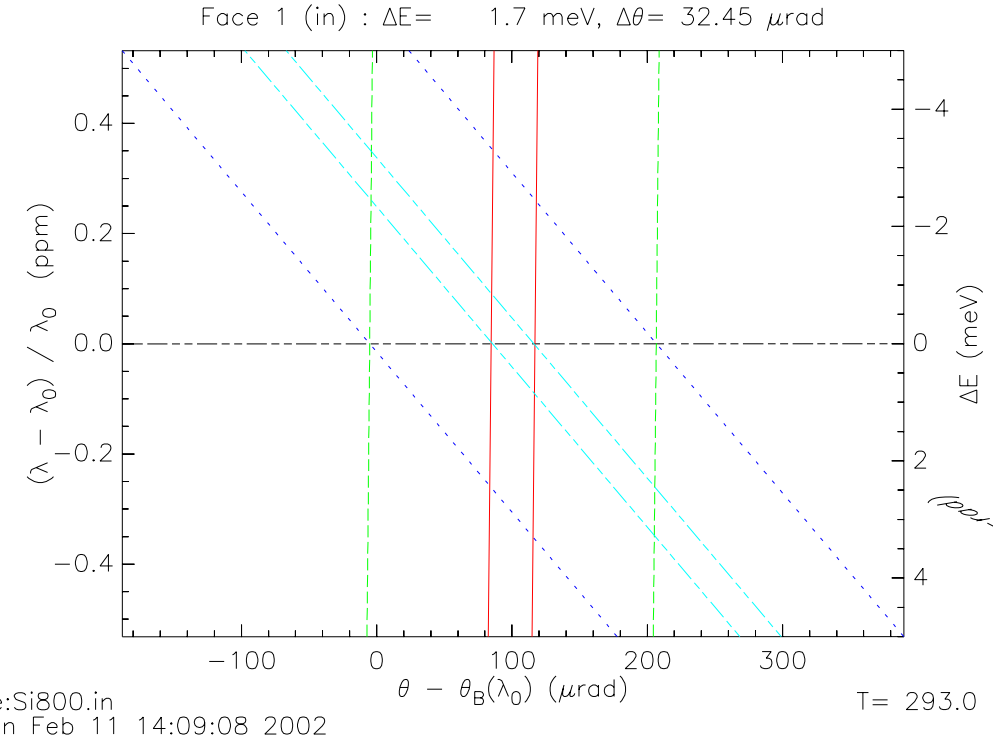

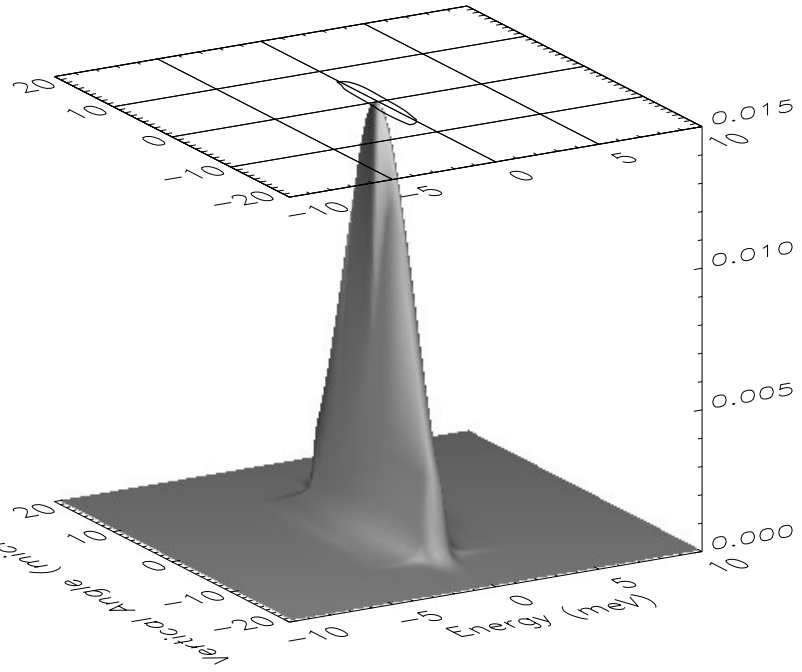

New monochromators with artificially linked, dispersive channel-cut configuration

^{83}Kr, E= 9.401 keV, ΔE= 1.0 meV

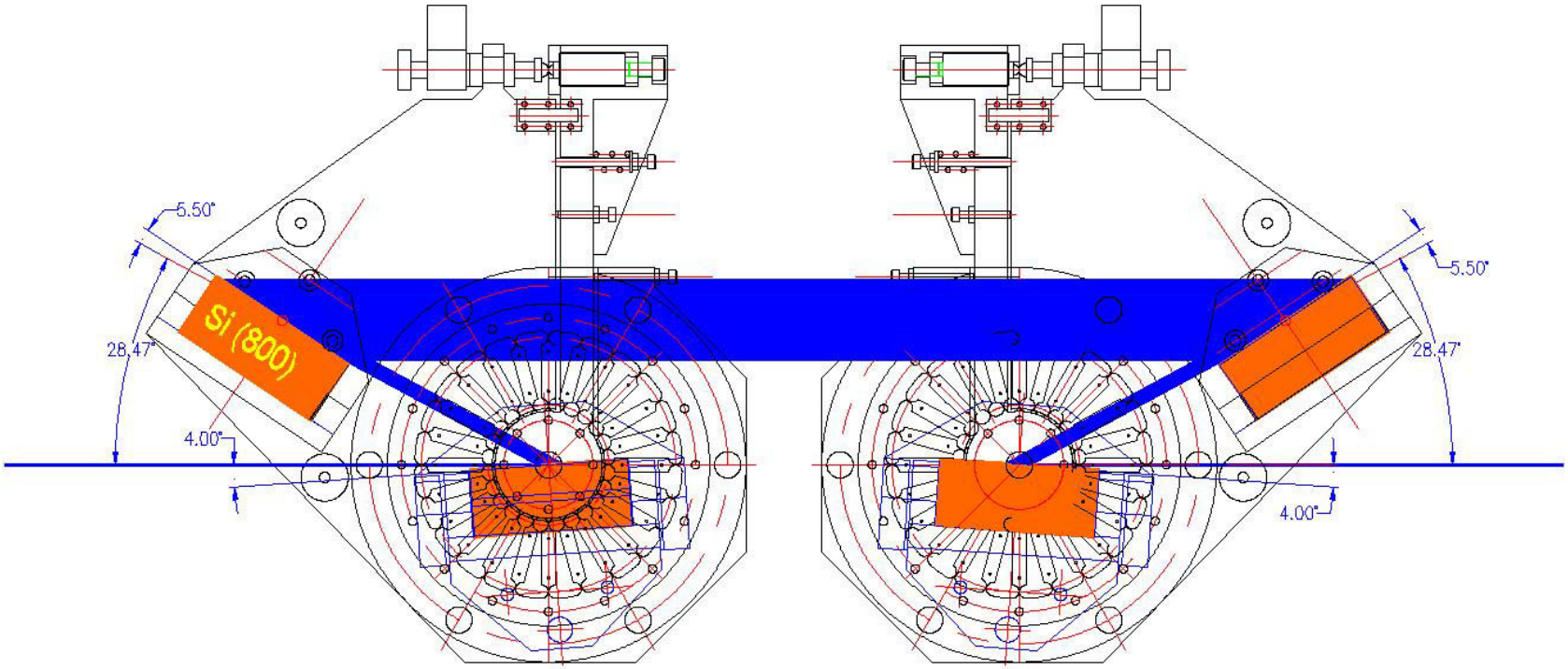

sub-meV mono's between 9-30 keV

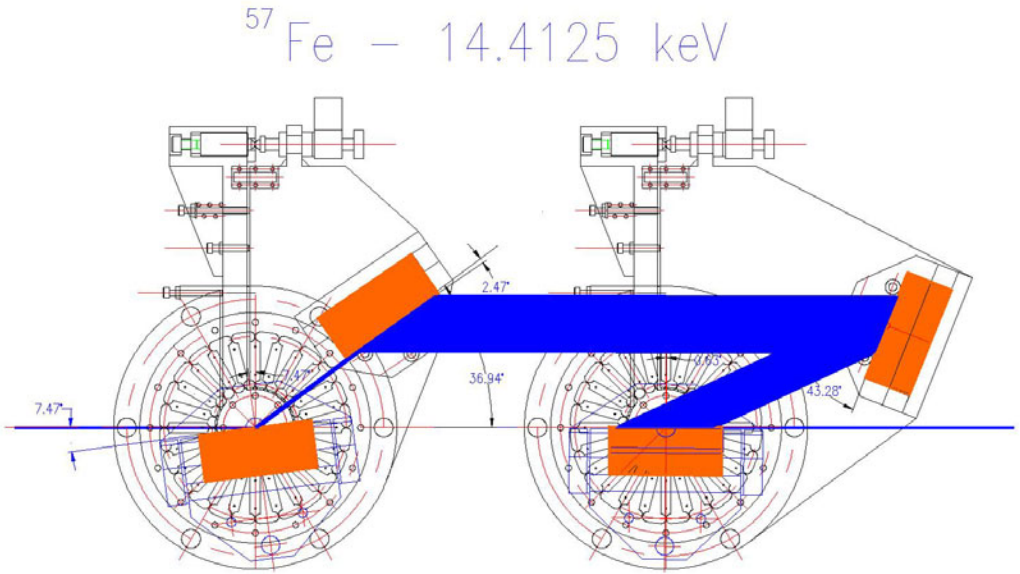

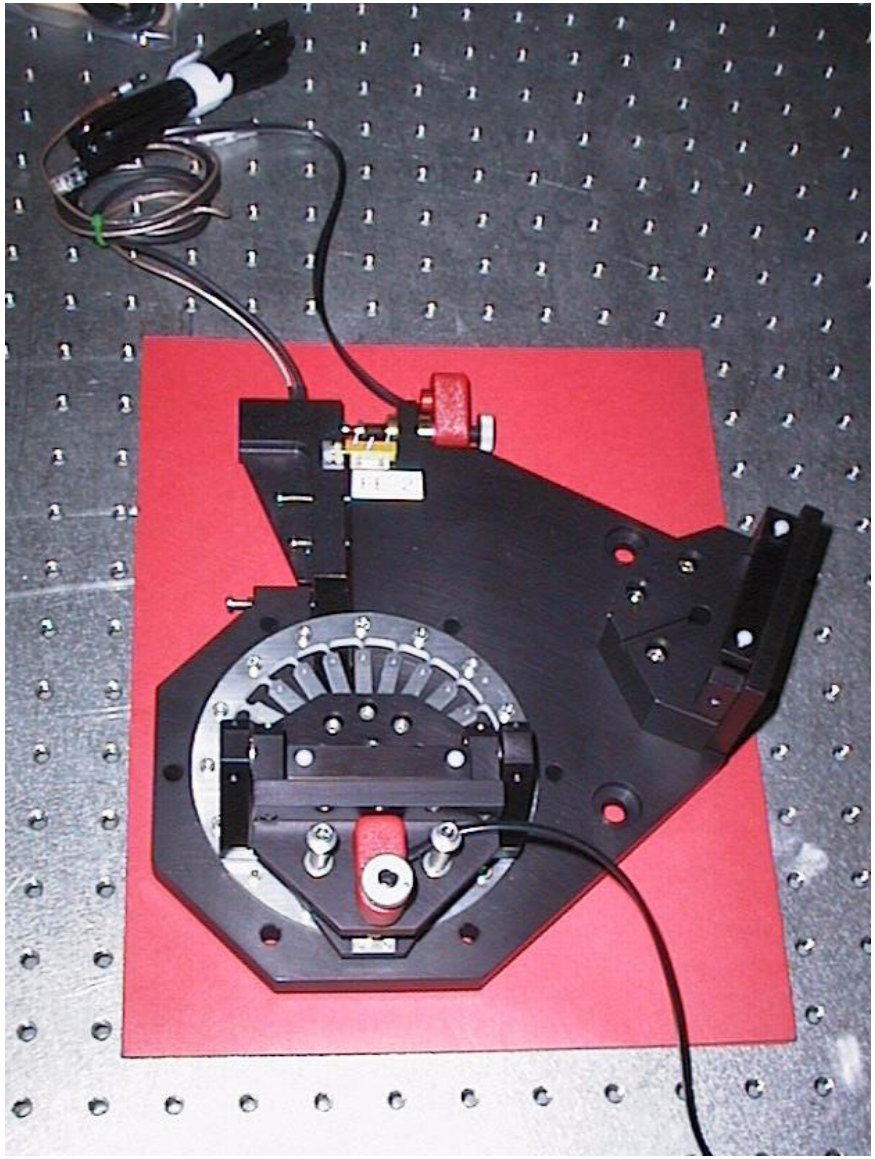

^{57}Fe , E= 14.4126 keV, ΔE=1.1 meV

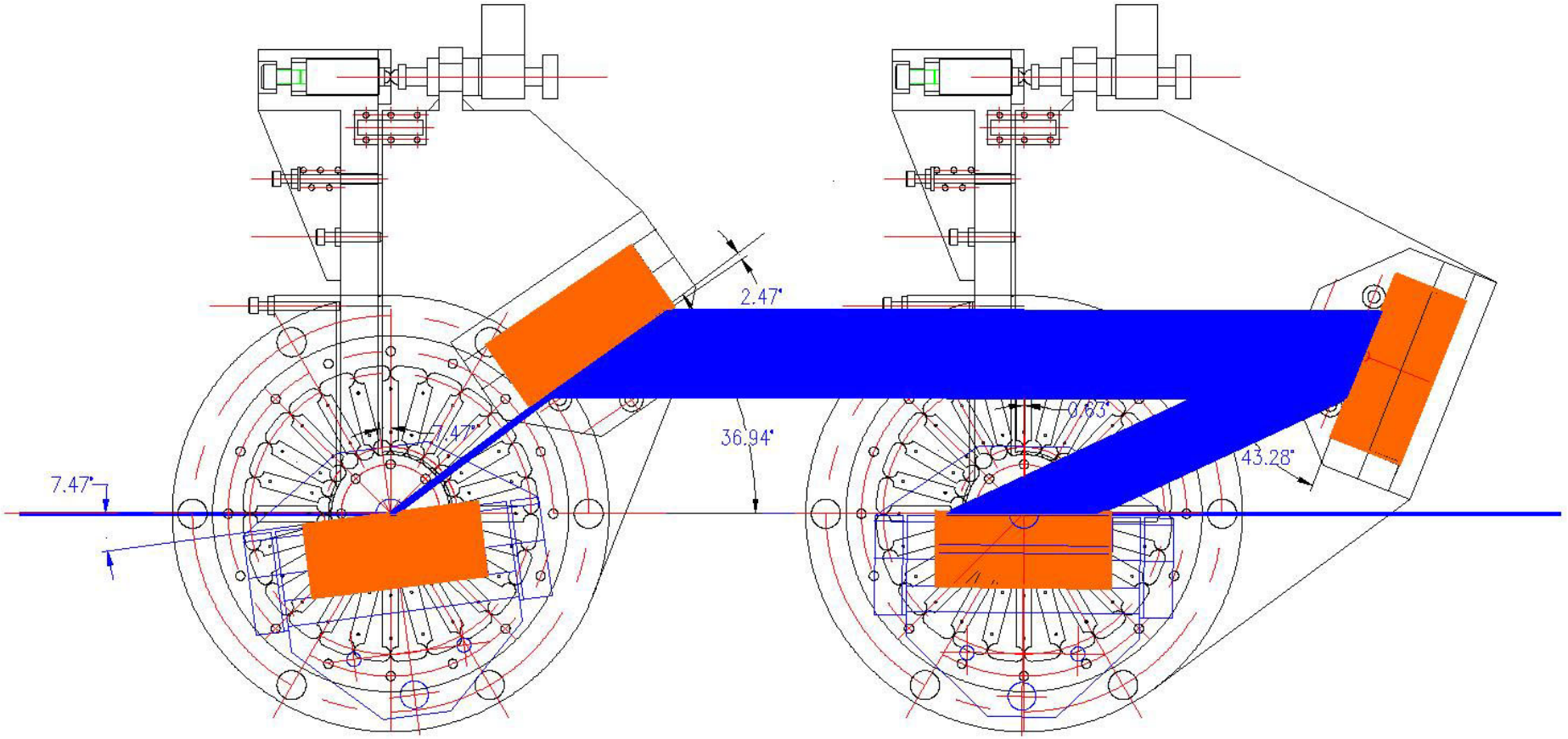

Artificially linked nested mono's

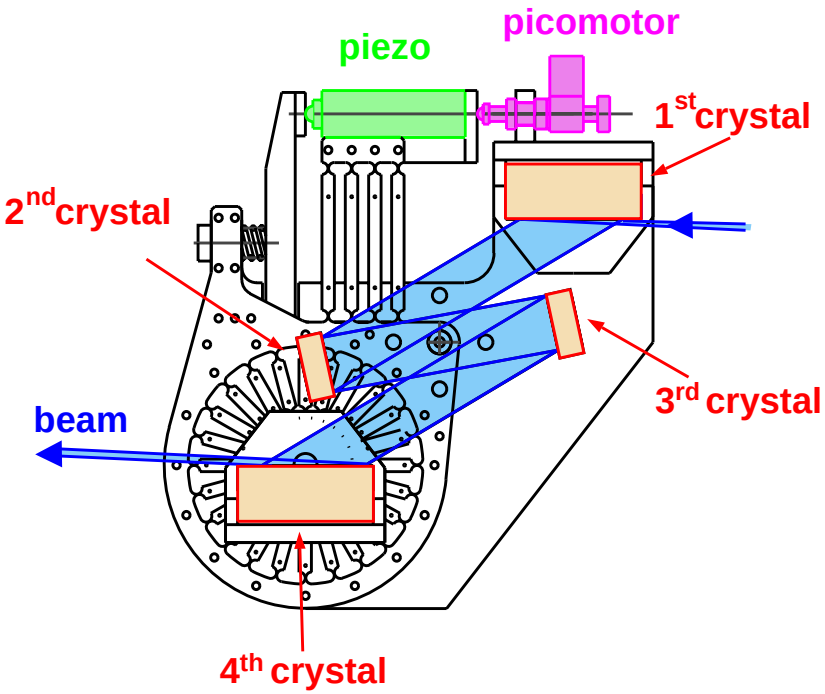

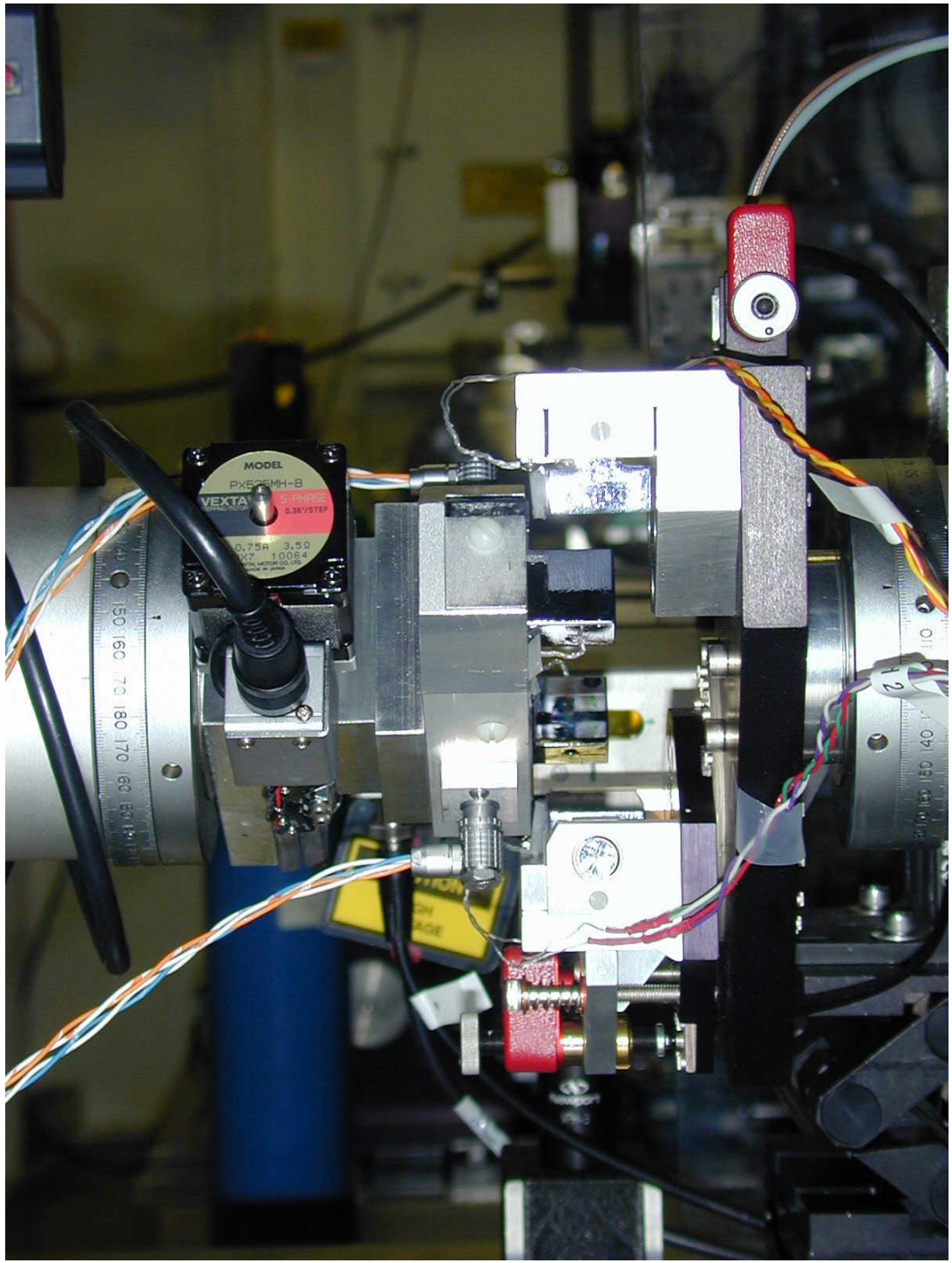

3-ID-B
APS

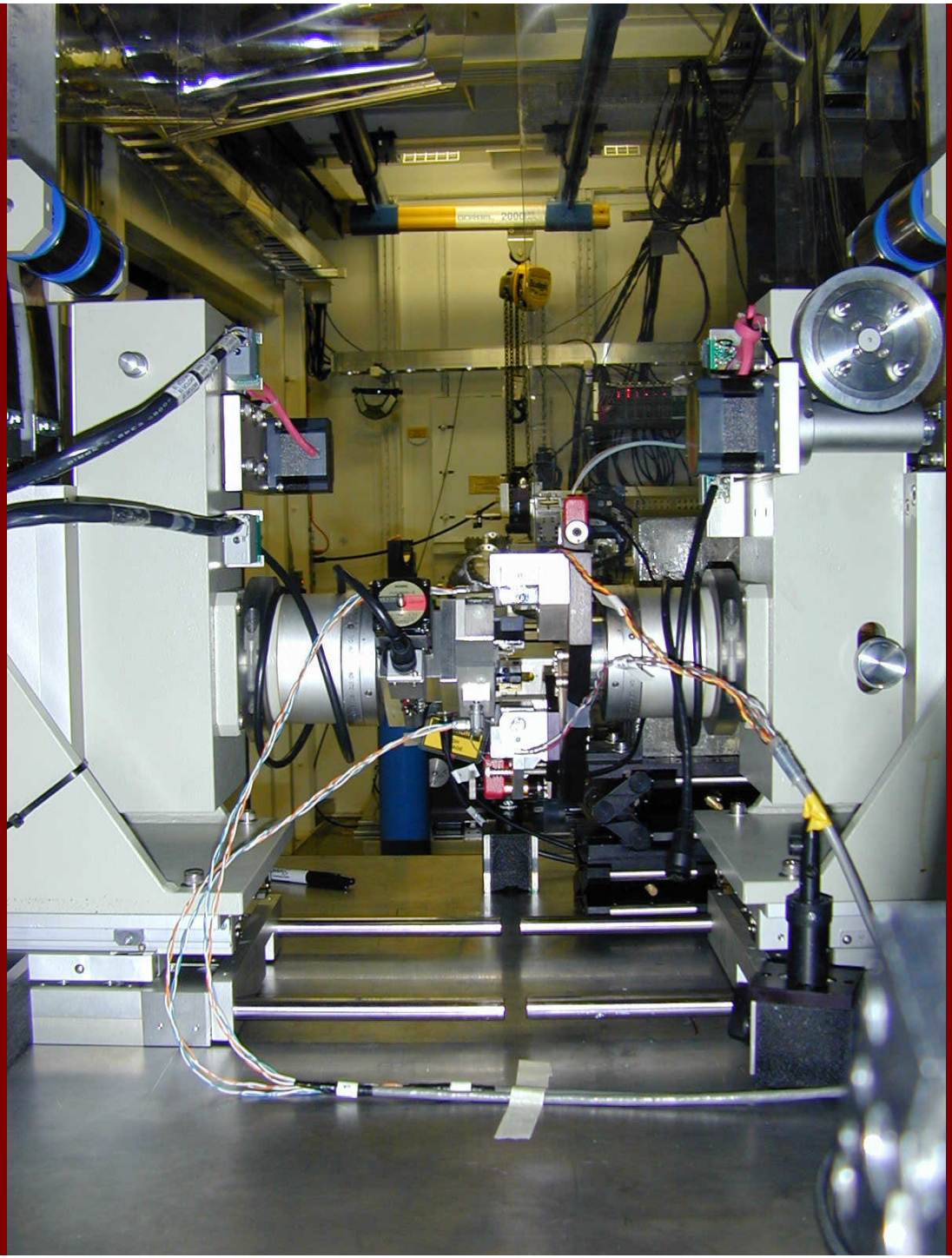

Advances in high energy resolution monochromators in the new century at the APS , 3-ID beamline

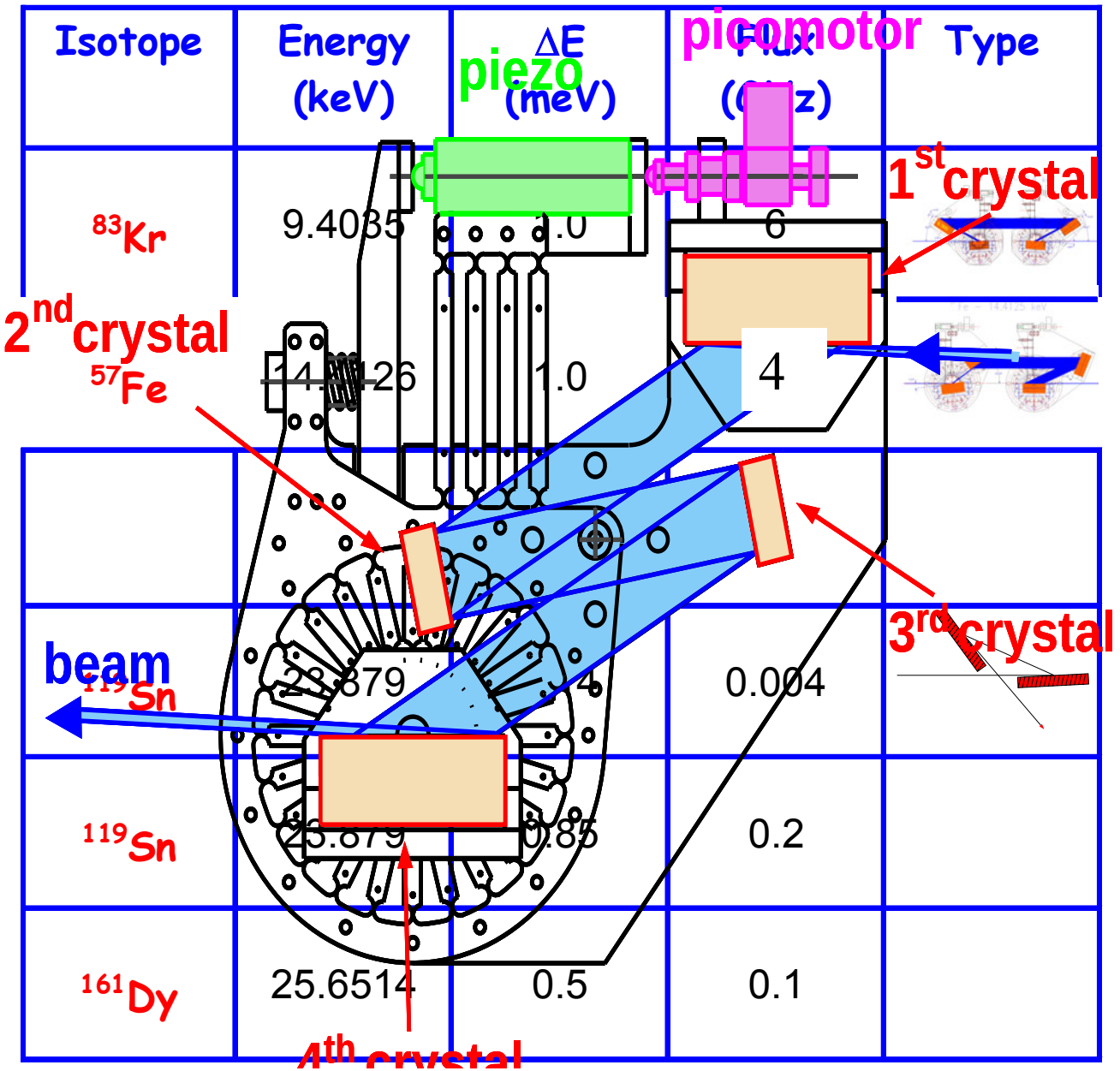

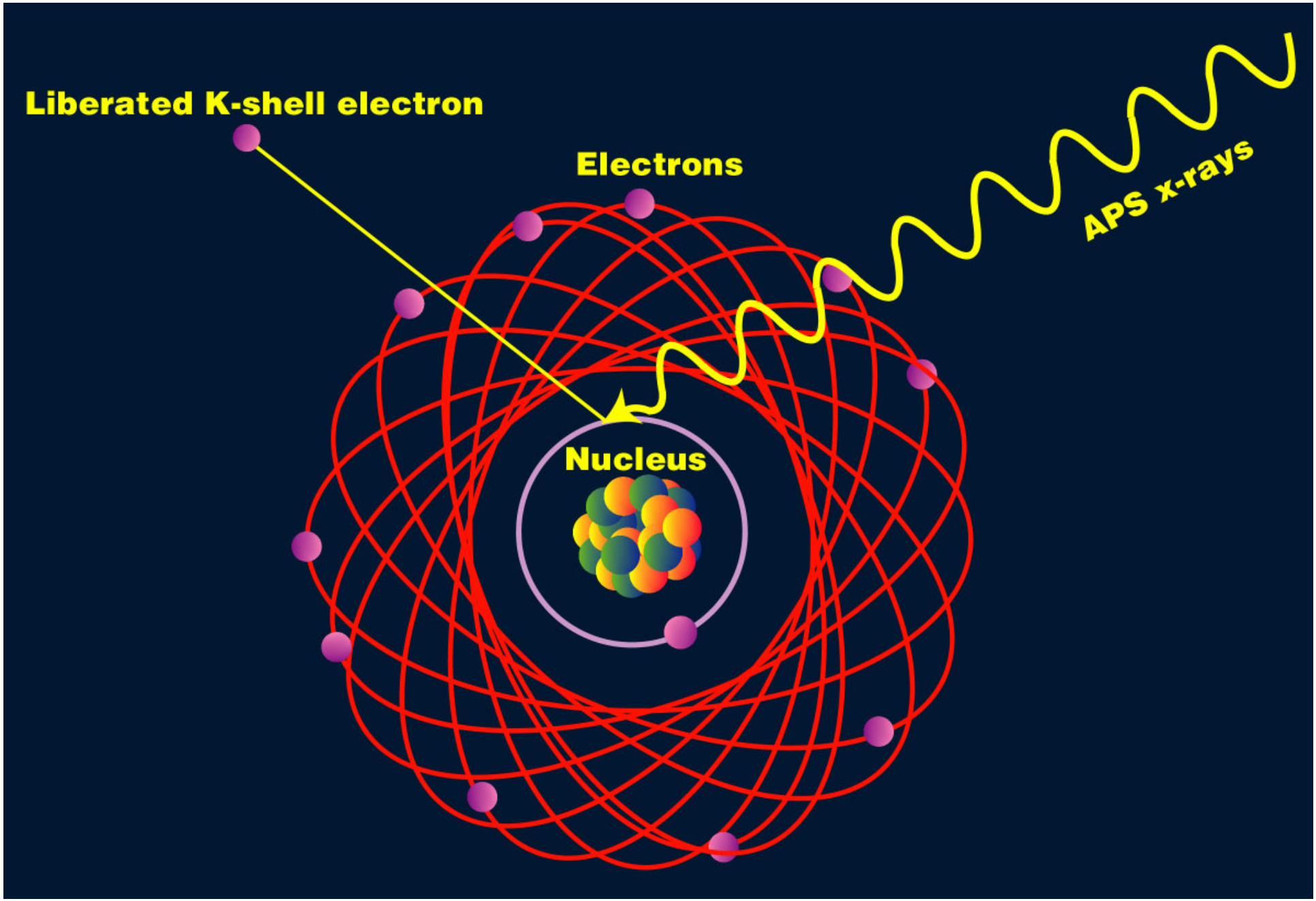
Liberated K-shell electron
Electrons
APS x-rays
Nucleus

Nuclear Resonance and Fallout in ^{57}Fe-decay

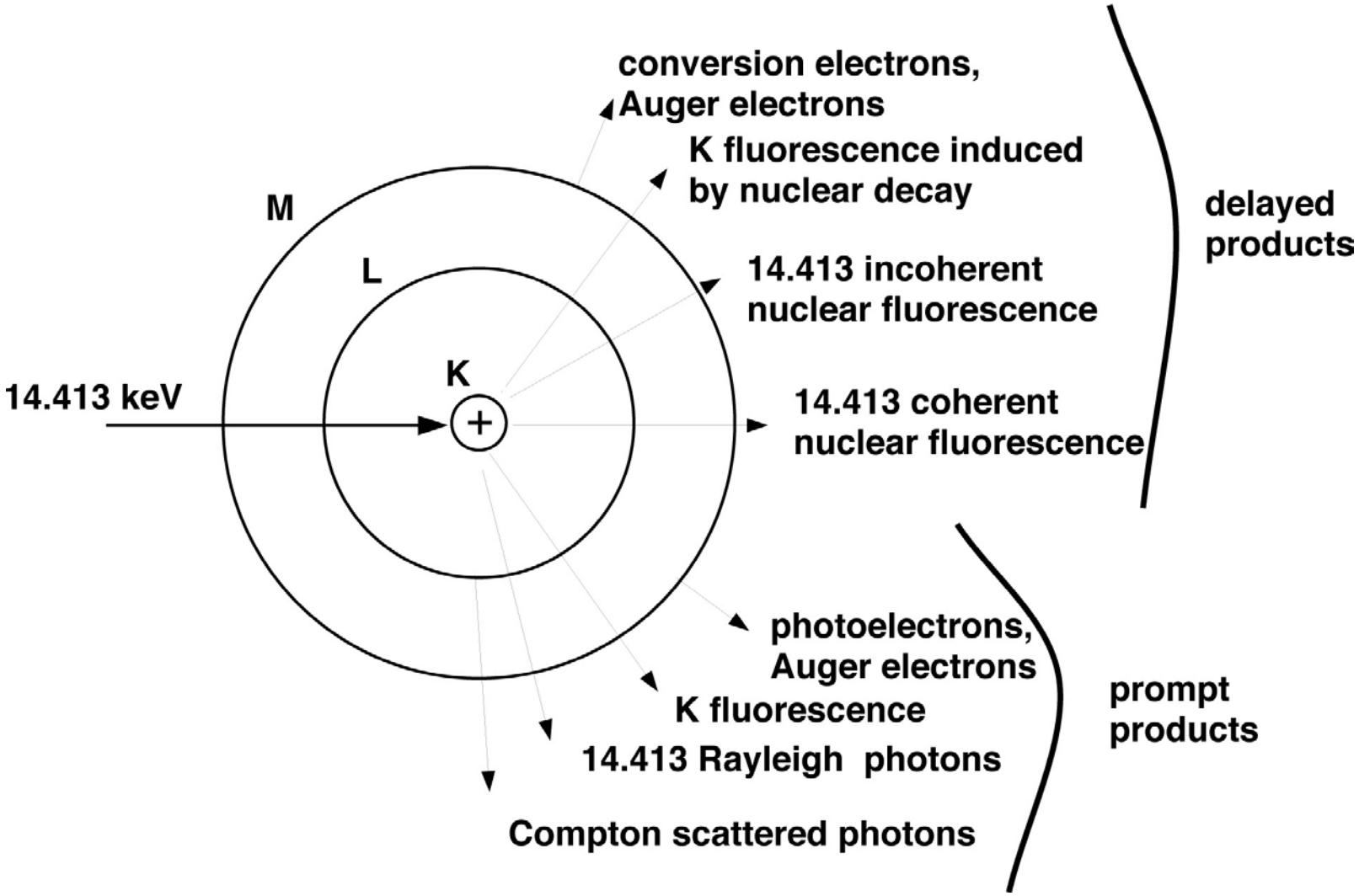

NR-IXS set-up

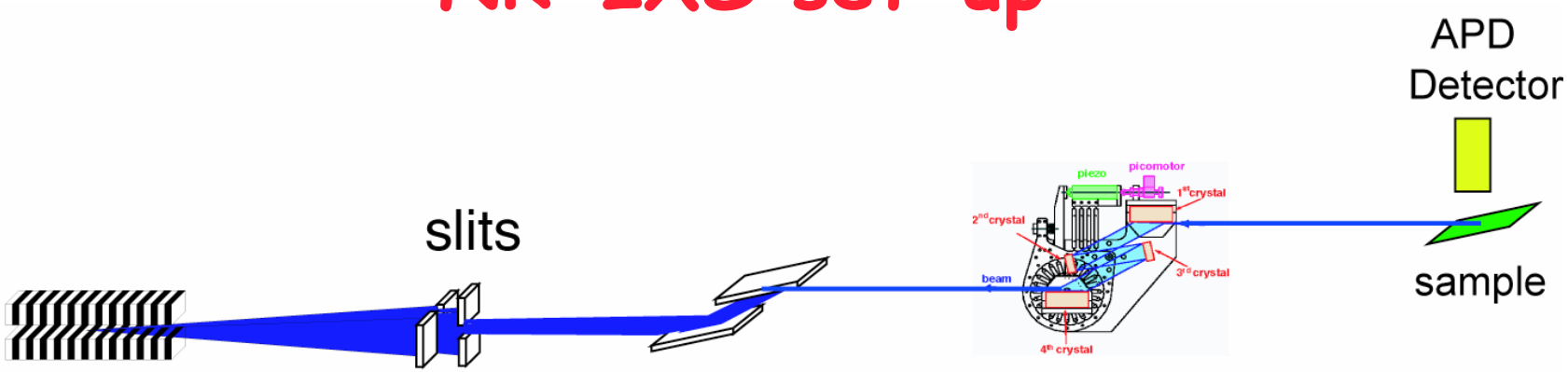

undulator

C (111), first monochromator.

high resolution monochromator

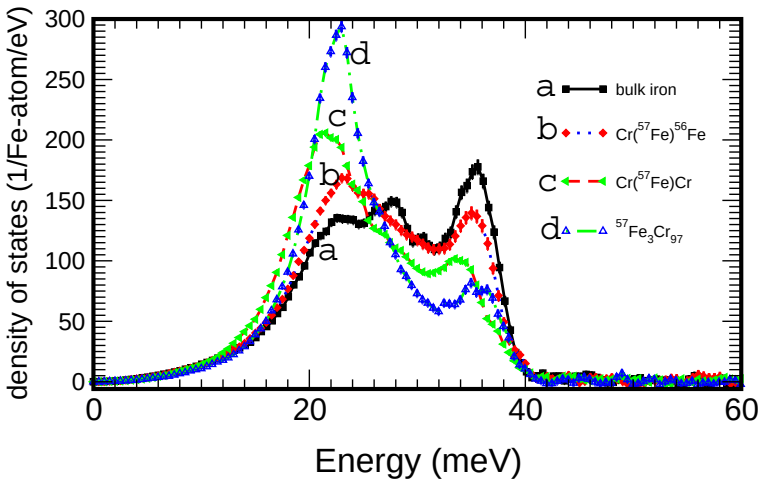

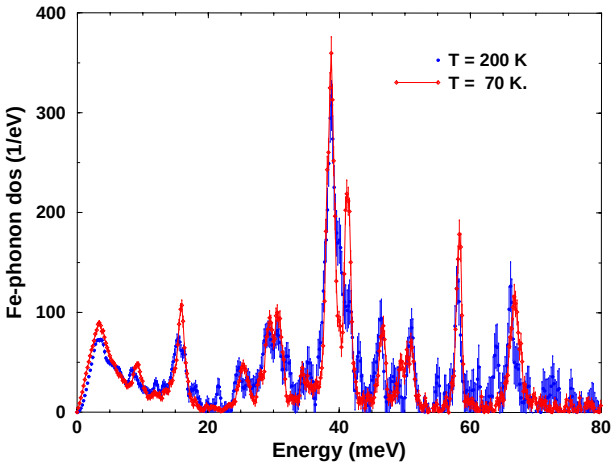

Time structure at APS (ca. 2002)

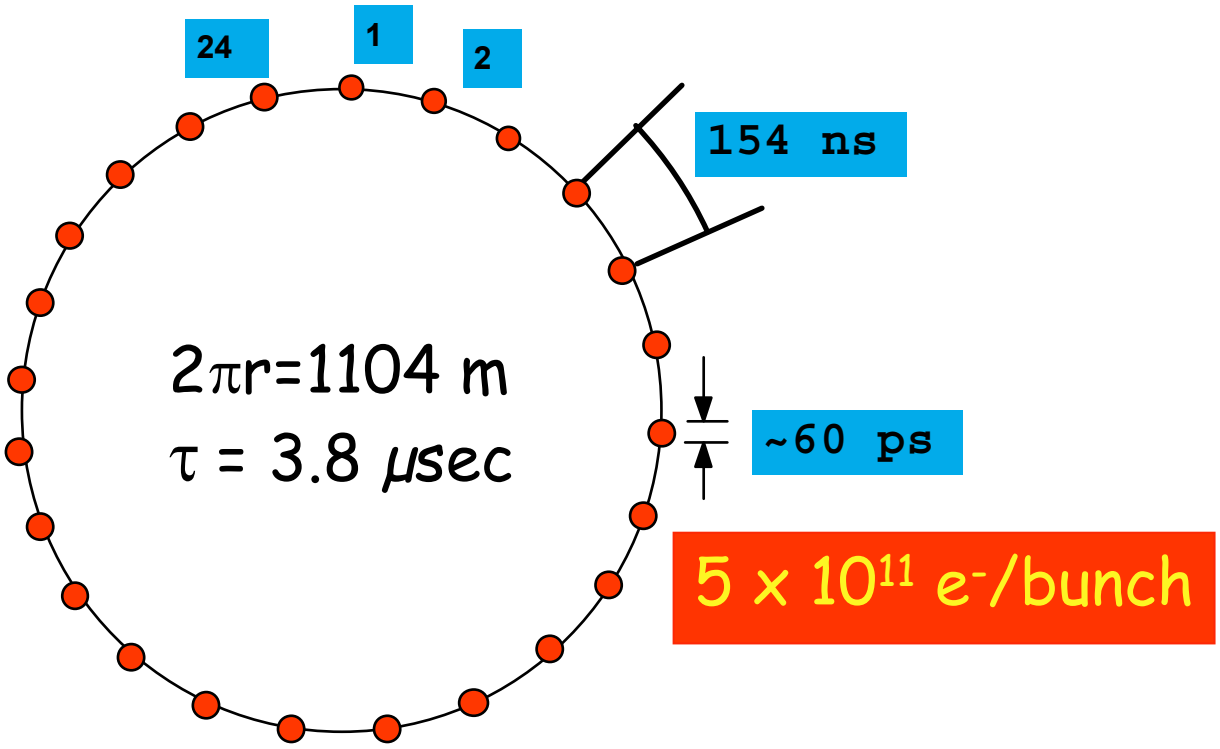

Detection of nuclear decay

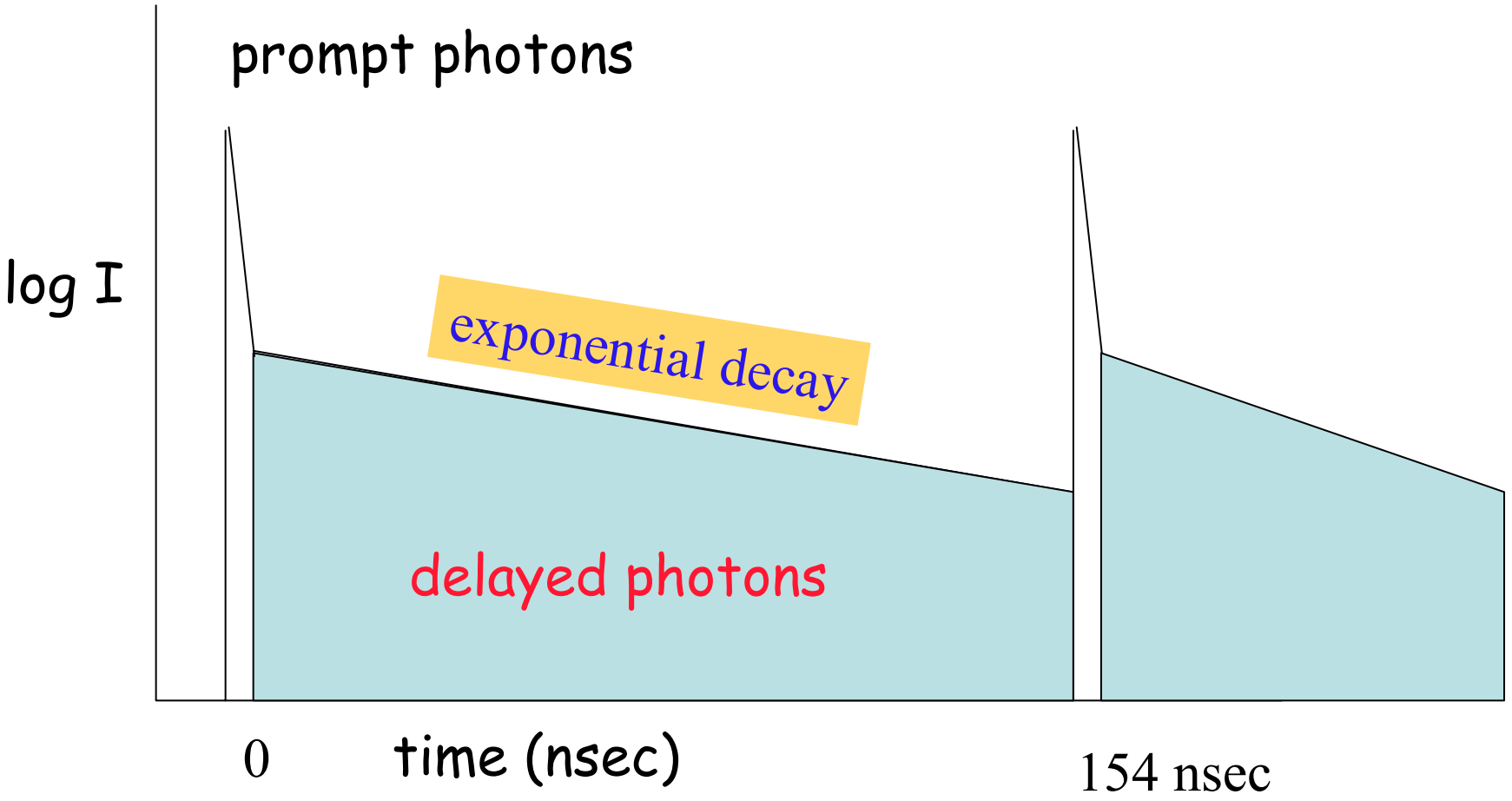

Bunch purity at the APS (2002)

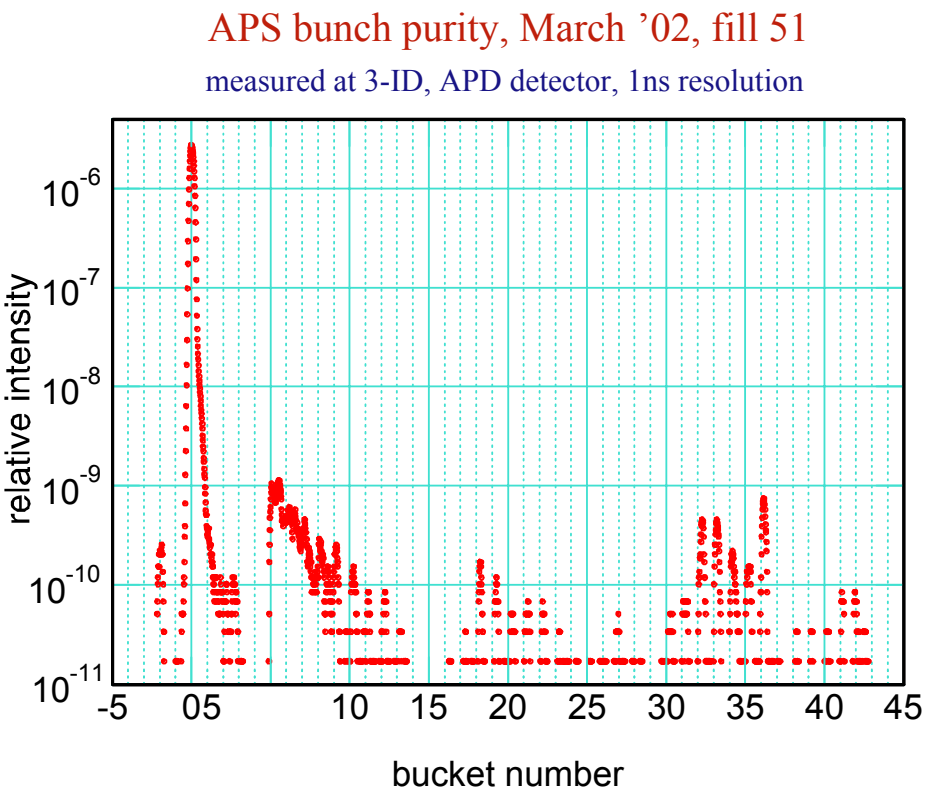

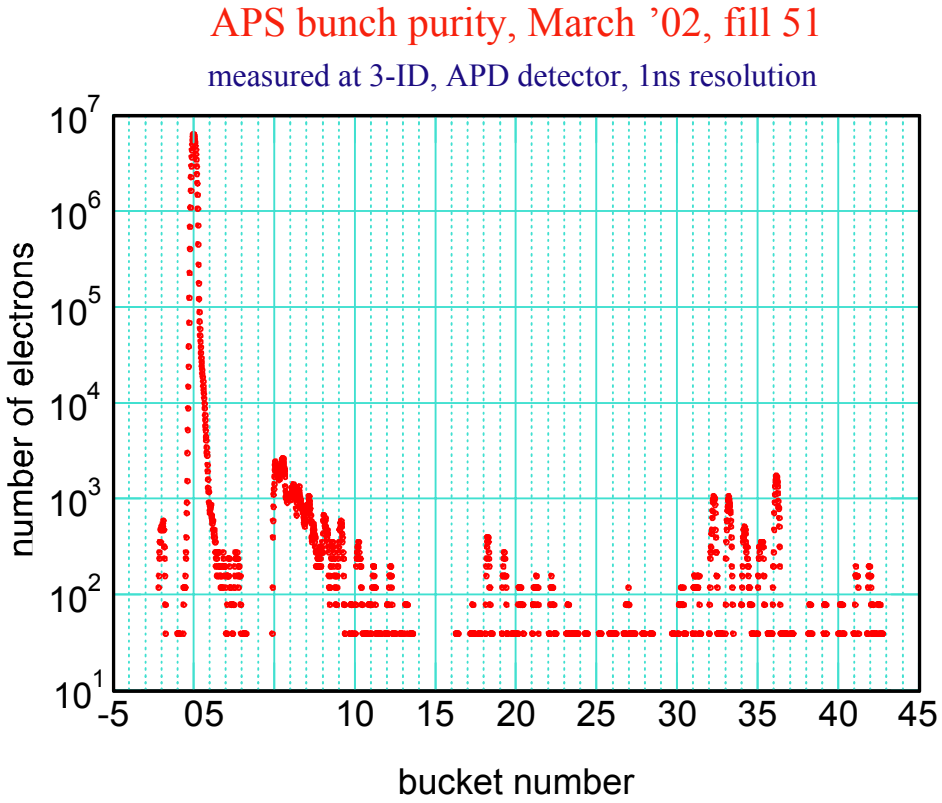

NR-IXS: What do we learn ?

Applications in biology, geology, and materials science to measure thermodynamic, magnetic and elastic parameters are derived from the fundamental phonon properties.

phonon density of state
specific heat
average force constant
vibrational entropy
Debye temperature

velocity of sound
mean displacement
bulk and shear moduli
magnetic phase transitions
Grüneisen constant

Classical thermodynamical quantities and phonon density of states

In the Harmonic Approximation (i.e. interatomic forces are linear in atomic displacement) the thermodynamic functions are additive functions of the normal mode frequencies. Thus, they are expressible as averages over frequency distribution function, **g**(ω), or phonon density of states.

1.Helmholtz Free Energy

$$F_V = 3RNk_BT\int \ln\left\{2\sinh\left(\frac{\hbar\omega}{k_BT}\right)\right\} \mathrm{g}(\omega)\mathrm{d}\omega$$

2.Vibrational Energy

$$F_V = 3RN\frac{\hbar}{2}\int \ln\left\{\coth\left(\frac{\hbar\omega}{k_BT}\right)\right\} \omega\cdot \mathrm{g}(\omega)\mathrm{d}\omega$$

3. Specific heat

$$C_{\mathrm{P}} = 3RNk_B\int\left(\frac{\hbar\omega}{2k_BT}\right)^2 \mathrm{csch}\left(\frac{\hbar\omega}{k_BT}\right) \mathrm{g}(\omega)\mathrm{d}\omega$$

4.Entropy

$$\mathrm{S} = 3RNk_B\int\left\{\left(\frac{\hbar\omega}{2k_BT}\right)\coth\left(\frac{\hbar\omega}{k_BT}\right) - \ln\left[2\sinh\left(\frac{\hbar\omega}{k_BT}\right)\right]\right\}\mathrm{g}(\omega)\mathrm{d}\omega$$

NR-IXS studies on Proteins and Model Compounds

Collaborations

S. Durbin, T. Sage, B. Rai, G. Wyllie, R. Scheidt, E. Prohofsy

Purdue University
Northeastern University
University of Notre Dame

K. Achterhold, F. Parak, U. van Bürck, W. Potzel

Technische Universität München

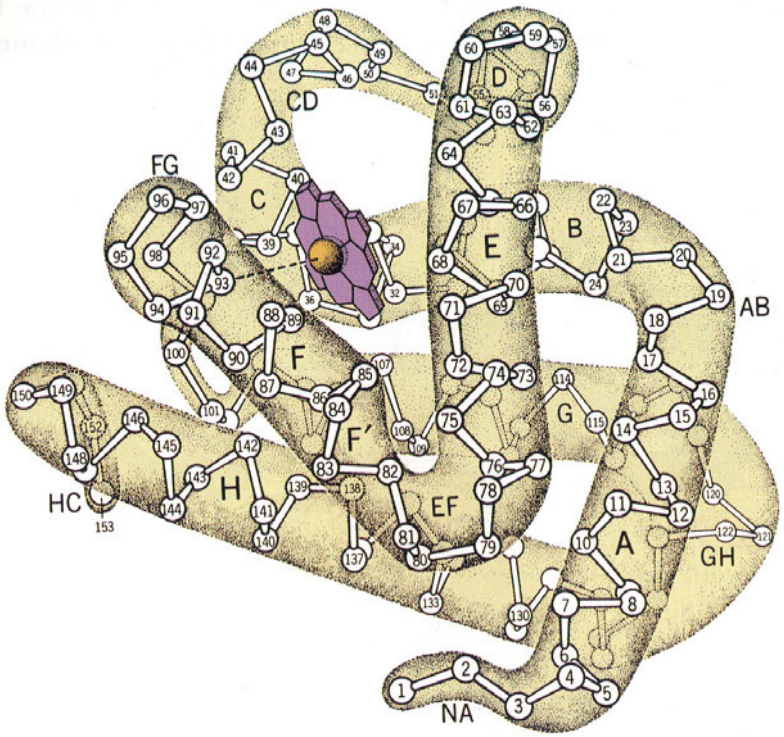

Myoglobin

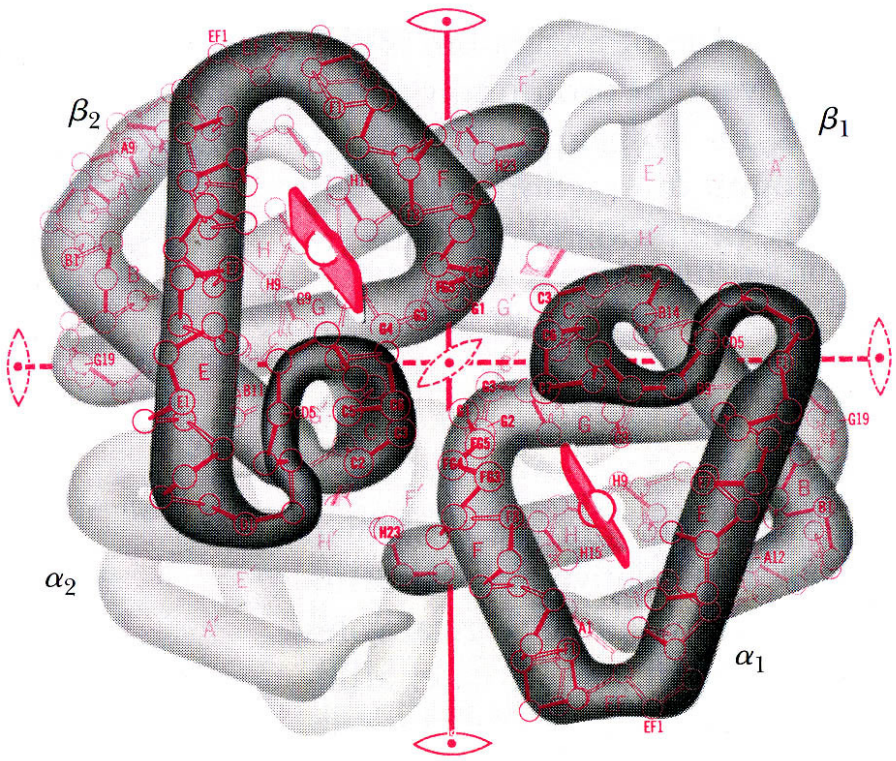

Hemoglobin

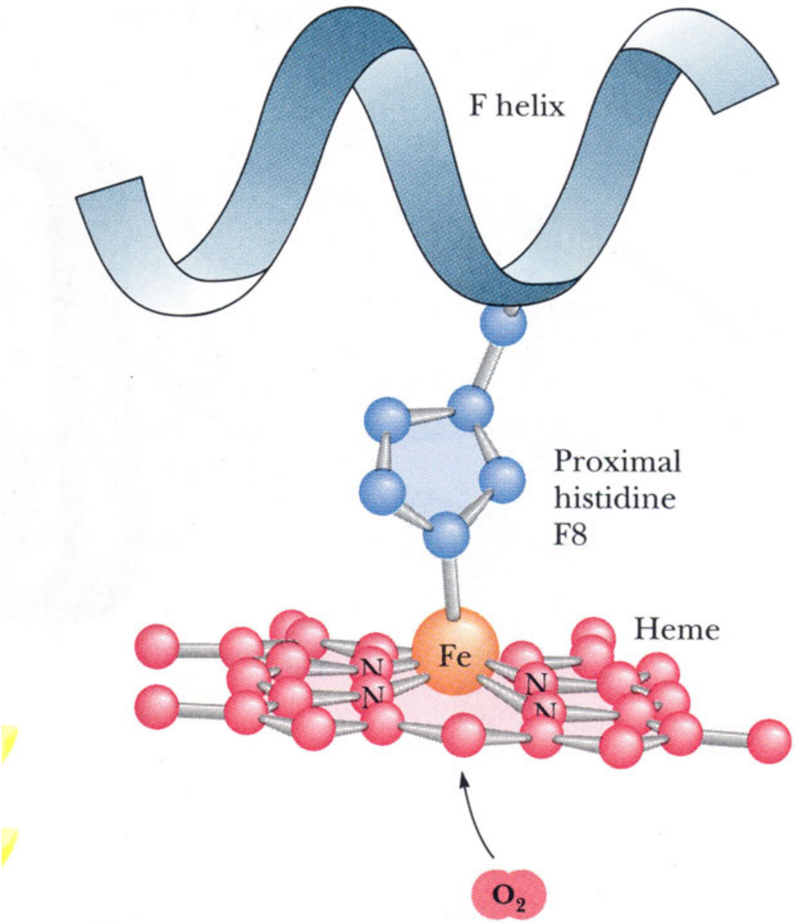

Binding of the heme to the protein

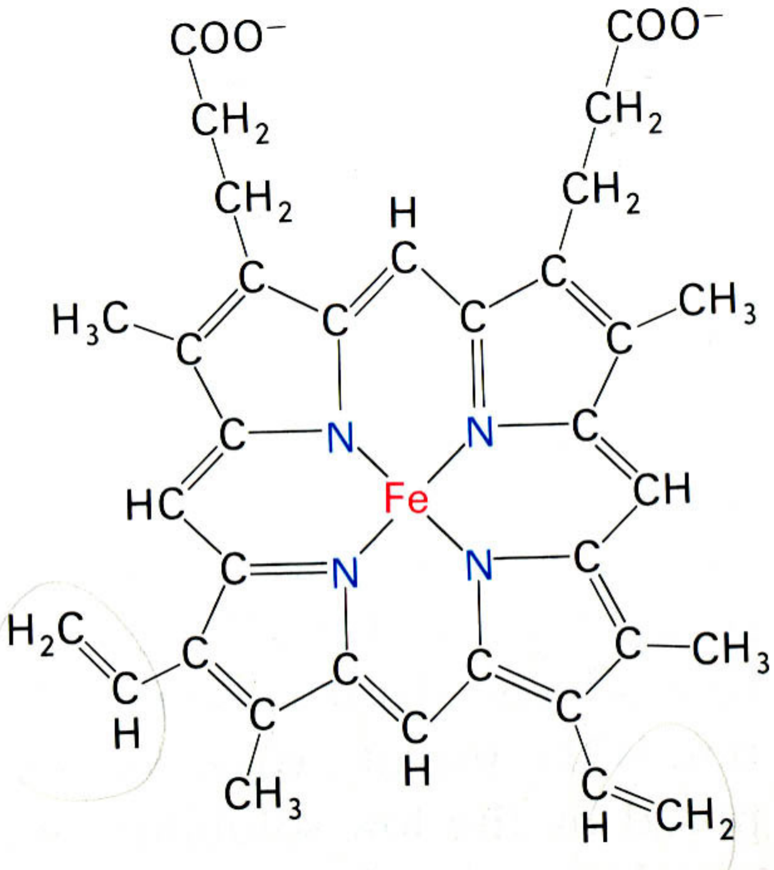

Heme
(Fe–protoporphyrin IX)

The heme molecule

Upon binding a ligand, Fe is pulled into the heme plane, putting a stress on the bond to the protein.

In response, the protein changes conformation, altering the environment of other hemes in Hb.

This simple shift in a single Fe atom plays the central role in the biological functioning of hemoglobin.

How does this couple to protein dynamics?

Polarization of phonon modes in 2-MeHIm-TPP

2-MeHIm-TPPO is a model system for deoxygenated myoglobin

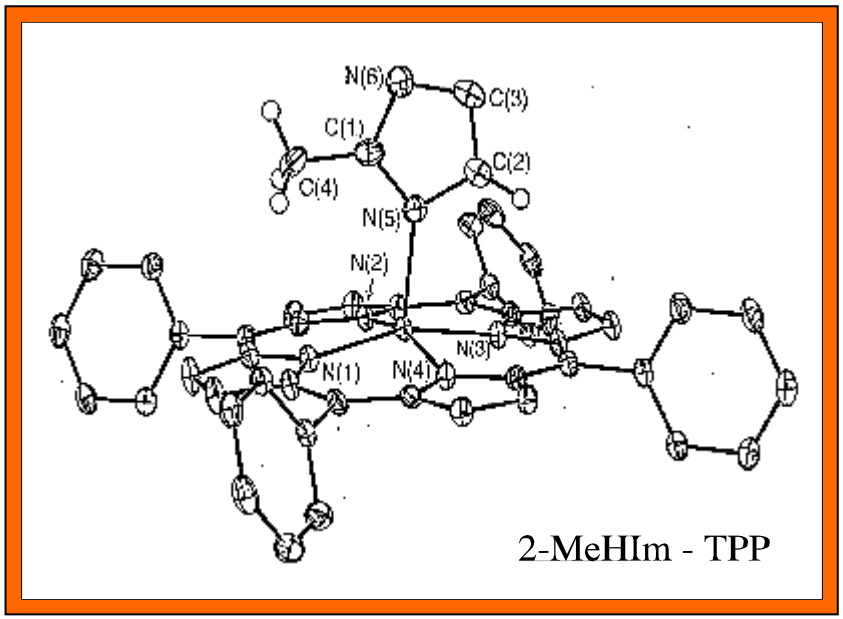

Out-of-plane vibrational modes dominate the low frequency region 7-20 meV.

Single crystal grown by: M.K. Ellison

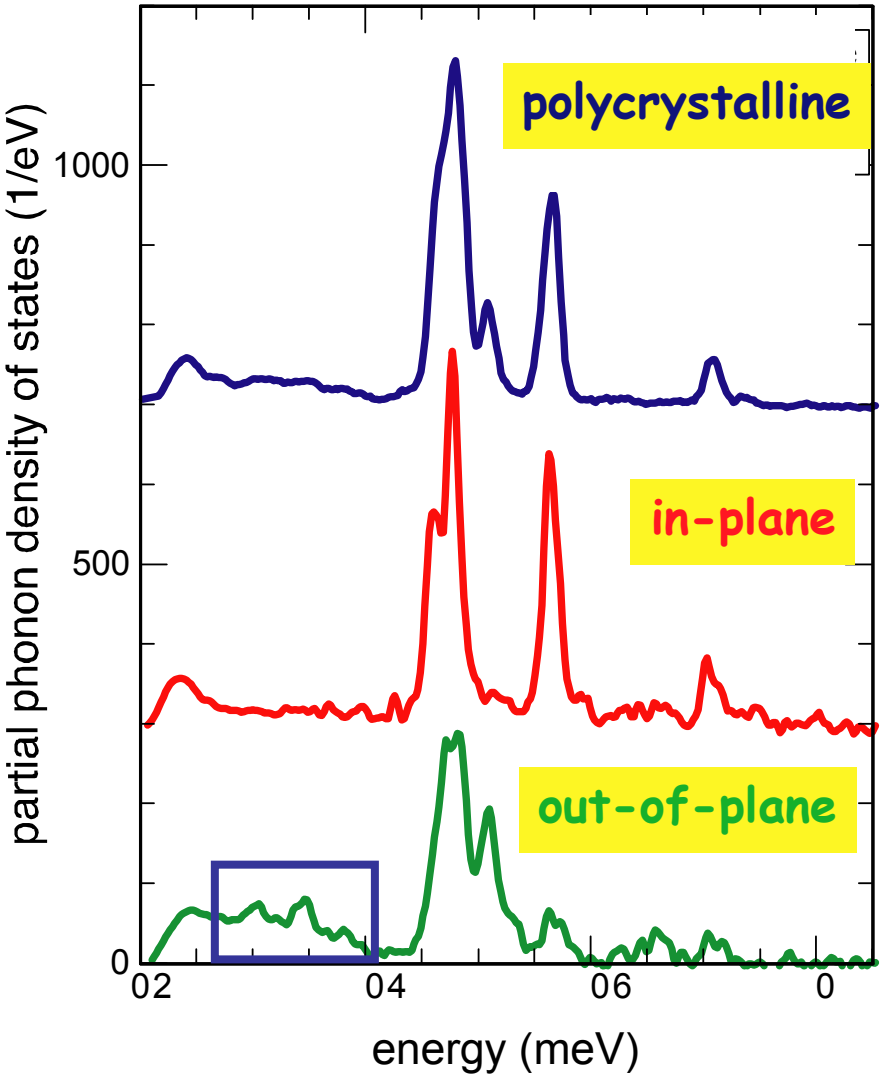

Porphyrin model compounds

J. T. Sage, et al, J. Phys. Cond. Matt, 13 (2001) 7707

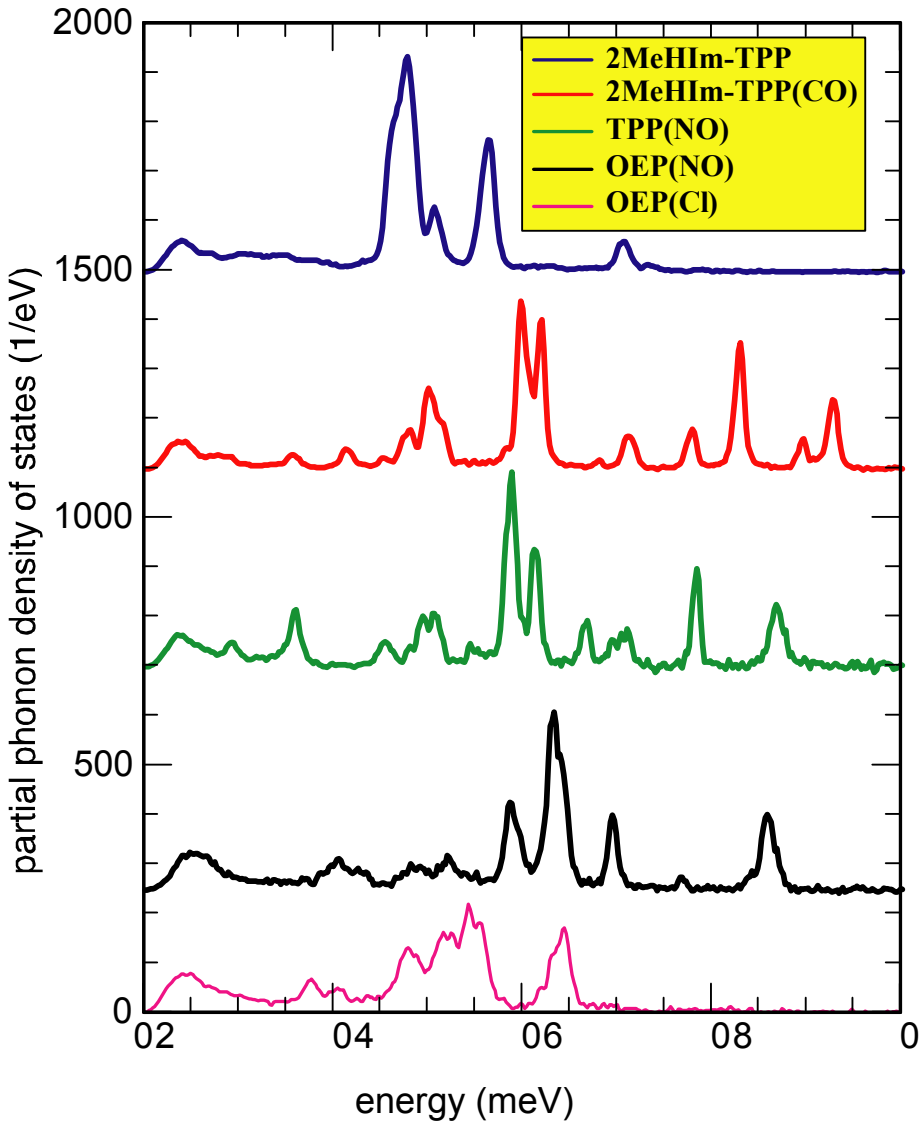

The heme doming coordinate is directly Involved in oxygen-binding reaction.

In proteins, it is important to know whether It acquires a global character.

Doming modes are expected in the range of 6-8 meV.

Porphyrin model compounds mimic the heme group found at the active site of many proteins involved in biological usage of oxygen and nitric oxide.

2MeHIm-TPP: Methyl-Hydrogen-Imidazole tetra phenyl porphyrin

OEP : Octo ethyl porphyrin

TPP : Tetra phenyl porphyrin

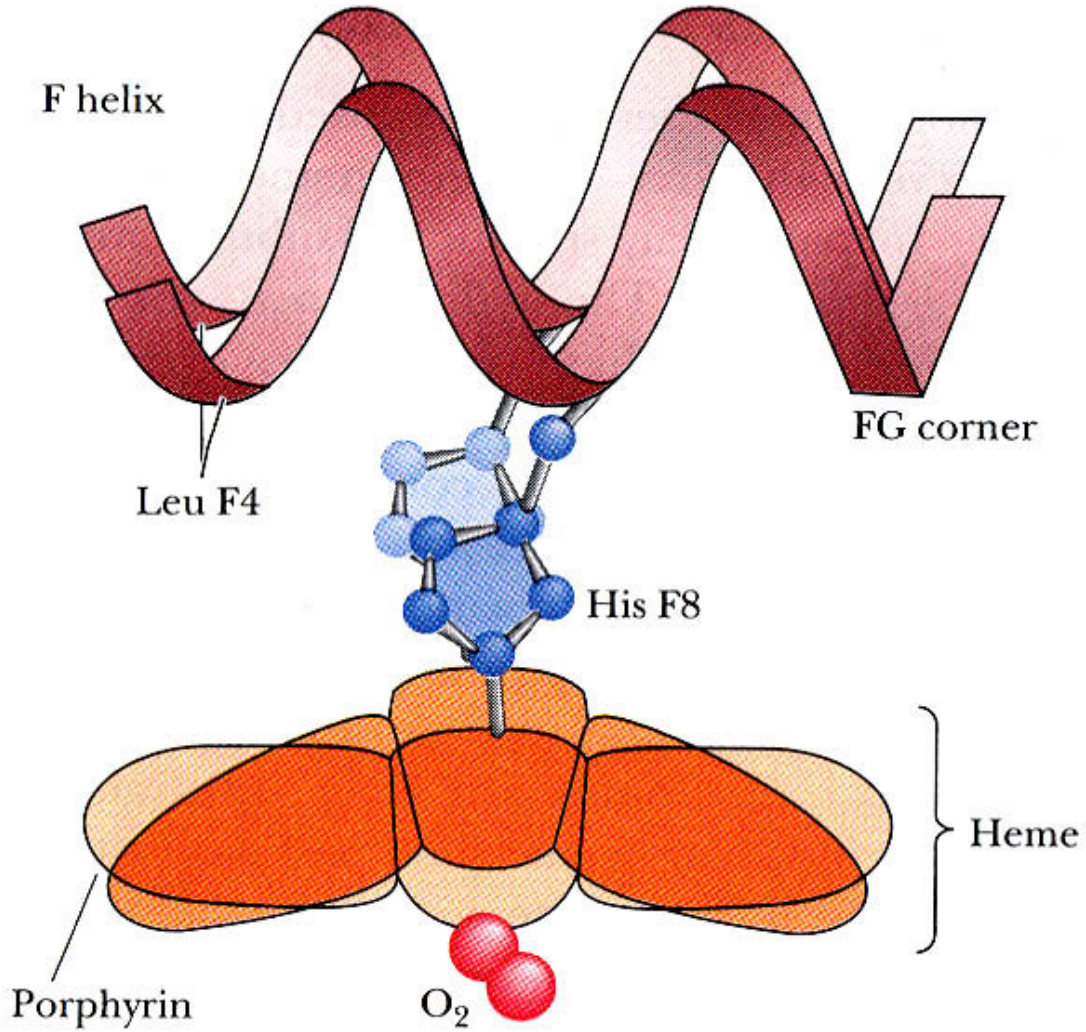

Changes in the position of the heme iron atom upon oxygenation lead to conformational changes in the hemoglobin molecule.

Heme Proteins

Heme proteins are exemplary systems to study the influence of protein dynamics on physiological functions.

Most reactions in proteins take place at the position of the heme group. The access to and reactivity of heme group is influenced by the dynamics of the entire surrounding of the protein structure.

Fe-ligand modes such as Fe-C, Fe-His can be identified.

CO-binding increases the complexity of the vibrational spectrum.

In cytochrome-f, the porphyrin group is more tightly attached to the surrounding protein.

The low energy modes at 5 meV is reduced compared to deoxygenated or carboxylized myoglobin.

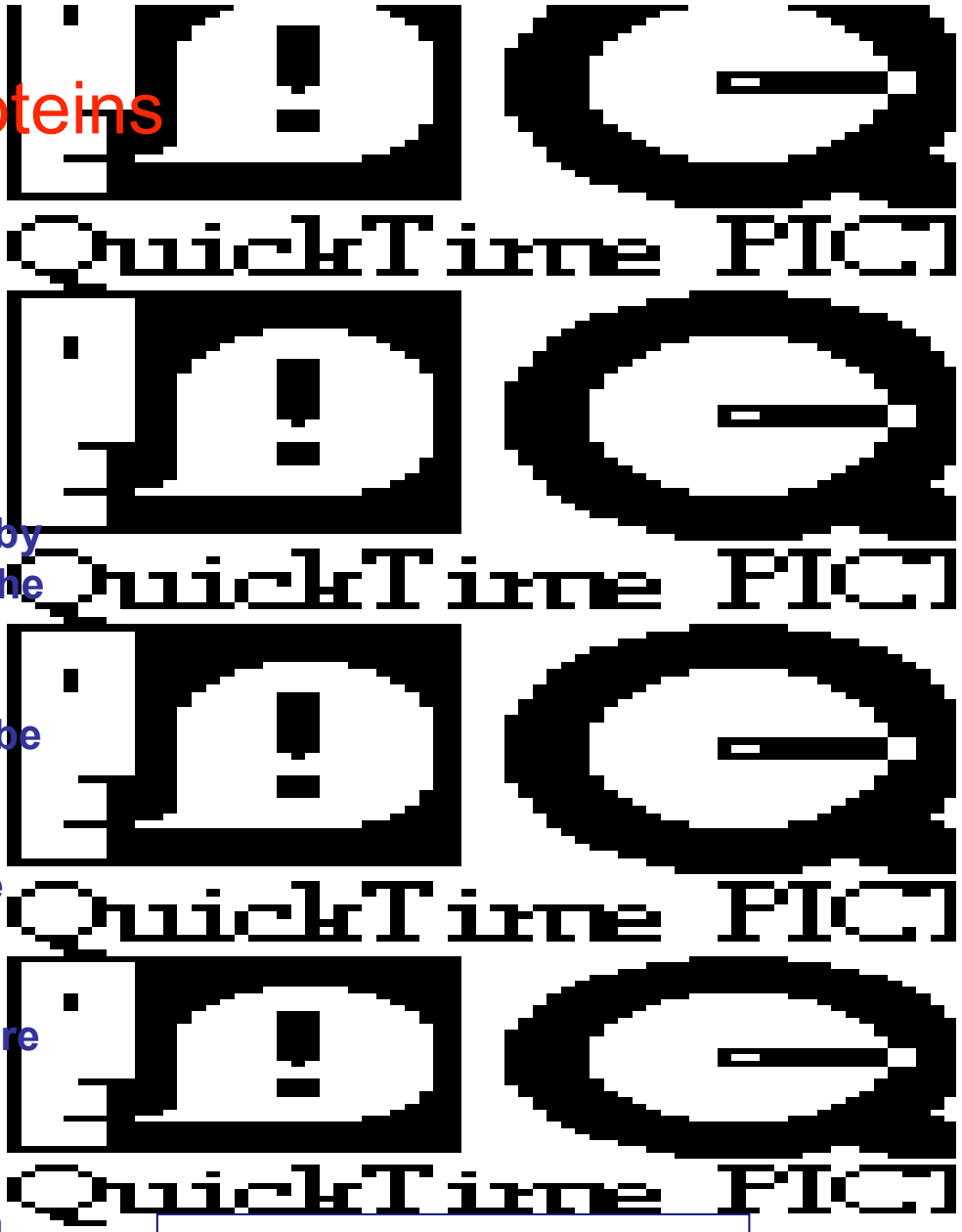

T. Sage, S. Durbin
K. Achterhold, F. Parak

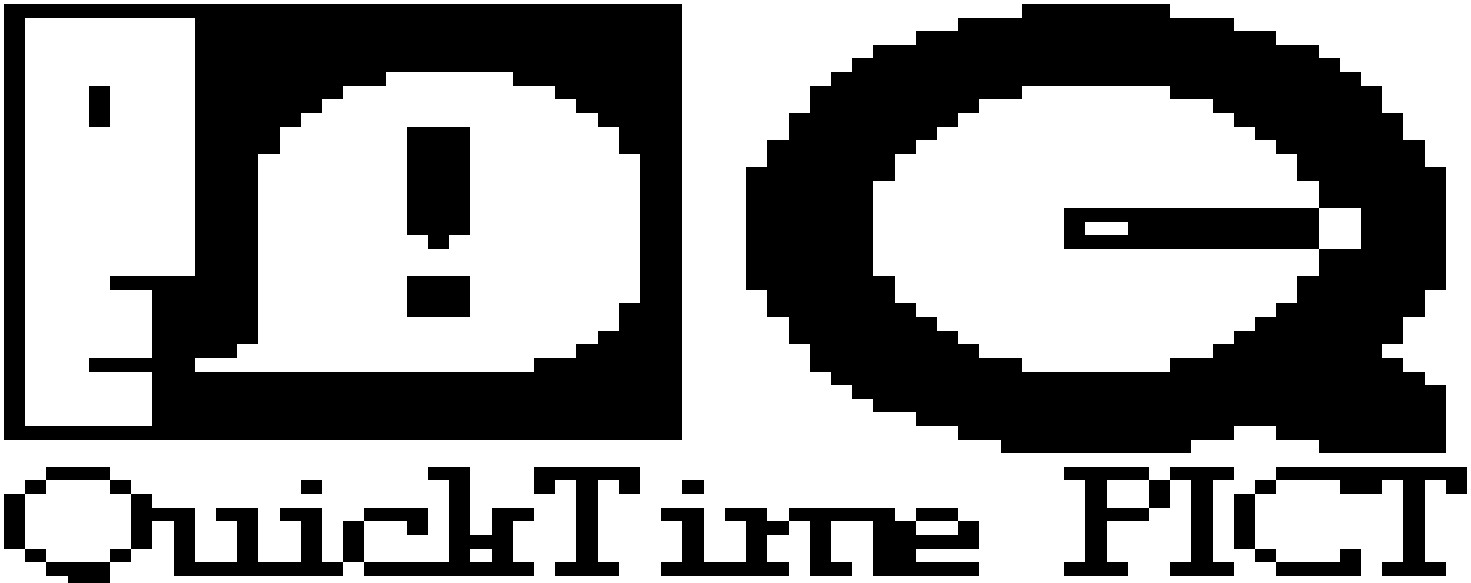
QuickTime PICT


QuickTime PICT

TPPO(NO)

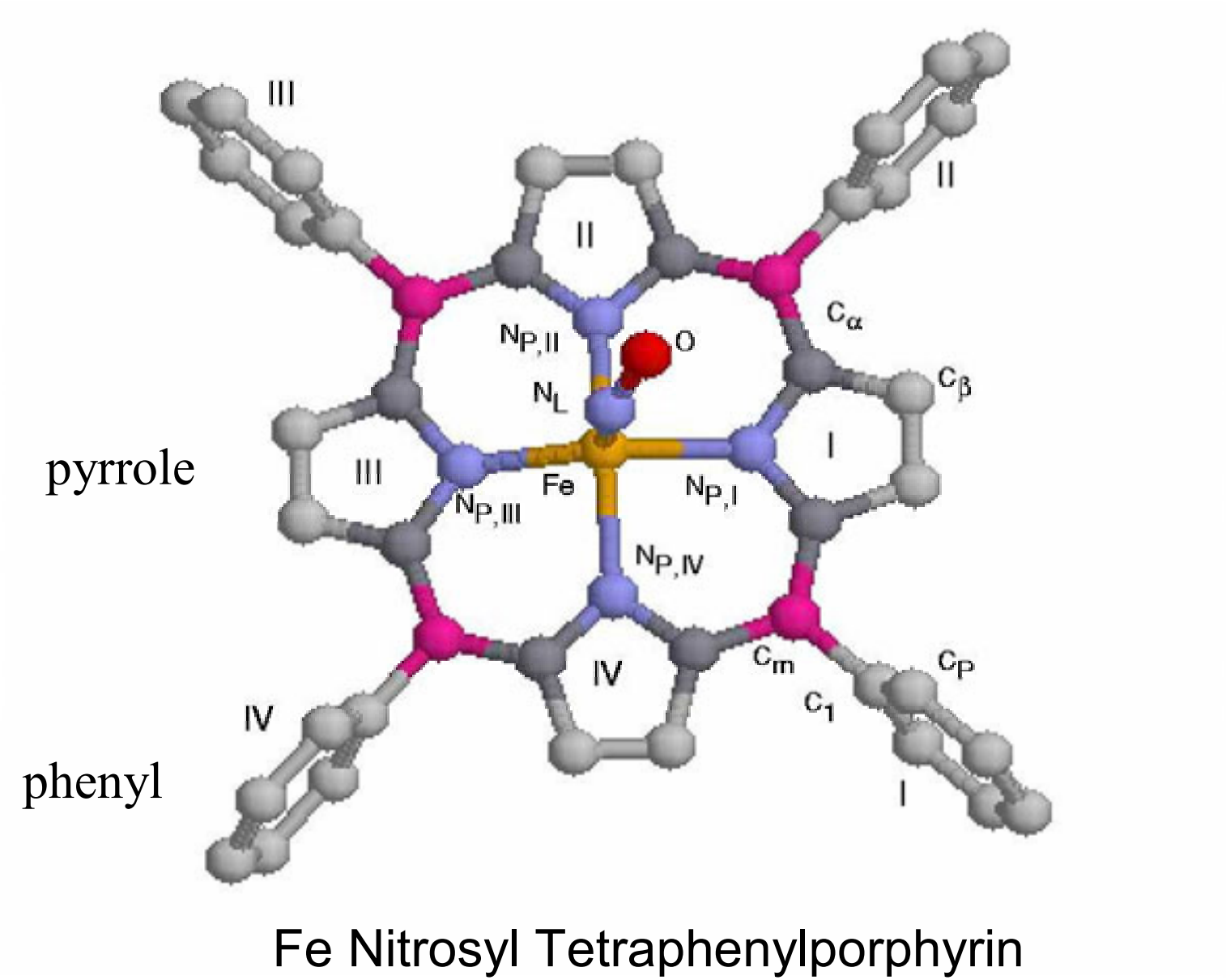

pyrrole

phenyl

Fe Nitrosyl Tetraphenylporphyrin

FeTPP-NO

N 42

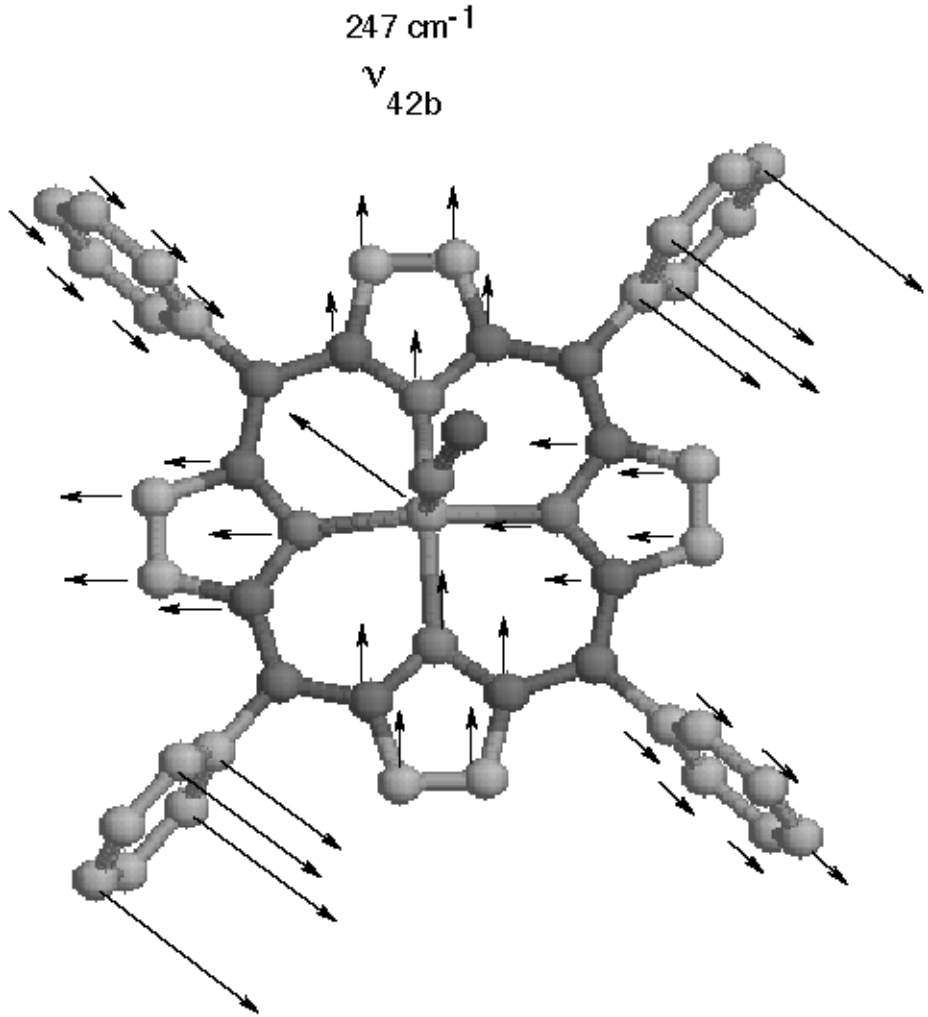

doming

QuickTime™ and a
decompressor
are needed to see this picture.

B. Rai, S. Durbin, W. Sturhahn, et al, Biophysics Journal, 2002

tilting

QuickTime™ and a
decompressor
are needed to see this picture.

B. Rai, S. Durbin, W. Sturhahn, et al, Biophysics Journal, 2002

in-plane

QuickTime™ and a
Video decompressor
are needed to see this picture.

B. Rai, S. Durbin, W. Sturhahn, et al, Biophysics Journal, 2002

Phenyl, out-of-plane

QuickTime™ and a
Video decompressor
are needed to see this picture.

B. Rai, S. Durbin, W. Sturhahn, et al, Biophysics Journal, 2002

Geology and high pressure physics

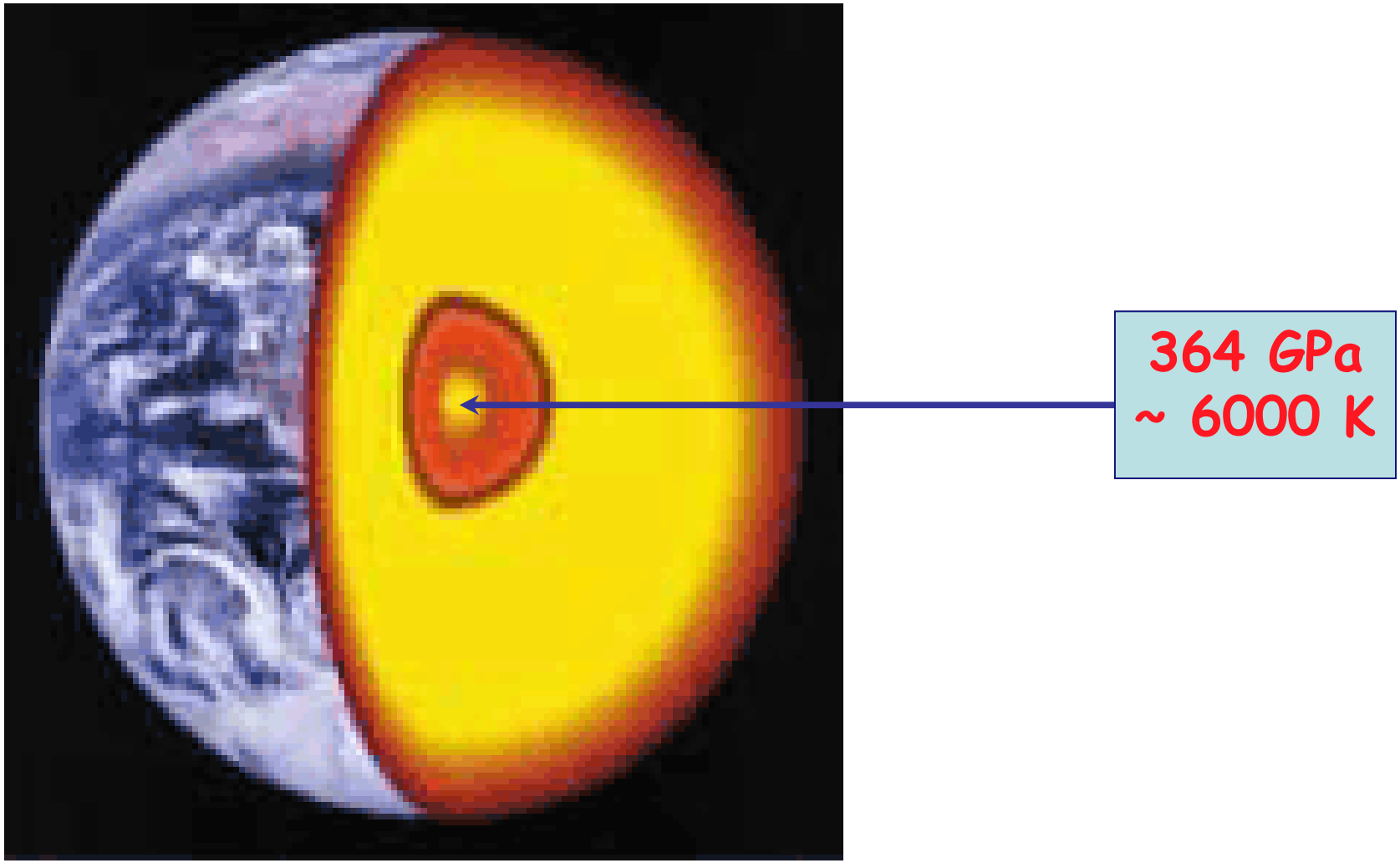

P vs. depth for Earth

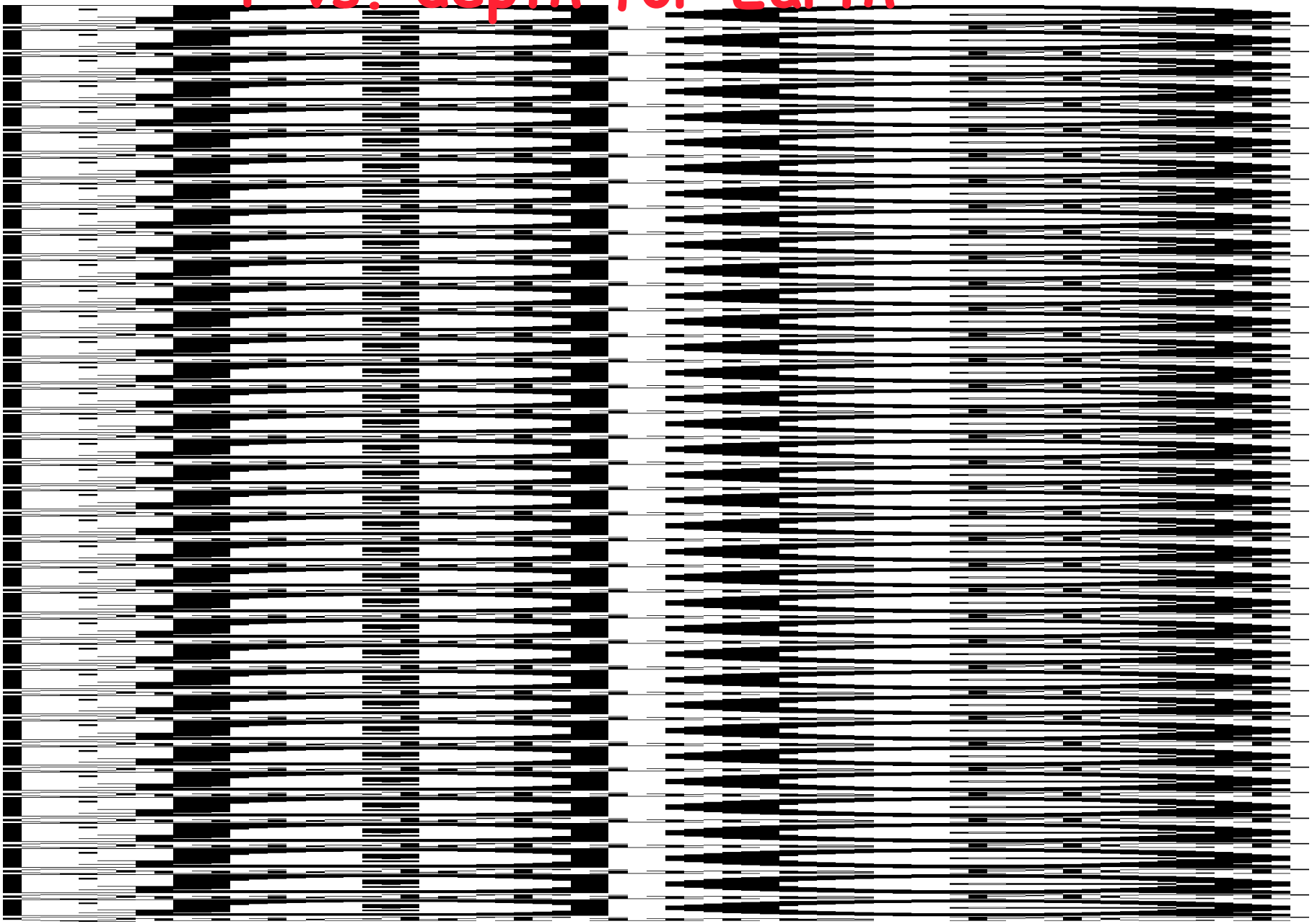

High pressure set-up with K-B mirrors

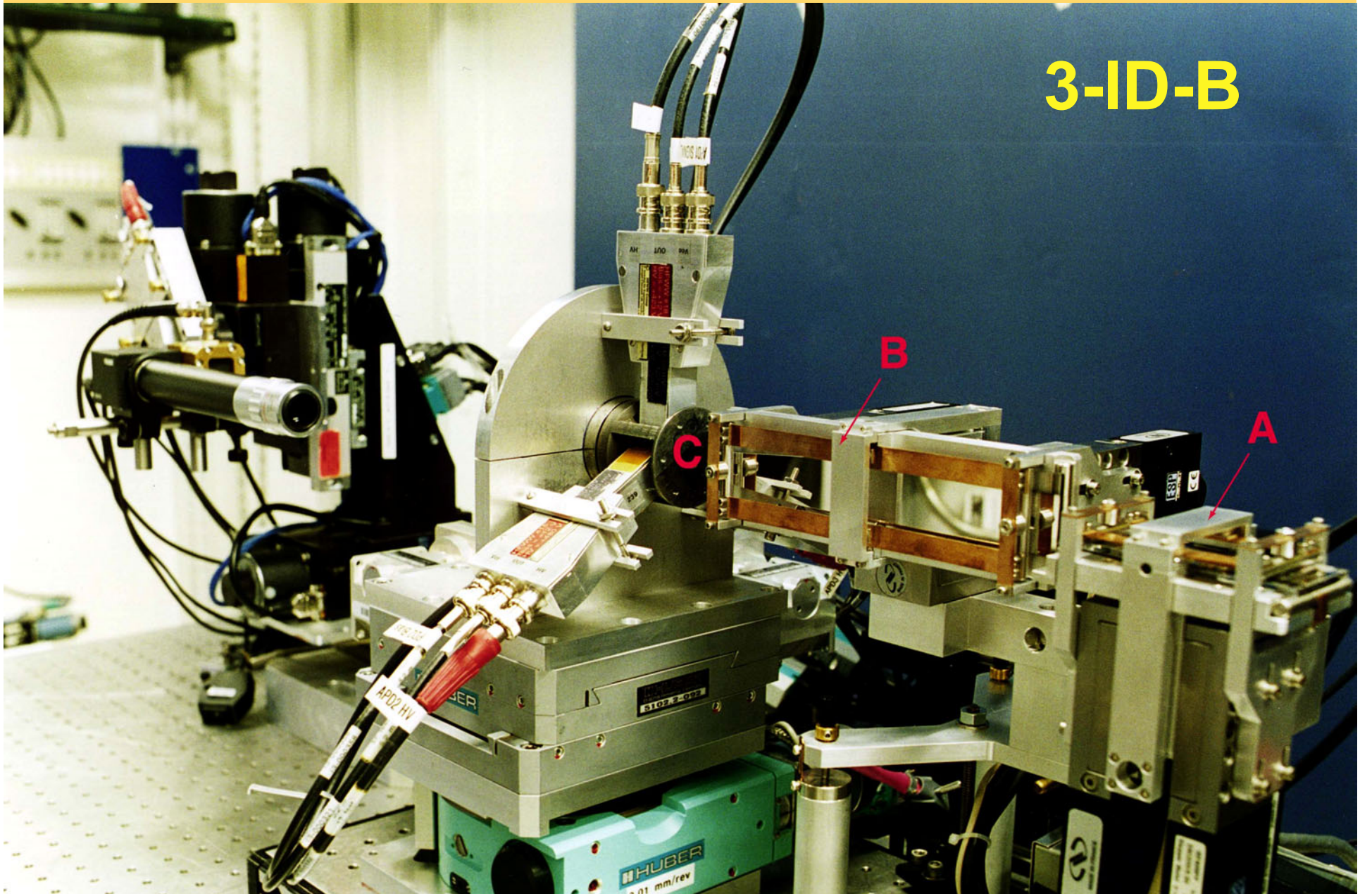

$Fe_{92.5}Ni_{7.5}$

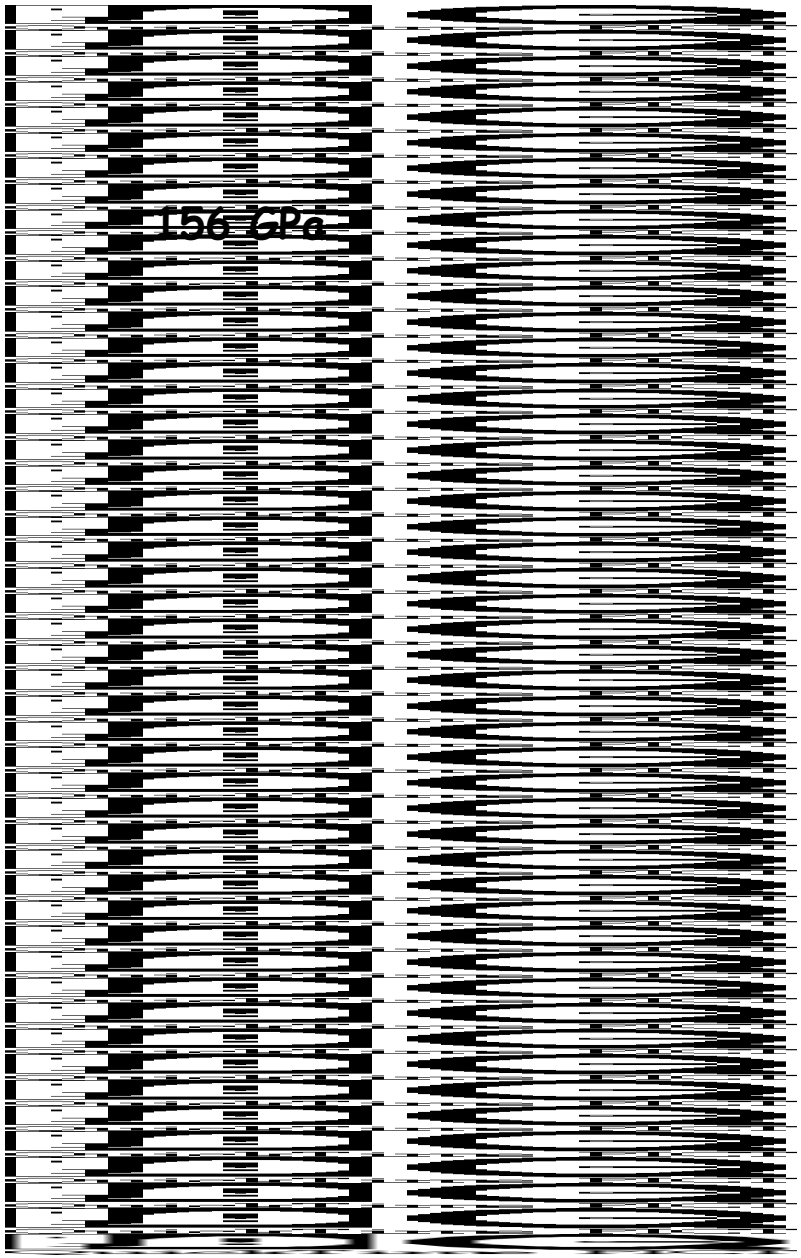

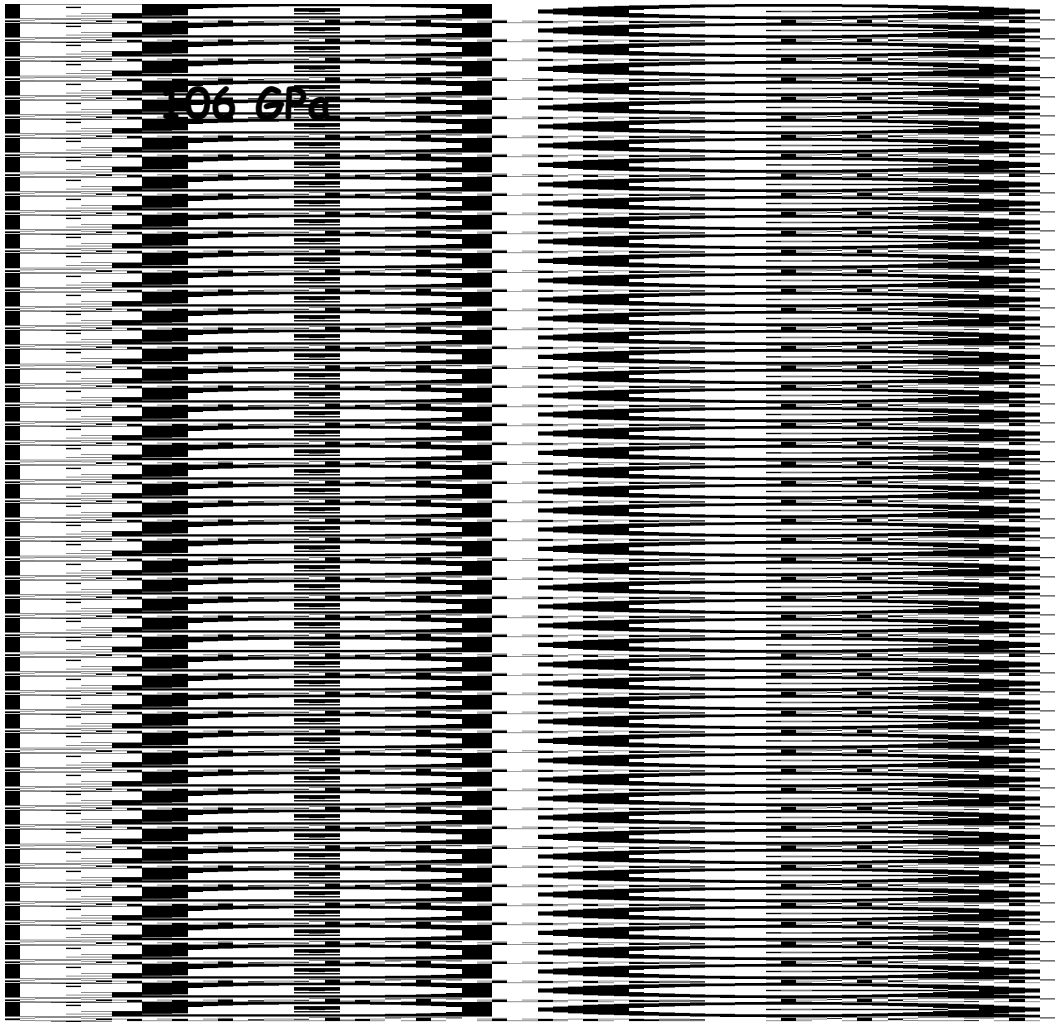

H.K. Mao, V. Sturzhkin (Carnegie Institute)
W. Sturhahn (APS)

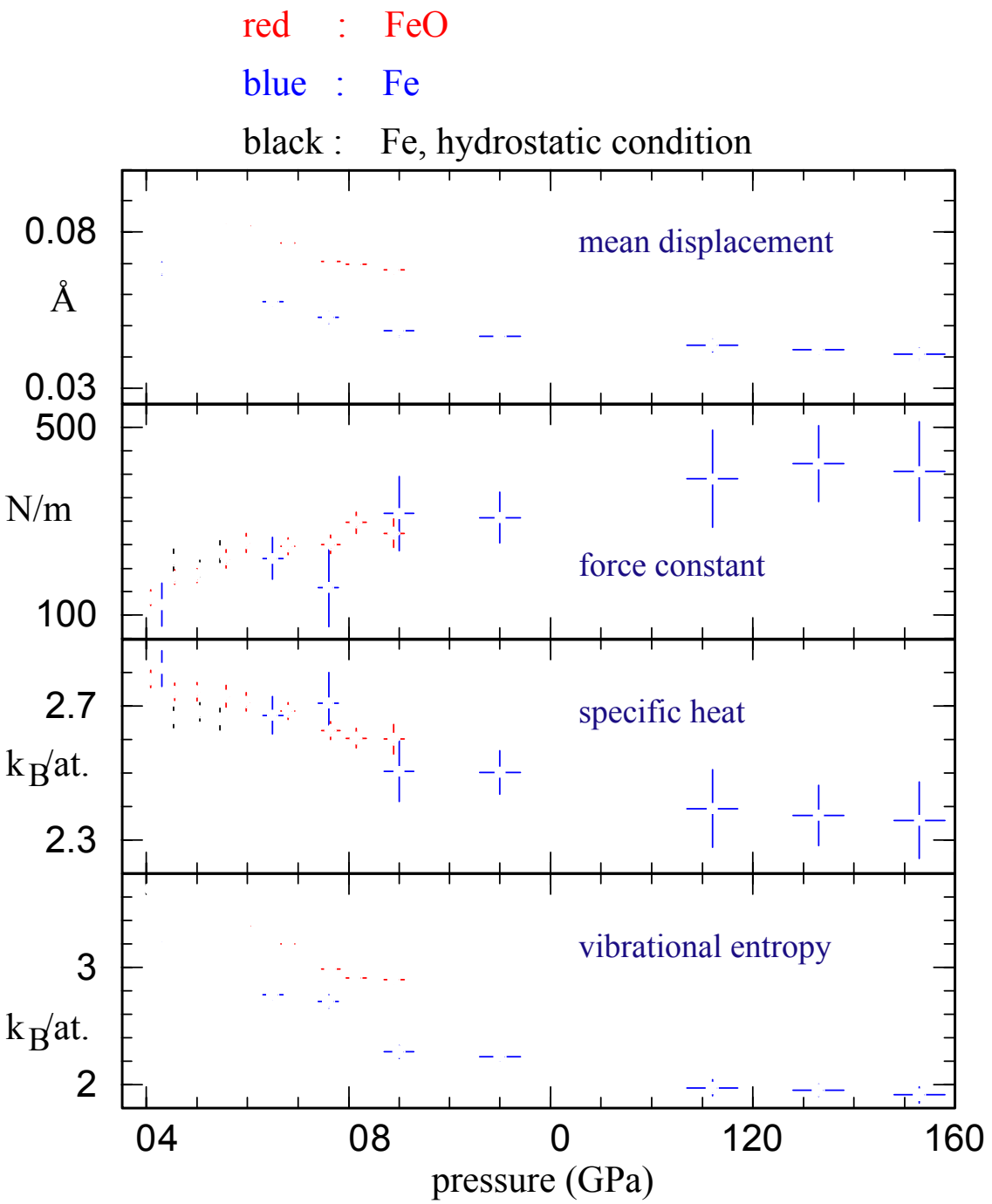
red : FeO
blue : Fe
black : Fe, hydrostatic condition
0.08
Å
0.03
mean displacement
500
N/m
100
force constant
2.7
k B/at.
2.3
specific heat
3
k B/at.
2
vibrational entropy
04
08
0
120
160
pressure (GPa)

Phonon-magnon coupling in FeO

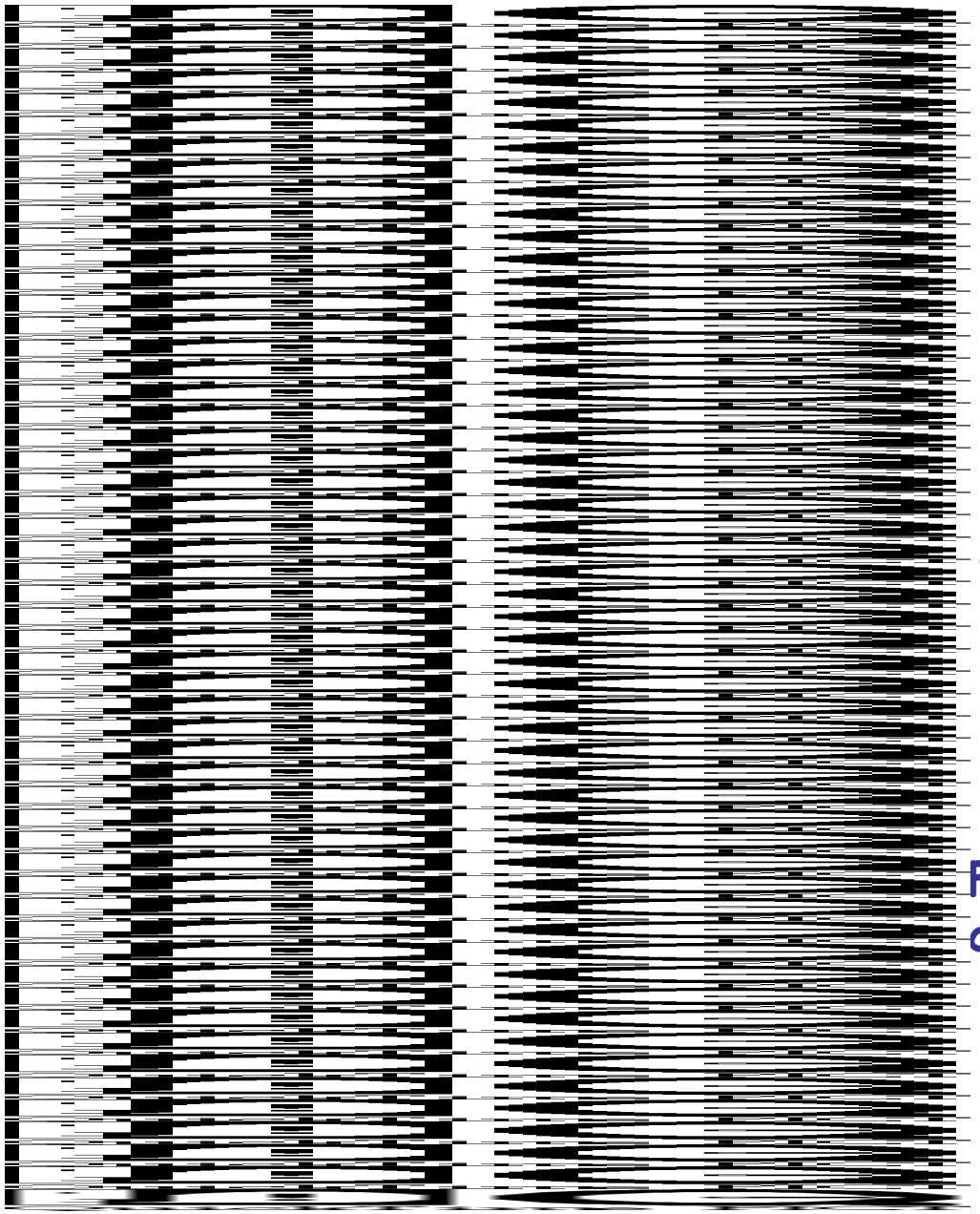

Pressure induced
phase transition

Rock-salt,
paramagnetic

Rhombohedral,
antiferromagnetic

16-20 GPa ⟶

First observation of magneto-elastic
coupling in the THz range

Phonon dispersion relations with magneto-elastic coupling

$$(\omega-\omega_m)^2(\omega-\omega_s)^2=\frac{gk^2B_2^2\Omega}{2\rho M_0}$$

ω_m = spin frequency = $\Omega g M_0(\beta+\alpha k^2)$

ω_s = sound frequency,

Ω = 11 meV (from Raman data)

M_0 = magnetic moment of the sublattice

B_2 = -2.5×10^{10} erg/cm^3

g = gyromagnetic ratio

α,β,γ = exchange interaction constants

k = wave vector

ρ = density, 6.2 g/cm^3

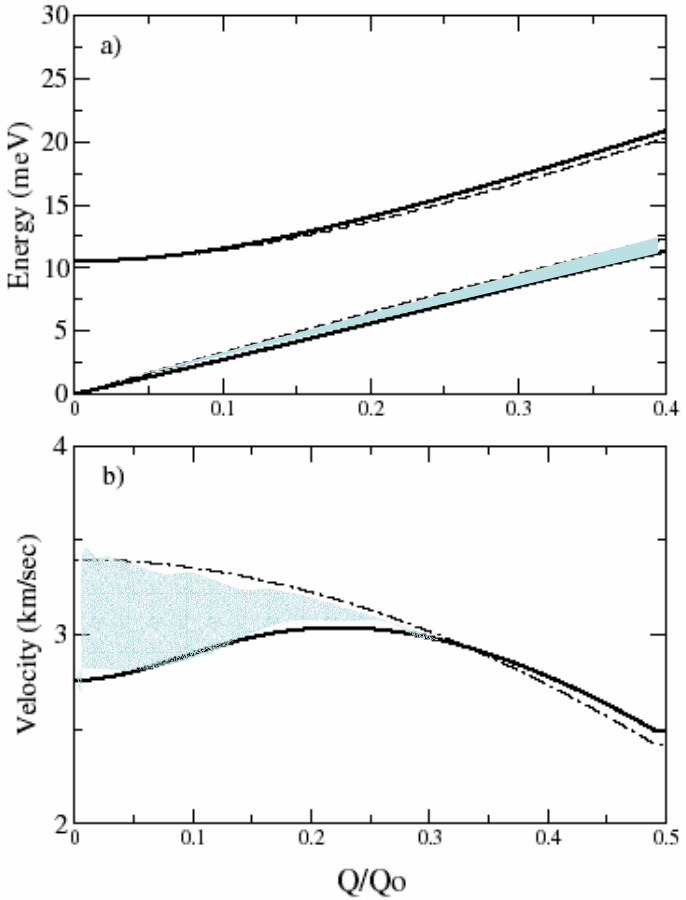

FIG. 4. Model for the magnetoelastic coupling in FeO. (a) The interacting transverse phonon and magnon branches. Noninteracting bare frequencies are shown with dashed lines, the dispersion branch for magnons is calculated according to [31], the phonon dispersion was approximated by $E(Q)=2Q_0v_s/\pi\sin[(\pi/2)(Q/Q_0)]$ using the sound velocity 3.4 km/sec at $Q=0$. (b) Calculated sound velocity including magnetoelastic coupling (solid line) and without magnetoelastic coupling (dash-dotted line).

Measurement of partial vibrational density of states on both elements in the same compound

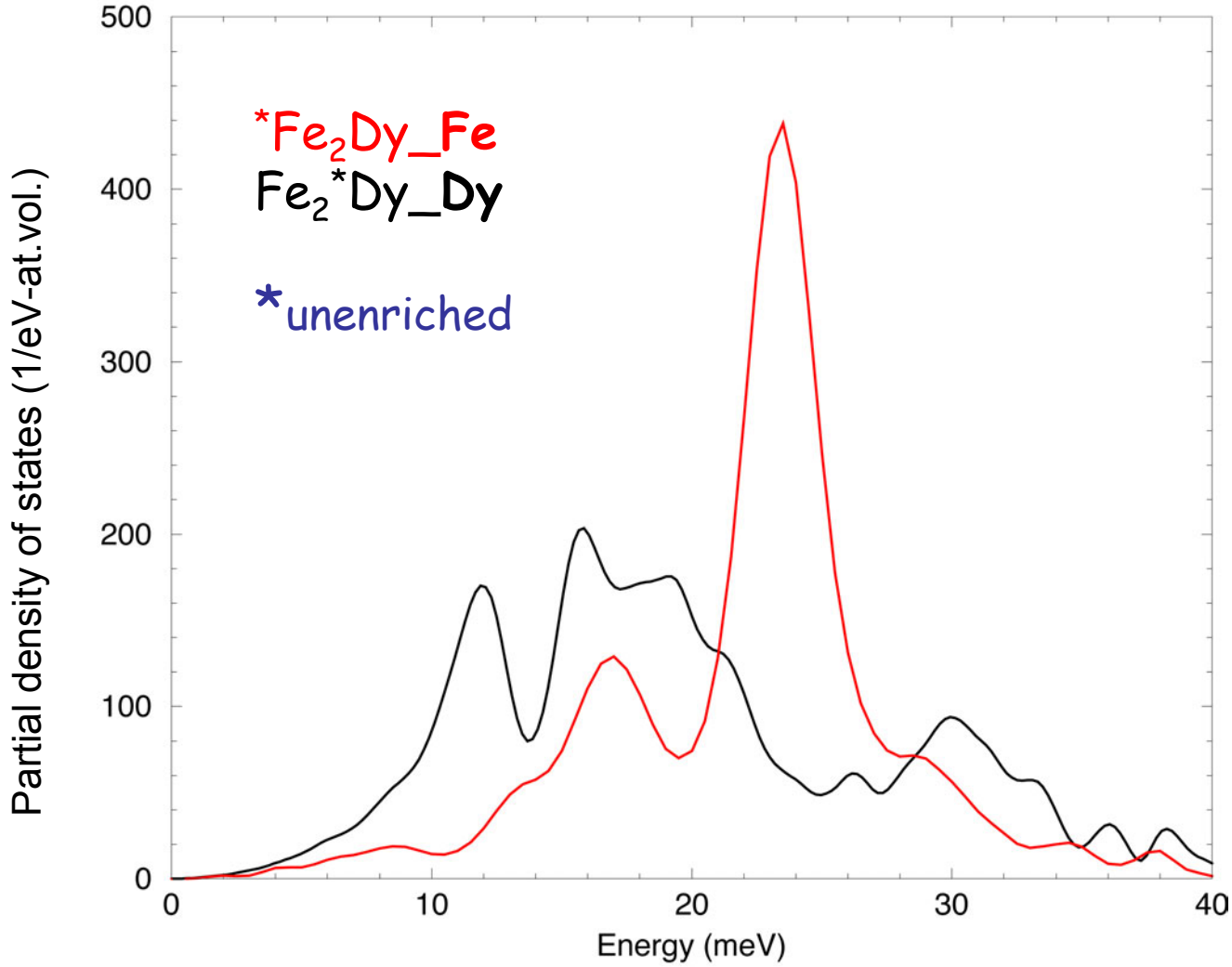

In collaboration with D. Brown, Northern Illinois University

Crystalline-amorphous transformation

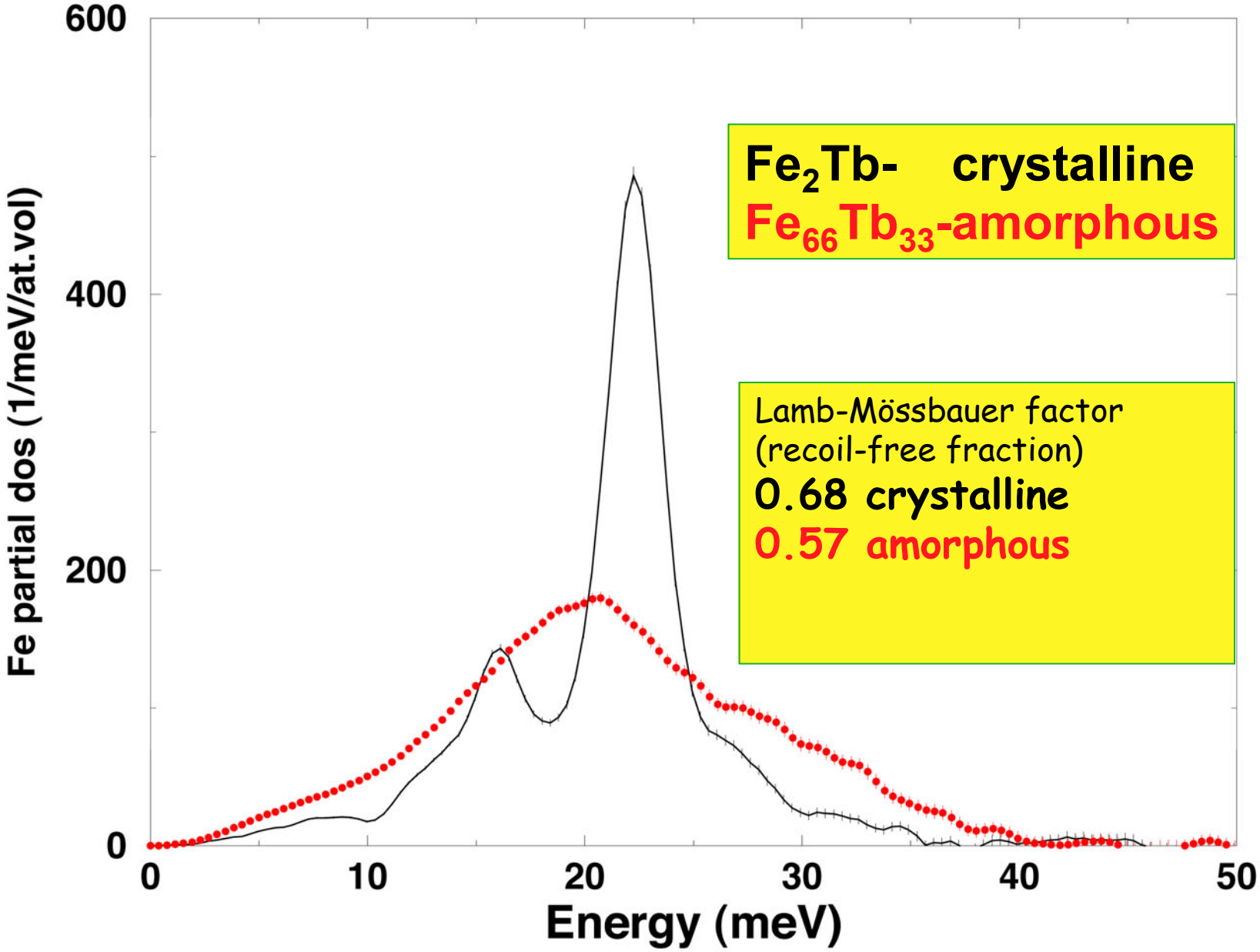

Crystalline and amorphous Fe_2Tb, raw data

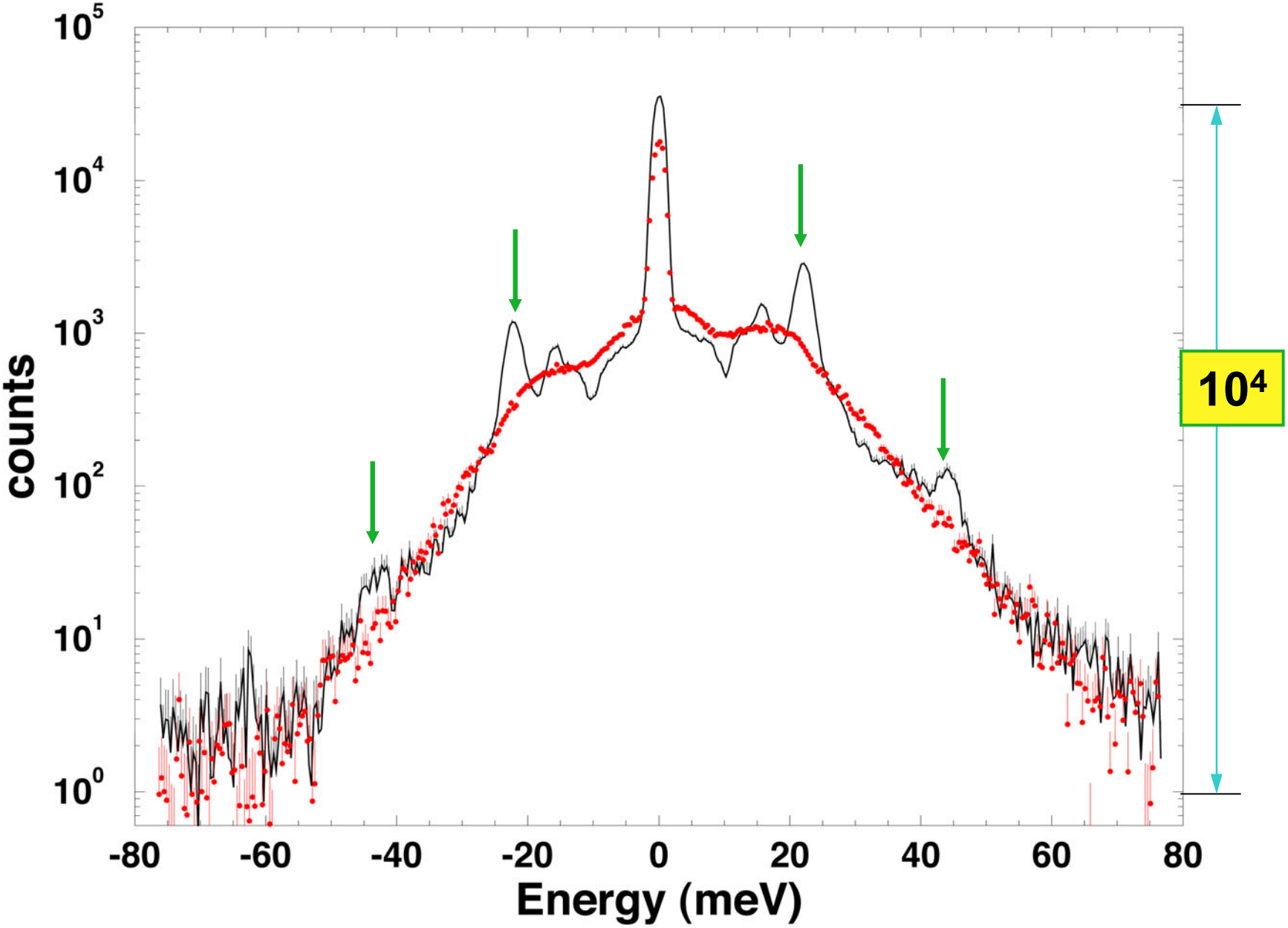

Effect of order-disorder in a crystalline compound

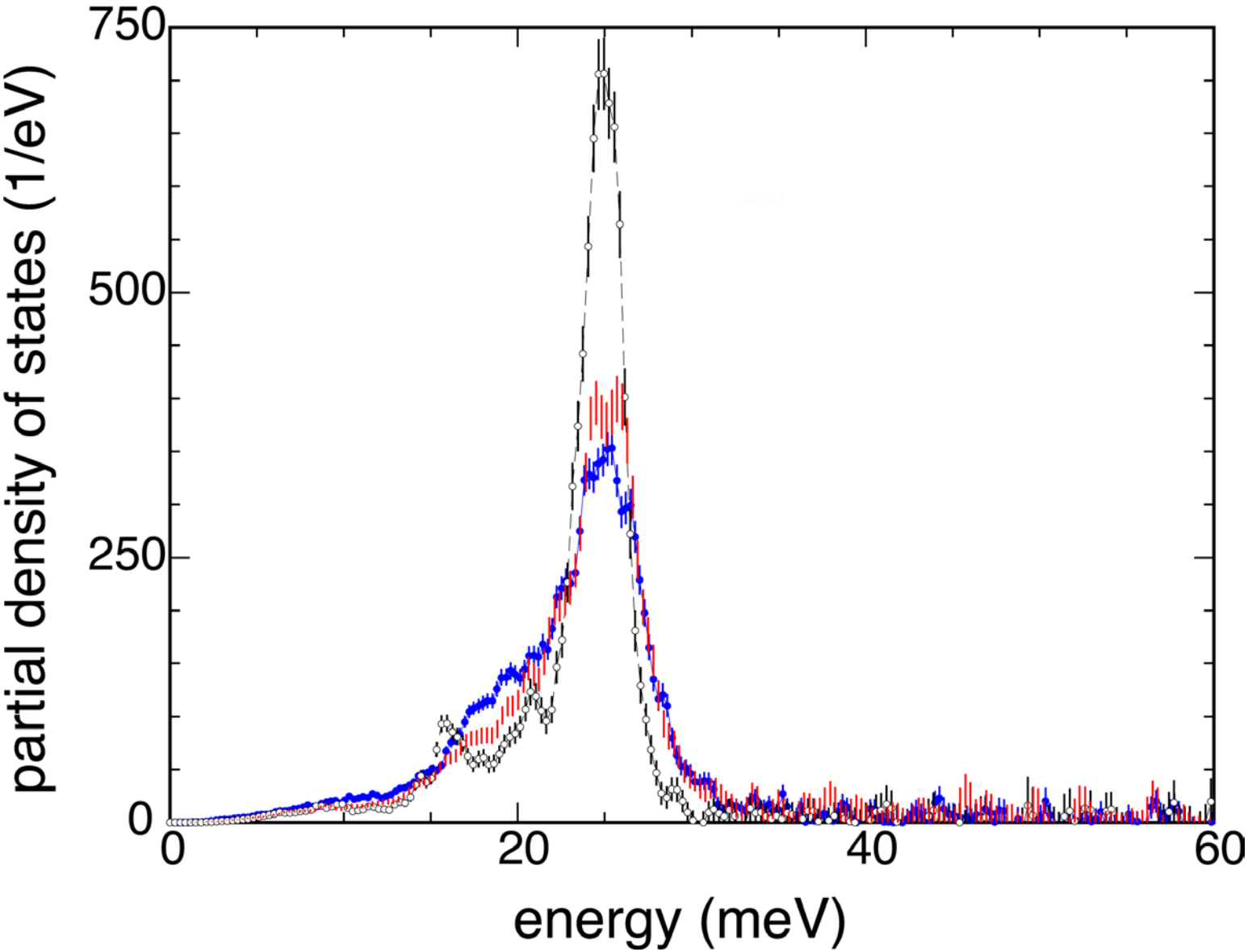

Determination of sound velocity

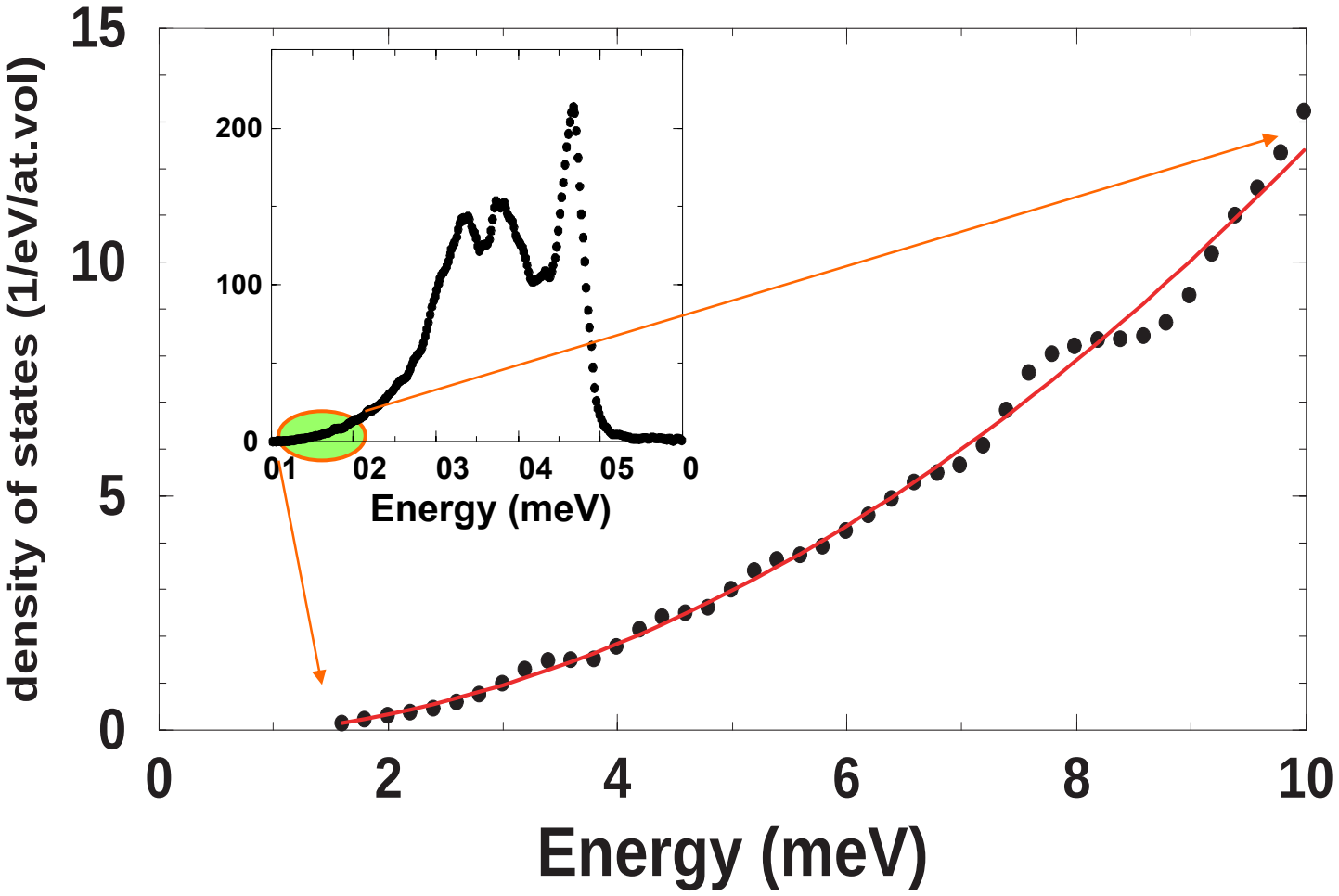

Sn impurities in Pd

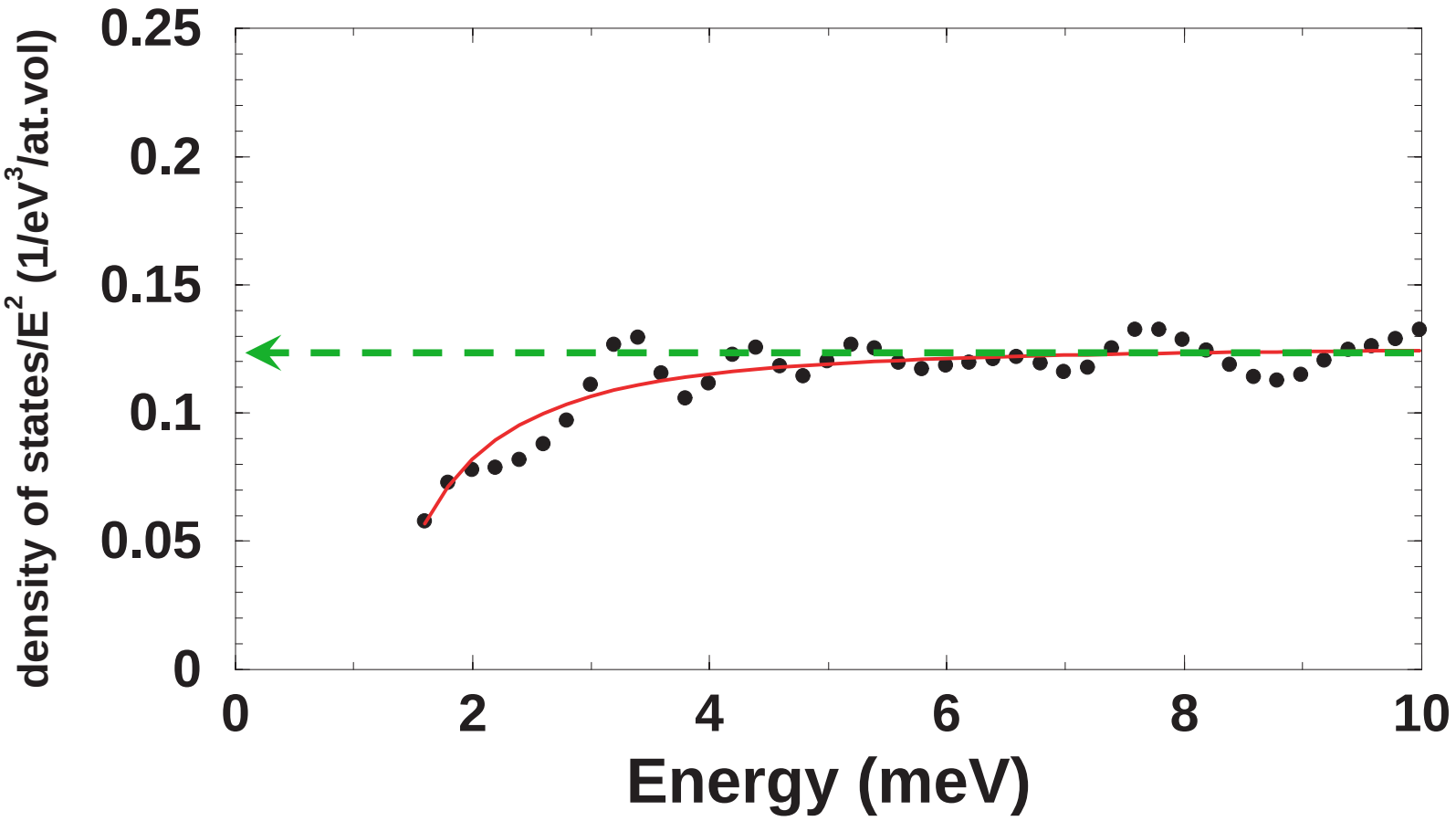

Sound velocity

$$D(E) = \frac{V}{2\pi\hbar^3 c_s^3} E^2$$

for cubic crystals

$$c_s = \left[2\pi\left(D(E)/E^2\right)\right]^{1/3} \frac{a(m)}{\hbar(eV.s)}$$

where a is the lattice constant.

For Pd

$$a = 389\ pm$$

$$D(E)/E^2 = 8.3\ THz/a(m) = 3228\ m/\sec$$

$$tabulated\ value = 3070\ m/\sec$$

Theory and experiment

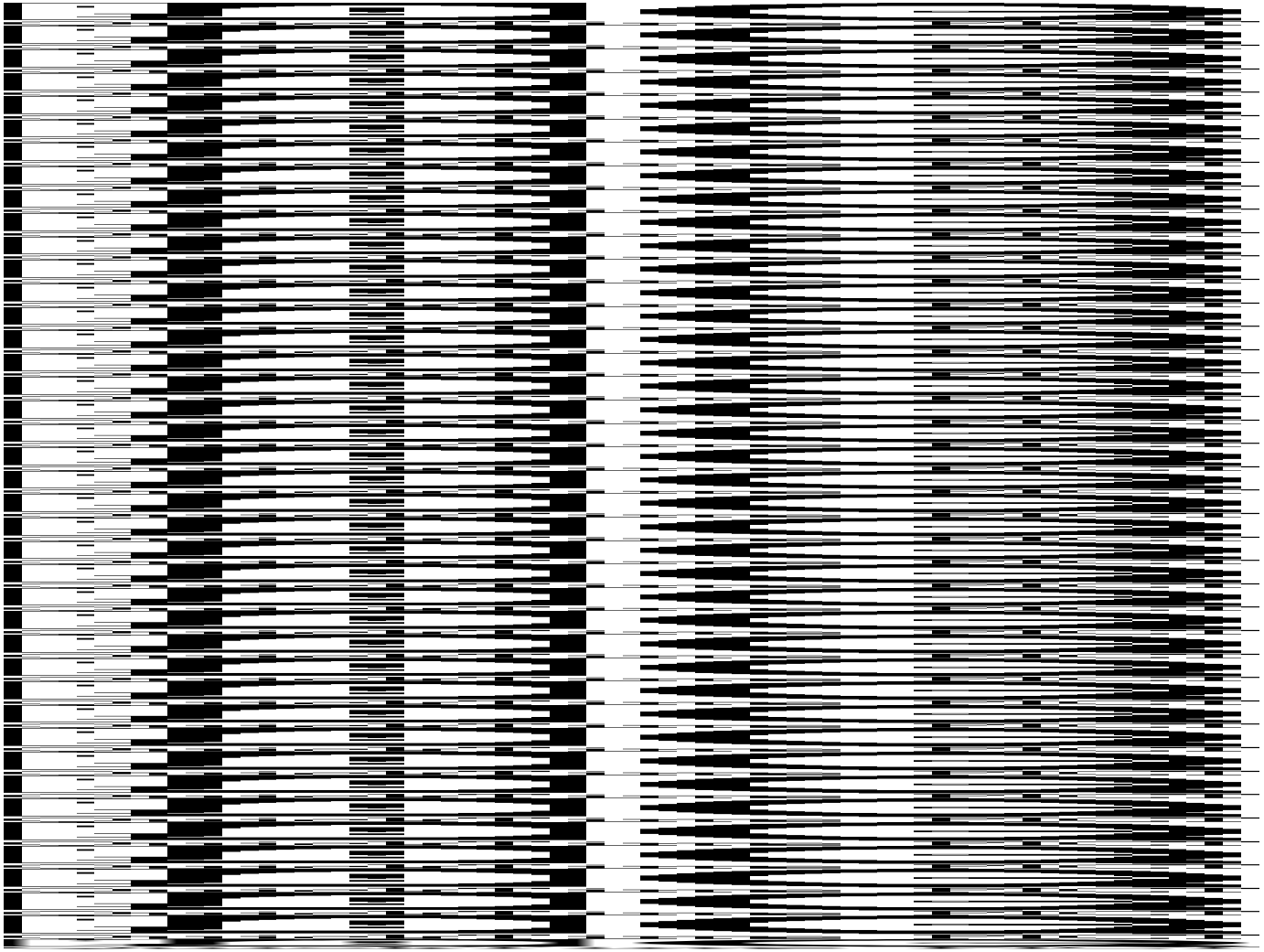

Kr under pressure in a DAC cell

J. Zhao, T. Toellner, W. Sturhahn, J. Tse (NRC)

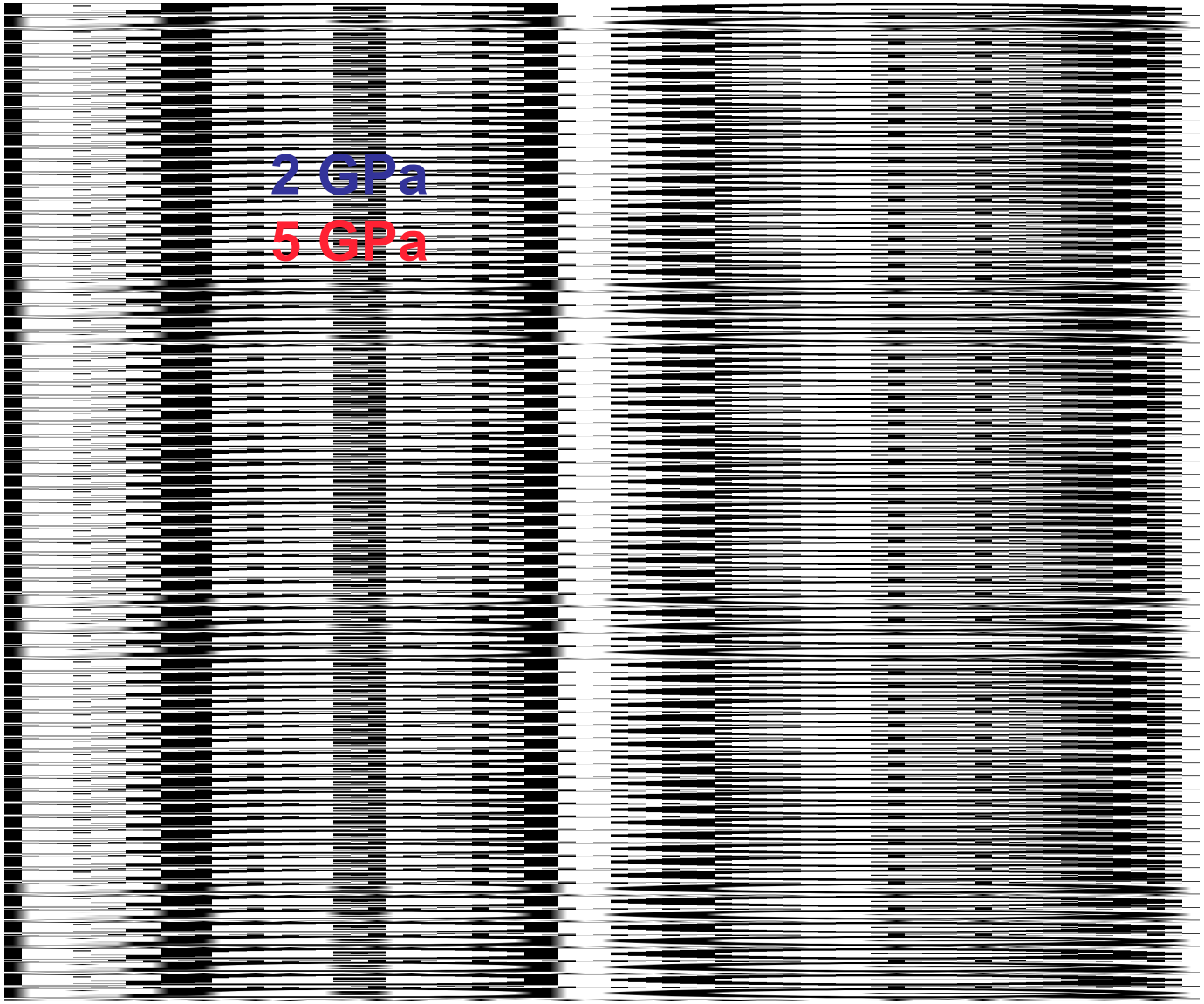

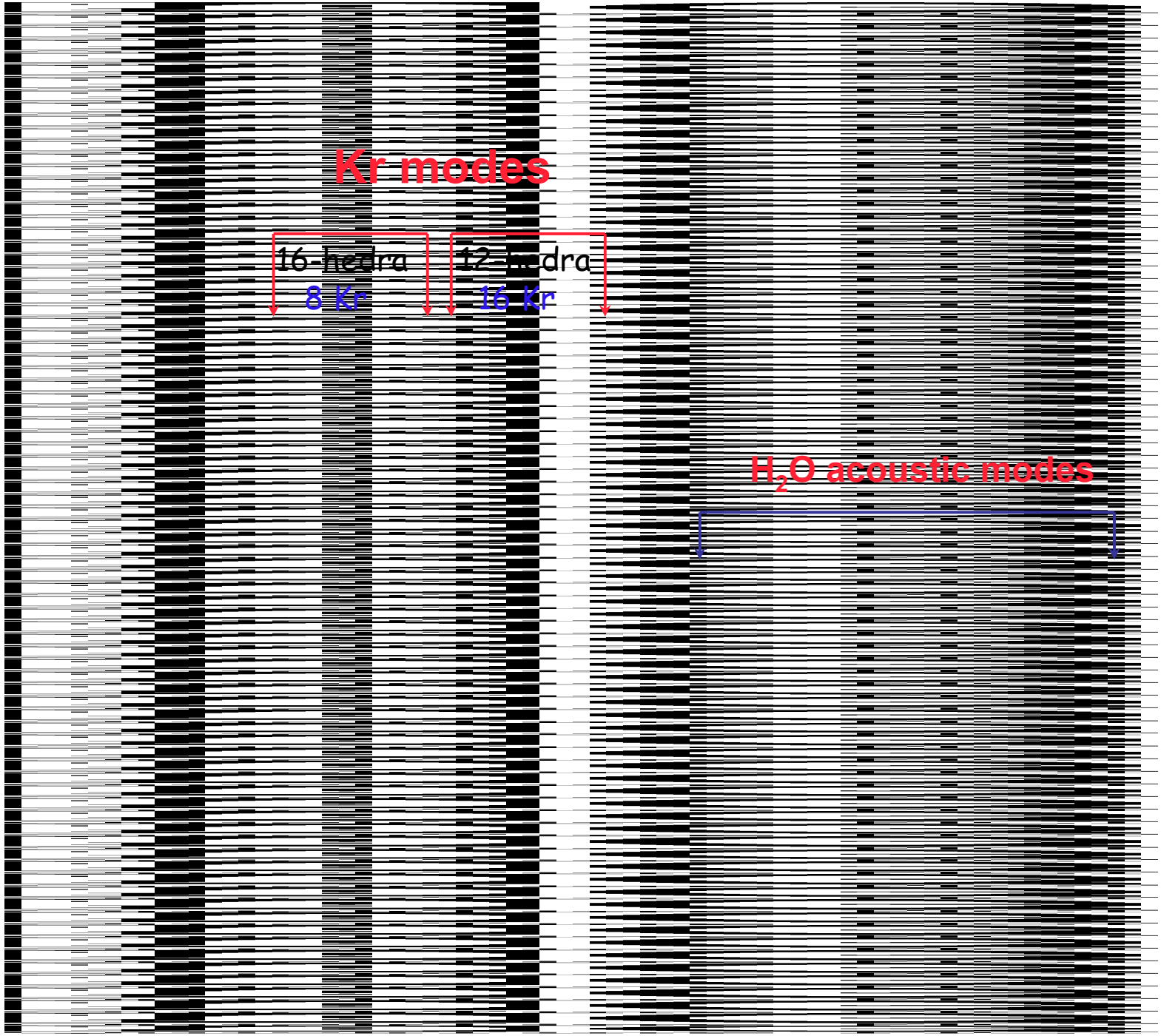
Kr modes
16-hedra
8 Kr
12-hedra
16 Kr
H2O acoustic modes

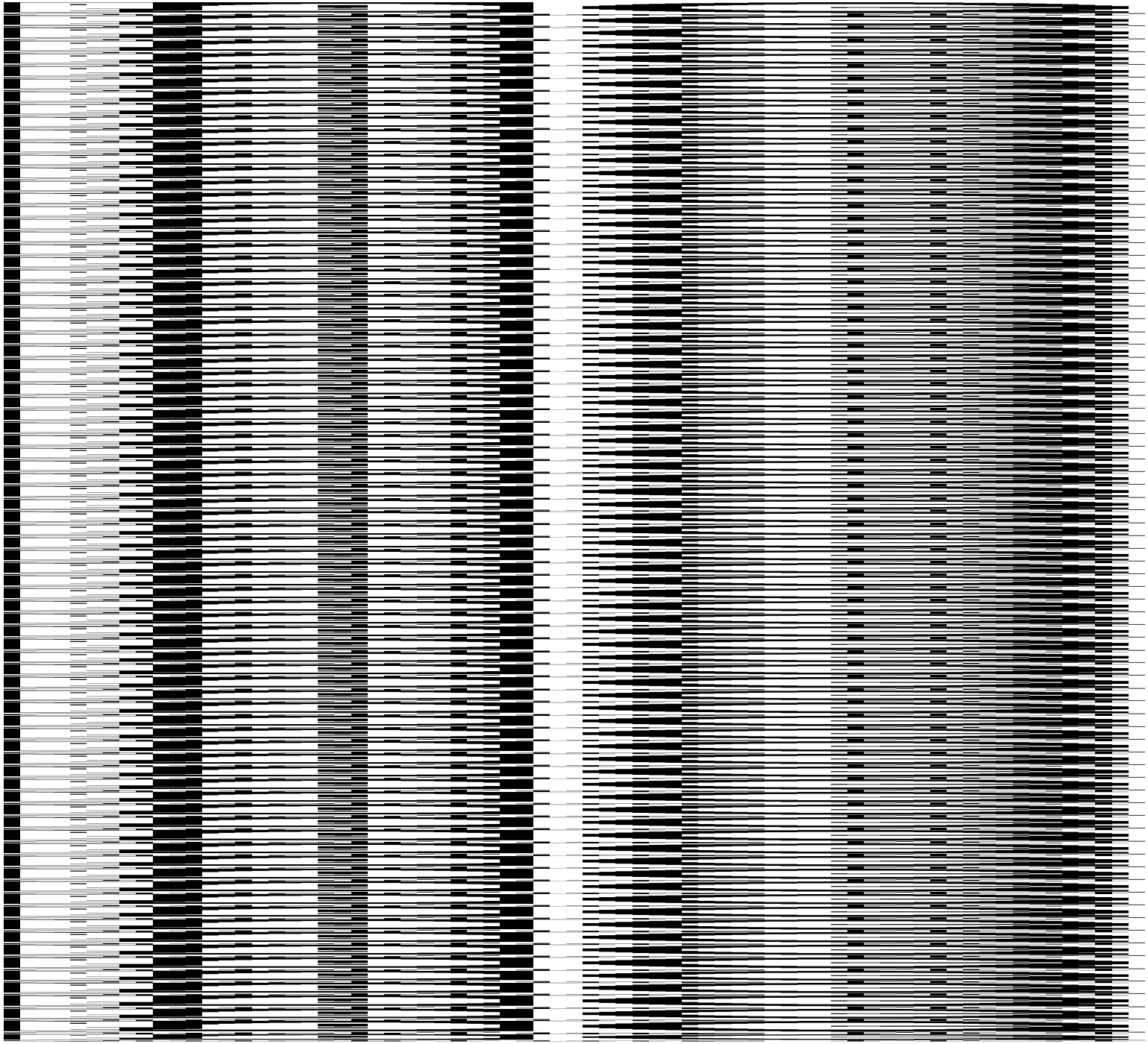

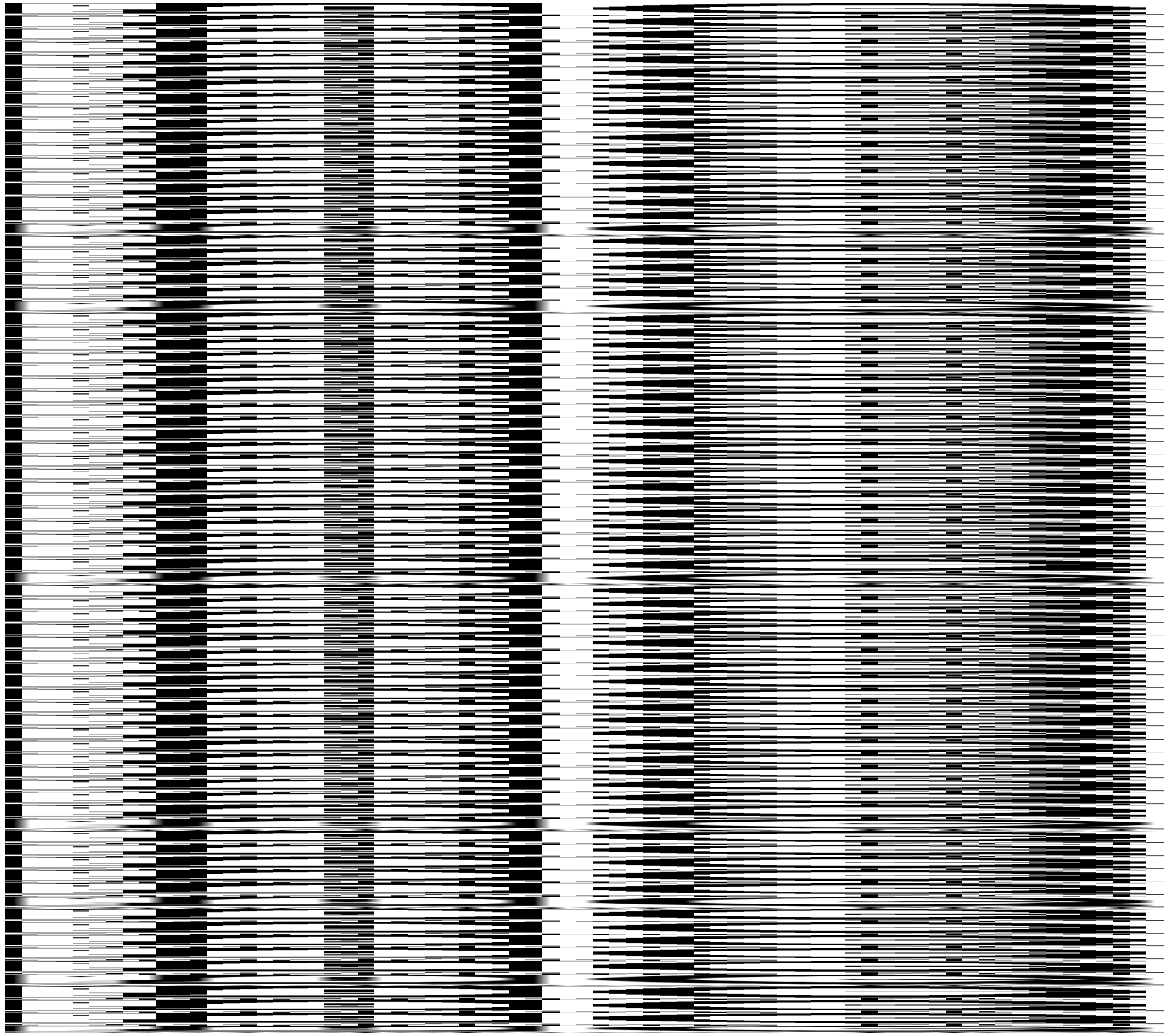

Large change in the speed of sound and similarly large change in thermal expansion are among the anomalous behavior of clathrate hydrates.

Progress in NRS between 1985-2002

Isotope	Tabulated E(eV)	Measured E(eV)	ΔE (neV)	Γ (nsec)
^{181}Ta	6238	6215.5	0.067	9800
^{169}Tm	8401	8401.3	114	4
^{83}Kr	9401	9403.5	3.1	147
^{73}Ge	13263	----	0.15	2953
^{57}Fe	14413	14412.5	4.67	97.8
^{151}Eu	21532	21541.4	47	9.7
^{149}Sm	22490	22496	64.1	7.1
^{119}Sn	23870	23879.5	25.7	17.8
^{161}Dy	25655	25651.4	16.2	28.2
^{129}I	27770	---	27.2	16.8
^{40}K	29560	29834	107	4.25
^{145}Nd	67100	---	6.8	67.1
^{61}Ni	67400	67419	89	5.1
^{193}Ir	73000	---	72.3	6.3
^{133}Cs	81000	---	71.5	6.4
^{67}Zn	93300	---	0.049	9200

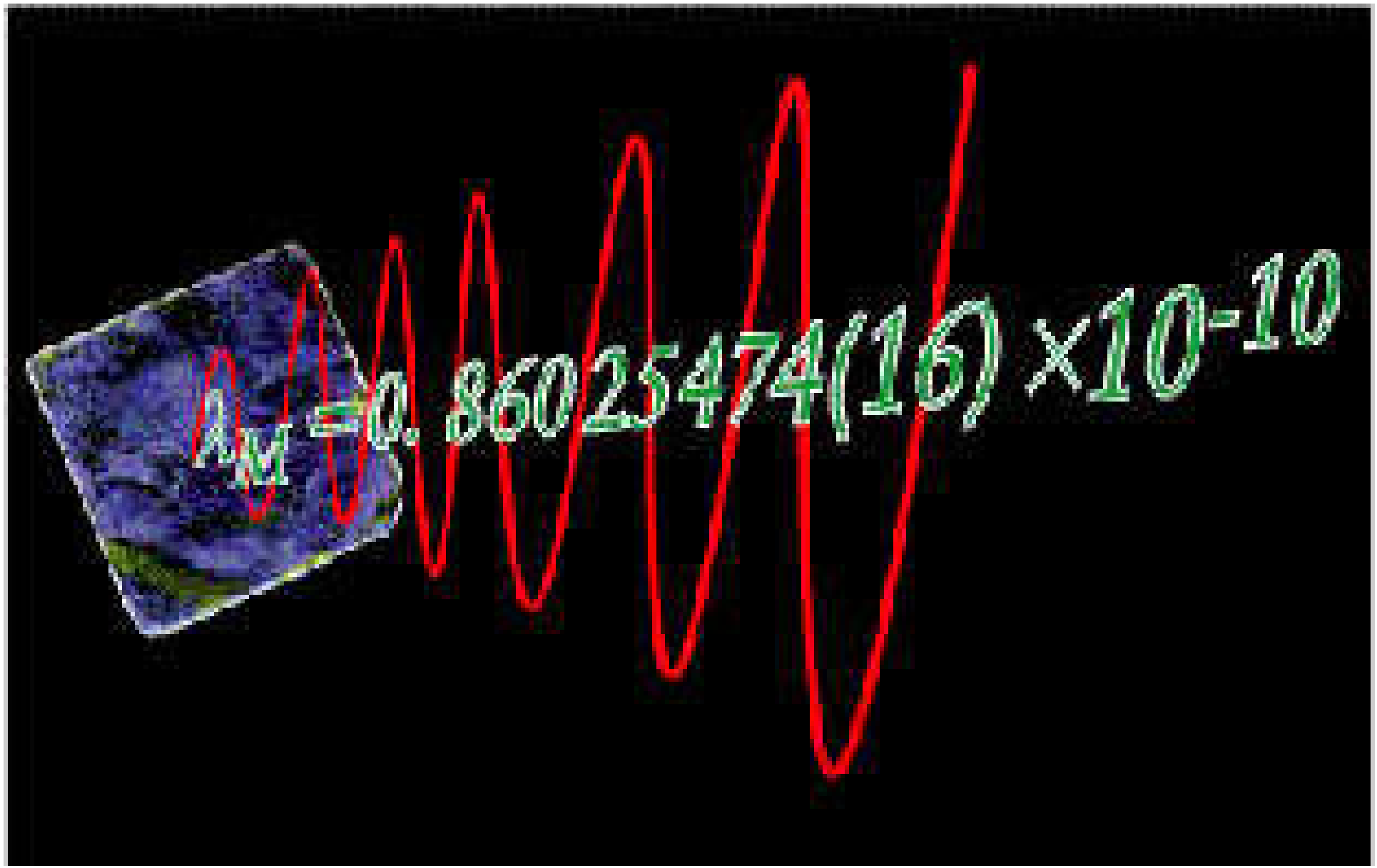
λM = 0.8602547(16) ×10-10

Measuring wavelengths and lattice constants with Mossbauer wavelength standard

Higher accuracy ($\Delta E/E \sim 10^{-13}$ possible)

Reproducible independent of temperature, pressure, composition, and other parameters

Available between 6-100 keV range at more than a dozen energies

Y. Shvydko, et al, Phys. Rev.Lett., 45 (2000) 495
J. Synchrotron Rad. 9 (2002) 17

Wavelength & energies of Mossbauer isotopes determined at a synchrotron radiation source

isotope	E (eV)	λ (Å)	δλ/λ (10^{-7})
^{57}Fe	14412.497(3)	0.86025474(16)	1.9
^{151}Eu	21541.418(10)	0.57556185(27)	4.7
^{119}Sn	23879.478(18)	0.51920811(39)	7.4
^{161}Dy	25651.368(10)	0.48334336(19)	4.0

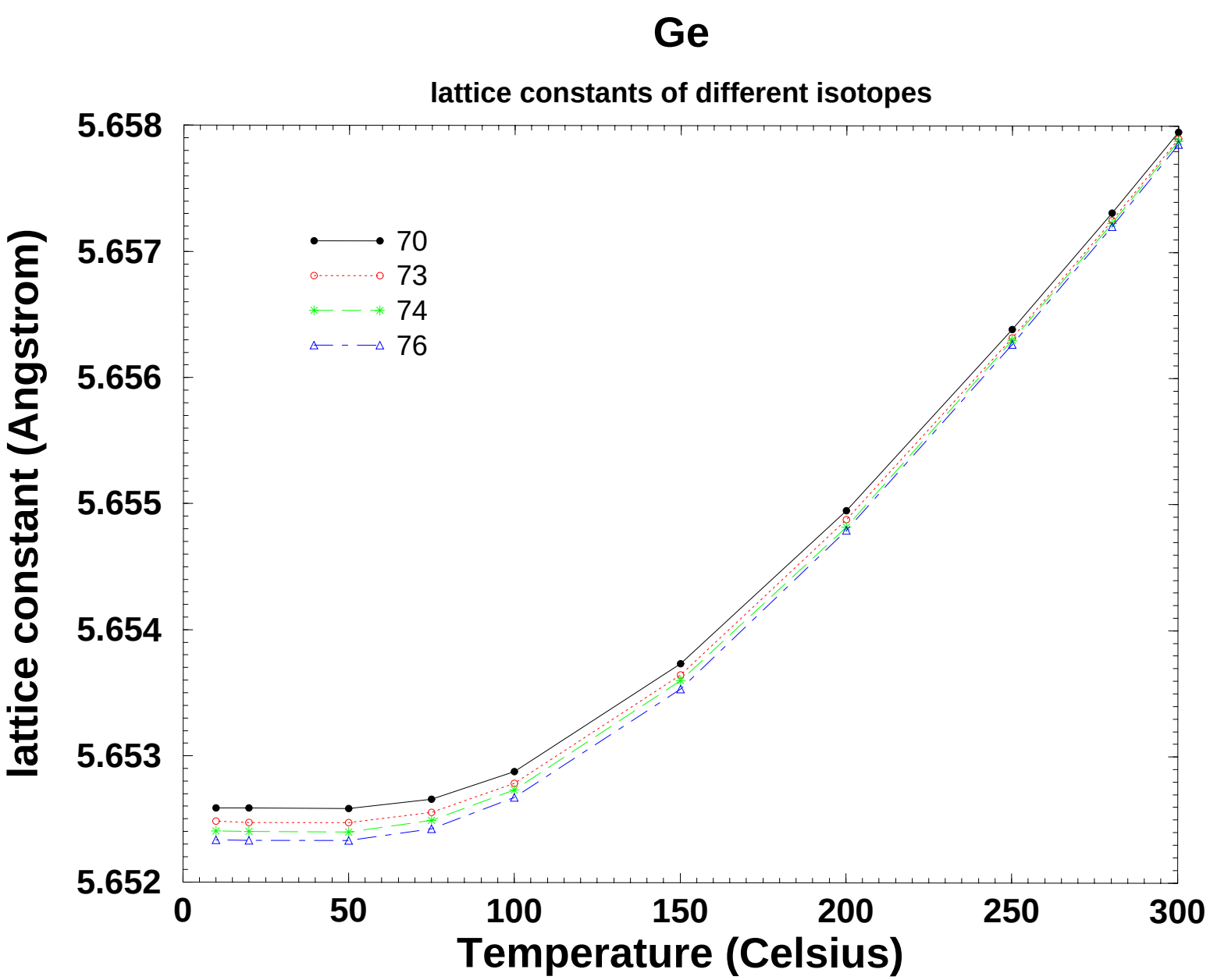
Ge
lattice constants of different isotopes
lattice constant (Angstrom)
Temperature (Celsius)
5.658
5.657
5.656
5.655
5.654
5.653
5.652
0
50
100
150
200
250
300
70
73
74
76

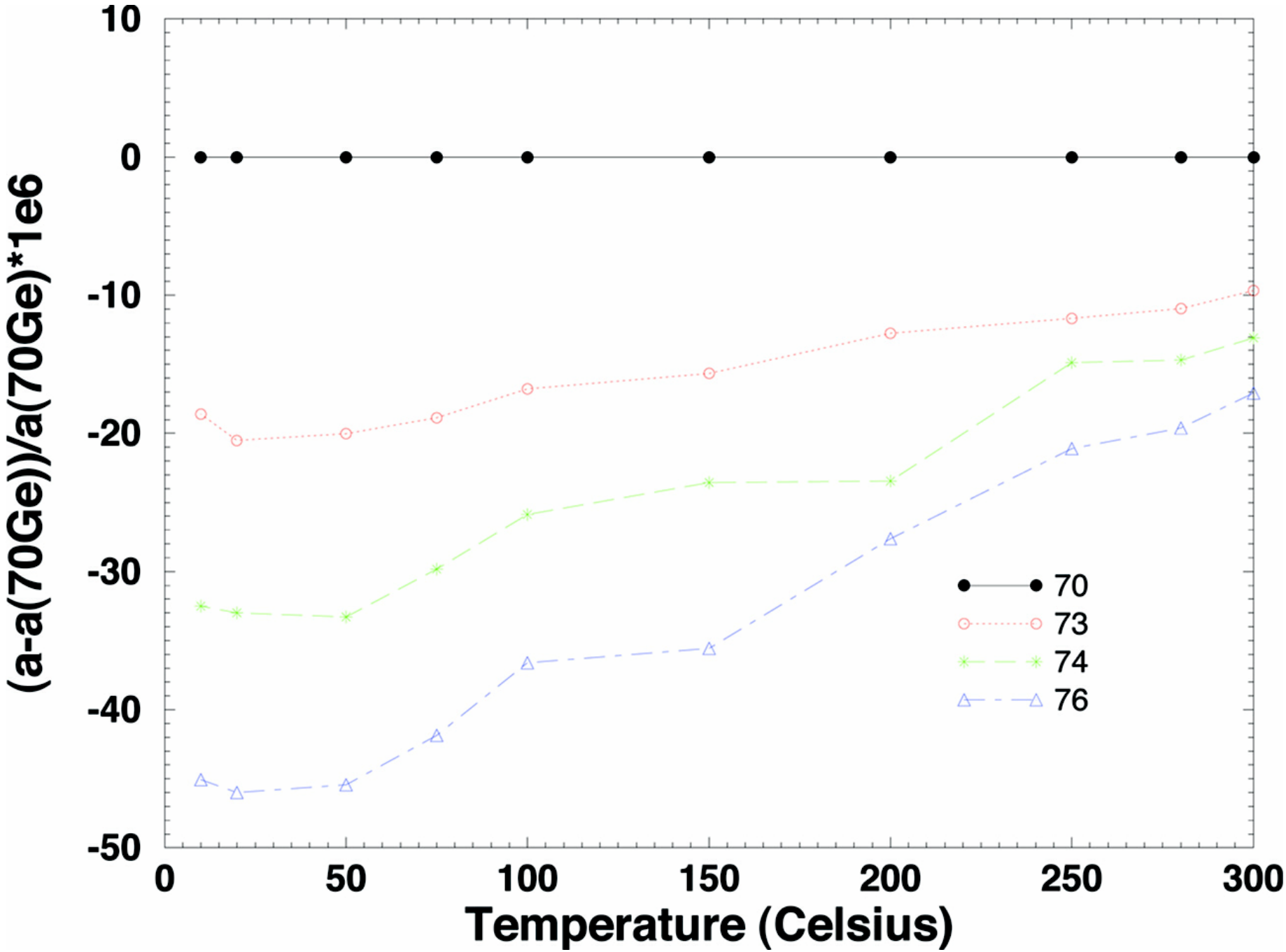
10
0
-10
-20
-30
-40
-50
0
50
100
150
200
250
300
(a-a(70Ge))/a(70Ge)*1e6
Temperature (Celsius)
70
73
74
76

Normal Incidence Diffraction, NID, beamline

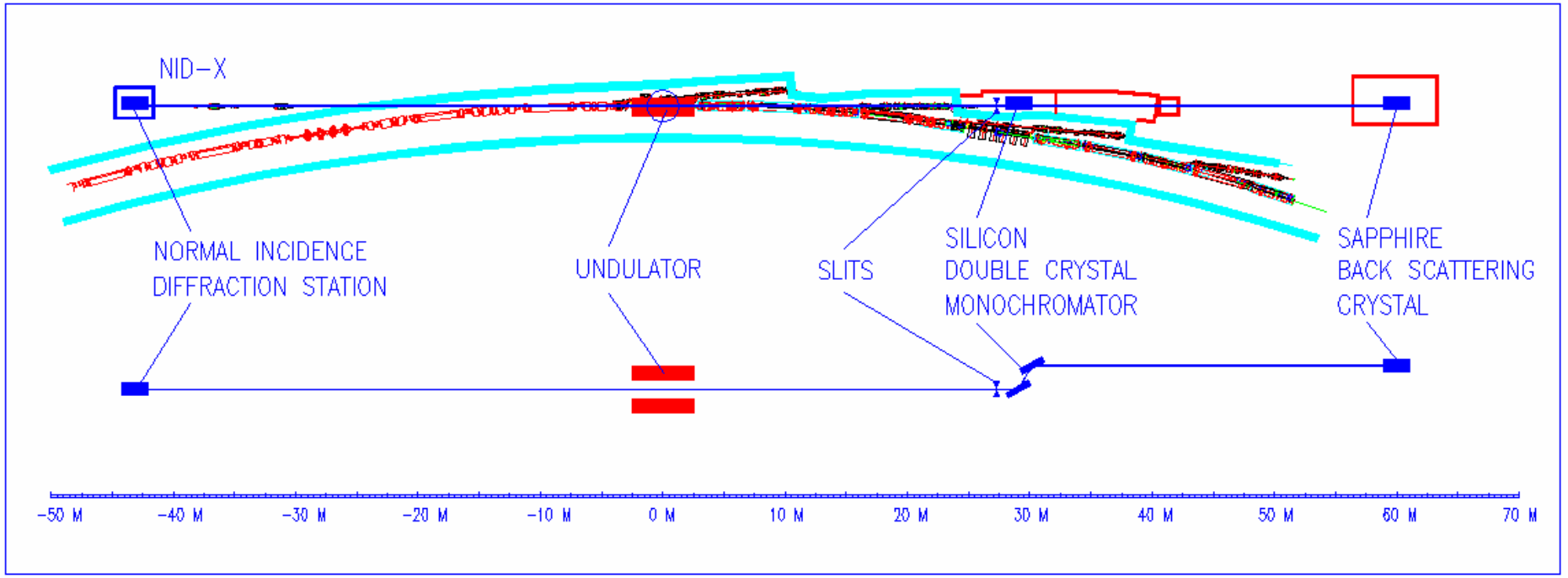

First scientific results from NID

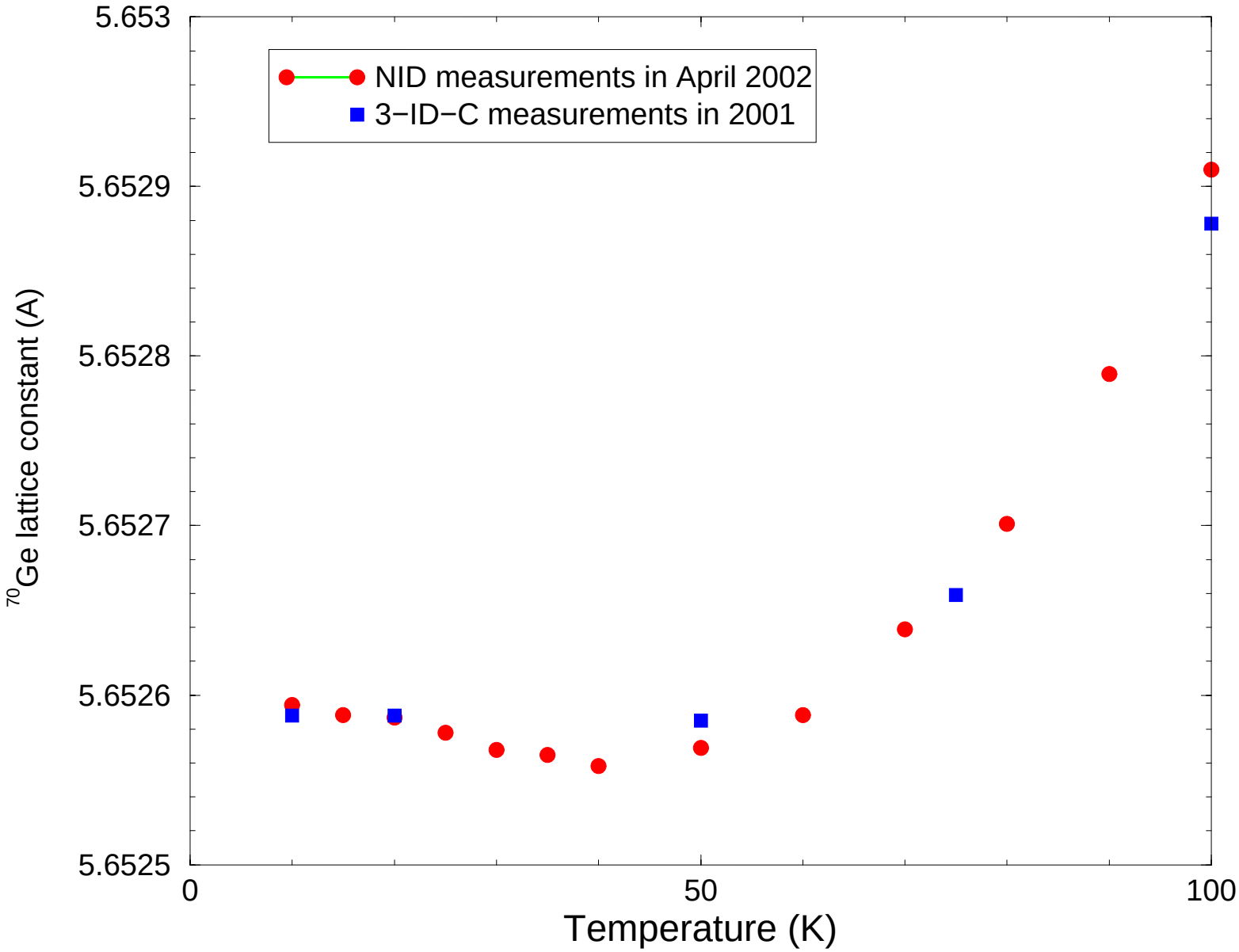

Fabry-Perot Interferometer for μeV

Free spectral range, $E_f = \dfrac{hc}{2d_g}$,

d_g **: gap between two mirrors**

Spectral width $\Gamma = \dfrac{E_f}{F}$

where F, finesse $F = \dfrac{\pi\sqrt{R}}{(1-R)}$,

R **: Reflectivity**

with R **= 0.85,** F **= 19.3,** d_g **= 50 mm,** Γ **= 0.73** μeV

Fabry-Perot interferometer

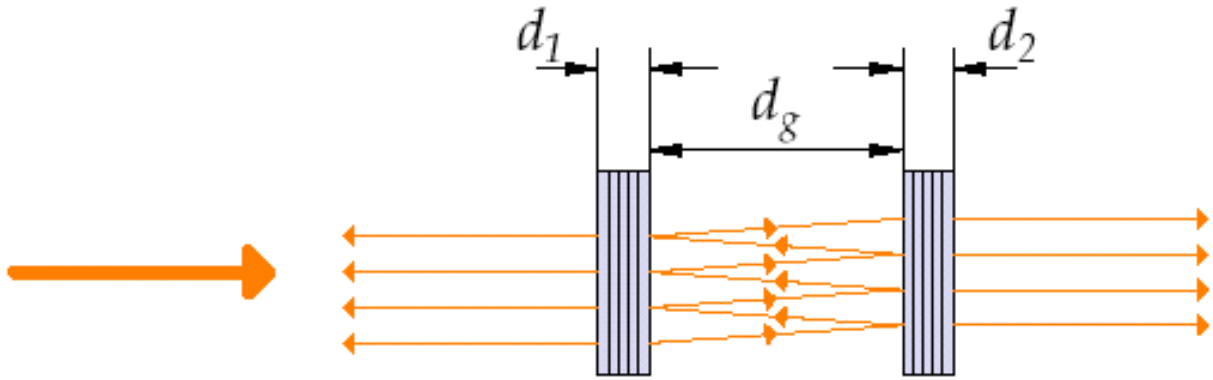

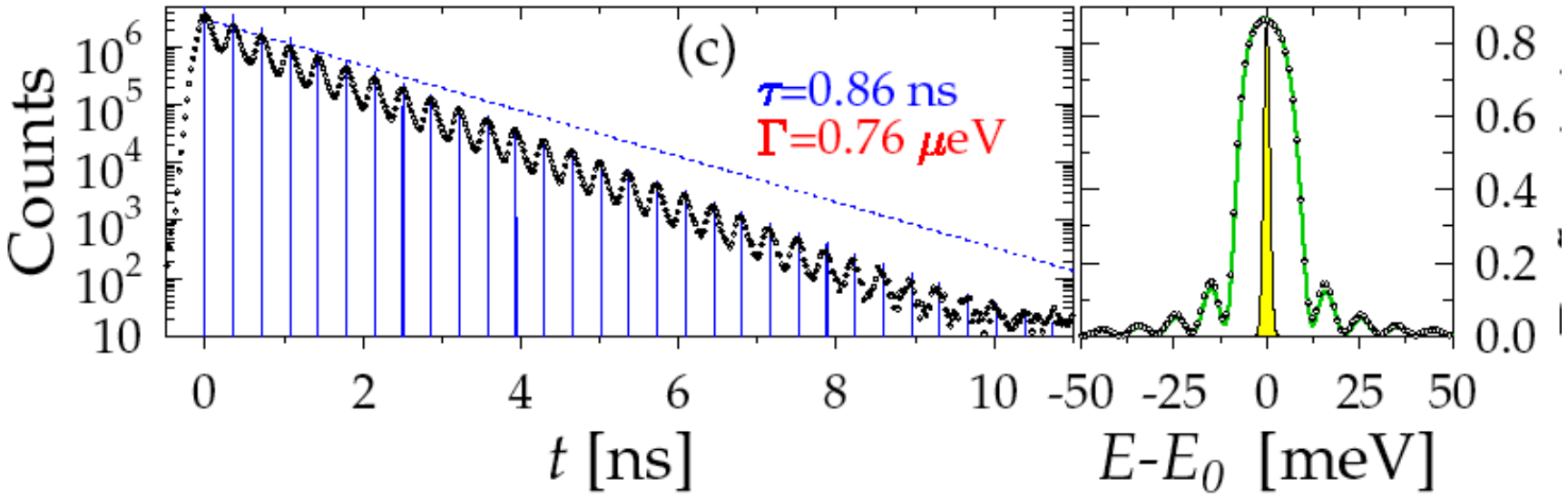

Y. Shvydko, M. Lerche, H.-C. Wille, E. Gerdau, M. Lucht, H.D. Rüter (Hamburg)
E. E. Alp, R. Khatchatryan (APS), Phys. Rev. Lett (accepted) 2002